Pipeline for the Classification of Subjects with Neurodegenerative Diseases Based on Biomedical Signal Processing and Machine Learning Techniques

Aura Cristina Puche Sarmiento

Tesis de maestría presentada para optar al título de Magíster en Ingeniería

Tutor

John Fredy Ochoa Gómez, Doctor (PhD)

Universidad de Antioquia

Facultad de Ingeniería

Maestría en Ingeniería

Medellín, Antioquia, Colombia

2022

Cita	(Puche Sarmiento, 2022)
Referencia **Estilo APA 7 (2020)**	Puche Sarmiento, A. C. (2022). *Pipeline for the Classification of Subjects with Neurodegenerative Diseases Based on Biomedical Signal Processing and Machine Learning Techniques* [Tesis de maestría]. Universidad de Antioquia, Medellín, Colombia.

Maestría en Ingeniería, Bioingeniería.

Grupo de Investigación Bioinstrumentación e Ingeniería Clínica (GIBIC).

Centro de Investigación Ambientales y de Ingeniería (CIA).

Acknowledgment

I would like to thank Professor John Fredy Ochoa Gómez for his guidance, expertise and encouragement during this process. To all the members of GRUNECO for the academic support, criticism and advice. Thanks also to GIBIC and the Bioengineering program. I specially thank to my family, Marlene, Marco, Katy and Daniela for their unconditional support.

Many thanks to the examiners for taking the time to review this project.

Contents

List of abbreviations

AD	Alzheimer's Disease
ADNI	The Alzheimer's Disease Neuroimaging Initiative
AFNI	Analysis of Functional NeuroImages, Open-source environment
AIS	Active Information Storage
ALFF	Amplitude of Low Frequency Fluctuations
ALS	Amyotrophic Lateral Sclerosis
AUC	Area Under the Curve
BOLD	Blood-oxygen-level-dependent
CC	Clustering Coefficient
CDR-SB	Clinical Dementia Rating Scale Sum of Boxes
CN	Cognitively Normal
CONN	Open-source software for the computation, display, and analysis of functional connectivity Magnetic Resonance Imaging
CSF	Cerebrospinal Fluid
CV	Cross Validation
DMN	Default Mode Network
DPABI	A Toolbox for Data Processing & Analysis for Brain Imaging
DPARSFA	Data Processing Assistant for Resting-State fMRI advanced edition
EEG	Electroencephalography
ES	Effect Size
FA	Flip Angle
fALFF	Fractional Amplitude of Low Frequency Fluctuations
FDG-PET	Positron Emission Tomography with 18F-fluorodeoxyglucose
FDR	False Discovery Rate
fMRI	Functional Magnetic Resonance Imaging
FN	False Negative
FP	False Positive
FTD	Frontotemporal Dementia
GE	Global Effiency
HD	Huntington's Disease
Hipp	Hippocampus
ICA	Independent Component Analysis
IPL	Bilateral Inferior Parietal Lobes
LOOCV	Leave One Out Cross-Validation
MCI	Mild Cognitive Impairment
MDS	Multidimensional Scaling
MEG	Magnetoencephalography
MES	Measures of the Effect Size

MI	Mutual Information
MMSE	Mini-Mental State Examination
MPFC	Medial Prefrontal Cortex
MRI	Magnetic Resonance Imaging
ND	Neurodegenerative Diseases
ND	Node Degree
OASIS	The Open Access Series of Imaging Studies
PCA	Principal Component Analysis
PCC	Posterior Cingulate Cortex
PD	Parkinson's Disease
PE	Permutation Entropy
PET	Positron Emission Tomography
PL	Characteristic Path Length
RBF	Radial Basis Function
ReHo	Regional Homogeneity
ROC	Receiver Operating Characteristic
ROI	Region of Interest
rs-fMRI	Resting State Magnetic Resonance Imaging
SMOTE	Synthetic Minority Oversampling Technique
SVM	Support Vector Machine
SWP	Small World Propensity
TA	Acquisition time
TDA	Topological Data Analysis
TE	Echo Time
TN	True Negative
TP	True Positive
TPOT	Open-source library for performing automatic machine learning in Python
TR	Repetition Time
t-SNE	t-Distributed Stochastic Neighbor Embedding

List of tables

List of figures

Abstract

Alzheimer's disease is the most common cause of dementia. It has been found that the Default Mode Network (DMN), one of the so-called resting state networks, is important in the study of Alzheimer's Disease (AD) given the loss of its integrity during its progression. Signals from the DMN were obtained from resting state functional Magnetic Resonance Imaging (rs-fMRI). The objective of this study was to develop a pipeline to classify subjects with neurodegenerative diseases using techniques from biomedical signal processing and machine learning over resting state fMRI BOLD signals. We implemented a static and dynamic approach to evaluate the brain function in cognitively normal individuals and subjects with Alzheimer's Disease over the default mode network. Metrics used for the estimation of brain function included spectral estimations, information theory measures and graph theory analysis. Machine learning techniques were applied to find the best model to classify AD subjects. Information theory analysis performed by the permutation entropy showed a statistically significant increase in AD compared to cognitively normal (CN) subjects, the difference was found in the Left Retrosplenial Cortex, Posterior Cingulate Cortex. The classification provided a recall of 0.74 ± 0.34, a ROC-AUC of 0.83 ± 0.07 and a specificity of 0.62 ± 0.05.

Keywords: Neurodegenerative disease, resting state functional magnetic resonance imaging, brain networks, default mode network, biomedical signal analysis.

1. Introduction

ND are a common cause of morbidity, most of them do not have cure or reduction of symptoms (Lassonde et al., 2017). In the coming decades an increase in cases of dementia is expected, with AD being the most prevalent one (Tom et al., 2015). In Colombia, AD affects 221,000 Colombians and is considered one of the pathologies that generate higher costs to the health system. The average minimum cost per patient is $ 1.5 million per year in the mild state, $4 million in the moderate state, and $ 8.5 million in the severe state. The total cost of treatment for a period of 8 years was established at $ 33.3 million, if the caregiver's costs were included, the figure would be $ 99 million (Prada, Takeuchi, & Ariza, 2014). On the other hand, PD is the second most common neurodegenerative disease, with an estimated prevalence of 0.3% of the population, median age of onset is around 60 years and the estimate mean illness duration to death is 15 years from diagnosis (Erkkinen, Kim, & Geschwind, 2017; Lees, Hardy, & Revesz, 2009).

The diagnosis of AD is based on clinical manifestations such as a gradual progression of memory loss and a loss of functional independence caused by alterations in visuospatial and executive function. The presence of amnestic symptoms was originally a requirement criterion according to The National Institute of Neurological and Communicative Disorders and Stroke and Alzheimer's Disease and Related Disorders Association (NINCDS-ADRDA) but in 2011 there were included more clinical phenotypes based on 27 years of clinical experience (McKhann et al., 2011). Therefore, its diagnosis is highly dependent of the clinical manifestations and the performance of the person during the implementation of cognitive tests. However, there are other formal diagnostic criteria based on the use of biomarkers, in which imaging modalities have been widely studied given its promising potential to detect even pre-symptomatic neurodegenerative stages (Dickerson, Agosta, & Filippi, 2016).

In patients with AD, structural magnetic resonance imaging (MRI) has revealed disproportionate atrophy in the hippocampus and other structures (Baron et al., 2001; Erkkinen et al., 2017; Frisoni et al., 2002; Ishii et al., 2005). Functional imaging modalities such as FDG-PET in PD have shown a greater hypometabolism in patients compared to controls. Amyloid-PET is available clinically in the United Stated, however it is highly dependent of the approval of insurance carries given its high cost.

A less expensive modality that allows the study of functional brain function is functional magnetic resonance imaging (fMRI). During task performance patients with AD exhibit decreased activation in hippocampal and parahippocampal regions compared to controls and PD patients showed reduced neural responses in the pre-supplementary motor area during the execution of a variety of tasks (Dickerson et al., 2016). In resting state fMRI (rs-fMRI), studies showed that one of the most reproduced findings is the reduction of brain connectivity over the Default Mode Network (DMN) in AD (Dickerson et al., 2016). In ALS has been found that patients have a reduction or mixed changes in brain connectivity compared to controls, these patients have also showed reduction and increase in brain connectivity over the DMN.

In contrast to task-based fMRI, rs-fMRI is more accomplishable in clinical practice being not dependent on the performance of the subjects. Additionally, oscillations can be studied through rs-fMRI given its advantage for capturing brain dynamics during rest by means of the Blood Oxygenation Level Dependent (BOLD) effect (B. Biswal, Yetkin, Haughton, & Hyde, 1995). rs-fMRI allows the implementation of several techniques over the BOLD signal looking for patterns related to the physiological phenomena. Nowadays the methods for the analysis of rs-fMRI relies on the processing BOLD signal through two main approaches: functional integration and functional segregation metrics (Lv et al., 2018). Functional integration refers to the analysis of

functional relationship between regions, this analysis is commonly known as connectivity analysis. On the other hand, functional segregation refers to the analysis of local function over specific brain regions (Lv et al., 2018).

The most common segregation analysis of rs-fMRI includes spectral metrics such as the Amplitude of Low Frequency Fluctuations (ALFF) and its fractional version (fALFF), both metrics are computed using the Fast Fourier Transform (Cheng et al., 2017; Hu, Chen, Huang, Qian, & Yu, 2017; Liu et al., 2014; P. Wang et al., 2019). In addition, previous works have reported altered patterns in ALFF and fALFF in neurodegenerative diseases (J. Wang, Zhang, Zang, & Wu, 2018; Yang et al., 2018).

Functional Integration analysis is commonly accessed by seed/region-of-interest, ROI-based functional connectivity analysis, independent component analysis (ICA), and graph analysis (Lv et al., 2018). This analysis is commonly computed based on the averaged behavior of the BOLD signal, rather than spatiotemporal dynamic features of the signal. Several papers have been published recently around this topic being the sliding window technique the most common approach to access changes in between-network connectivity (Schumacher et al., 2018). It has been pointed out that the use of rectangular windows has negative effects related to sudden changes in the signal, one of the most recent advances to solve this issue was a modulated rectangular window (Mokhtari, Akhlaghi, Simpson, Wu, & Laurienti, 2019), in this study authors suggested that future work is needed in order to evaluate the performance of different windows for getting real fMRI connectivity data.

The human brain has been described as a complex system (Telesford, Simpson, Burdette, Hayasaka, & Laurienti, 2011), in addition, neuroscience data is highly noisy and usually describes non-linear relationships (Timme & Lapish, 2018). Integration and segregation approaches rely on

the use of biomedical signal processing methods, however there exist a lack of works exploring methods based on spectral analysis that reduce the bias or variance of the estimates such as Multitaper (Babadi & Brown, 2014), researchers have highlighted the need to develop software tools that enable the routine application of power spectral density analysis (Duff et al., 2008) and the use of information theory for understanding brain function given its power for capturing nonlinear interactions (Timme & Lapish, 2018).

The integration and segregation metrics are usually done in the toolboxes DPABI/DPARSFA (http://rfmri.org/DPARSF), CONN (https://www.conn-toolbox.org), AFNI (https://afni.nimh.nih.gov/) and FSL (https://www.fmrib.ox.ac.uk › fsl). To date, none of them allows the computation of spectral nor connectivity metrics from a voxel wise approach over a resting state network of interest, instead the computation is done over averaged signals within a region of interest. Metrics based on information theory are not even available in those toolboxes, however dynamic analysis is included in some of them, it is the case of DPABI and CONN.

Recent advances have allowed the development of machine learning techniques, becoming a highly used approach in neuroimaging applications given its potential for the search of biomarkers (Pellegrini et al., 2018) and achieving individual diagnosing tools (Rathore, Habes, Iftikhar, Shacklett, & Davatzikos, 2017). However, features are traditionally extracted by seed-based ROI correlation, which mainly ignores the relationship between rs-fMRI voxels (Mevel, Chételat, Eustache, & Desgranges, 2011). Performing individual data classification based on the best characteristics as inputs will be more beneficial in the clinical field (Teipel et al., 2017). Studies concerning AD have used metrics values as inputs for classification algorithms to discriminate between AD and healthy controls (Ali Khazaee, Ebrahimzadeh, & Babajani-Feremi, 2017) and discriminate between healthy controls and mild cognitive impairment (MCI) subjects (Rathore et

al., 2017). For this purpose, ADNI and OASIS databases have been the most widely explored (Tom et al., 2015).

Looking for achieving the goal, it was proposed a pipeline for the diagnosis of AD, high and reproducible accuracy rates of $90.06 \pm 0.01\%$ with a sensitivity of $92.00 \pm 0.04\%$ and specificity of $87.78 \pm 0.04\%$ was obtained (Jha, Kim, & Kwon, 2017), they used 126 samples of structural MRI, including 28 subjects with AD and 98 healthy controls from OASIS database. They used a dual-tree complex wavelet transform for extracting features, this method processes properties including shift invariance and high directionality.

A multimodal study reported accuracy rates of 89.0 ± 0.7, sensitivity of 87.9 ± 1.2 and specificity of 90.0 ± 1.1 (Gray et al., 2013), features included regional MRI volumes, voxel-based FDG-PET signal intensities, CSF biomarker measures, and categorical genetic information. The diagnostic power of default mode network in the detection of Alzheimer's disease from rs-fMRI data was addressed by (Koch et al., 2012), they got a diagnostic power of 64% accuracy for one DMN region in independent component analysis. In this study prediction of mild cognitive impairment was not easily perceived, and complex models were used in order to optimize the diagnostic power given the small number of subjects: 21 healthy subjects, 17 subjects with mild cognitive impairment and 15 patients, accuracy was increased to 97% (sensitivity 100%, specificity 95%), however authors highlight the limitation in the number of subjects and that the use of methods of analysis considering activity and interconnectivity within the DMN are required to achieve optimal and clinically acceptable diagnostic power.

Imaging modalities under investigation are promising, however they do not have enough diagnostic power to be used in the clinic (Erkkinen et al., 2017). It has been reported that the desire to extract quantitative measures from medical imaging and used them with machine learning

techniques to improve the characterization and detection of diseases is limited given the variability of the measurements and its analysis, in addition there is “a paucity of evidence on how such quantitation potentially affects clinical decision-making and patient outcome” (deSouza et al., 2019). Additionally, according to a recent scientific report, the most significant challenge in single-subject prediction is that there is not an optimal connectivity metric nor a gold standard for the extraction of BOLD signals, they highlight that the deviations in prediction performance is due to previous factor and they suggest that methodological innovations, like metrics that reduce bias and variance, are necessary for improving the prediction accuracy that could end in the clinical practice (Khosla et al., 2019).

Previous needs are essential for the classification of neurodegenerative diseases (ND) and healthy subjects. Therefore, in this project was developed a pipeline for the classification of subjects with neurodegenerative diseases based on the extraction of brain function metrics from resting state networks using biomedical signal processing methods and machine learning techniques. Algorithms were designed for capturing static and dynamic brain function from blood-oxygen-level-dependent (BOLD) signals using region of interest (ROI) and voxel-based approaches, those algorithms were tested using rs-fMRI data of the Default Mode Network from 40 subjects with AD and 58 CN individuals. Metrics used for the estimation of the static brain function included spectral estimations, information theory techniques and graph theory analysis; dynamic brain function was accessed by a low dimensional manifolds’ analysis.

The dynamic approach was analyzed according to its visual representations. For the static approach, a statistical analysis was performed using a two-sample t-test non-parametric method and the effect size. Metrics from the static approach were used as features for the design of the classifier, data cleaning and a feature selection using the effect size and mutual information were

performed. Machine learning techniques were applied to find the best model to discriminate between AD and CN individuals, different strategies were implemented for model selection, such as support vector machine random search, automatization of the process of model selection using a data scientist assistant tool (TPOT) and an oversampling method for the imbalanced data (SMOTE).

Models were validated using k-fold cross-validation and the evaluation of its performance was accessed by the accuracy, recall, f1-score, the area under the receiver operator characteristic curve and the specificity. Results from previous steps were used to propose the pipeline for the classification of subjects with neurodegenerative diseases using techniques from biomedical signal processing and machine learning over resting state fMRI BOLD signals. The pipeline was validated with rs-fMRI data from the Alzheimer's Disease Neuroimaging Initiative: ADNI; 14 subjects with mild cognitive impairment and 14 control subjects were used for this purpose.

This document is distributed in sections as follows: *2. Objectives*, *3. Background Information*, *4. Measures for the Estimation of Brain Function* (development of objective 1), *5. Classification Capacity of Brain Function Features* (development of objective 2), *6. Pipeline for the classification of subjects with neurodegenerative diseases from rs-fMRI* (development of objective 3), *7. Validation of the pipeline on rs-fMRI data from subjects with MCI* (development of objective 4), *8. Overall Discussion*, *9. Overall Conclusion* and *10. Bibliography.*

2. Objectives

2.1. General Objective

To develop a pipeline to classify subjects with neurodegenerative diseases using techniques from biomedical signal processing and machine learning over resting state fMRI BOLD signals.

2.2. Specific Objectives

1. To develop algorithms to compute features on static and dynamic brain networks using spectral estimation, information theory and graph theory.
2. Evaluate the classification potential of the obtained features from the brain networks using machine learning techniques.
3. To develop a pipeline that integrates the measures for feature extraction and the classifier using open-source software.
4. Validate the pipeline with rs-fMRI data from healthy and AD subjects.

3. Background Information

3.1. Neurodegenerative Diseases

Neurodegenerative diseases (ND) are characterized by a progressive degeneration preceding clinical manifestations (Williams, 2002), in which genetic, sporadic, and unknown factors have been reported as causes of these diseases. The underlying physiology and clinical representations of ND are defined as heterogeneous. However, overlapping between features have been reported (Erkkinen et al., 2017). The most prevalent types of ND are Alzheimer's disease, Parkinson's disease (PD), Huntington's disease (HD), and multiple sclerosis (Hussain, Zubair, Pursell, & Shahab, 2018). Alzheimer's Disease (AD), Parkinson's Disease (PD), Frontotemporal Dementia (FTD) and Amyotrophic Lateral Sclerosis (ALS) share a common feature concerning the interaction of molecular and cellular alteration that ends up affecting specific groups of neurons at specific brain areas (R. Habib, Noureen, & Nadeem, 2018).

ND are a common cause of morbidity, most of them do not have cure nor reduction of symptoms (Lassonde et al., 2017). In the coming decades, an increase in cases of dementia is expected, with AD being the most prevalent one (Tom et al., 2015). Therefore, actions for developing strategies to treat and understand the mechanisms of ND are required.

3.1.1. Alzheimer's Disease

AD is the most prevalent ND, it is characterized by the presence of several changes in brain function typically extended over brain networks (Bayram et al., 2018). The main risk factor of sporadic AD is age where onset usually takes place at 60's (Strimbu & Tavel, 2010), in addition to this cause, there are genetic mutations that accelerate the beginning of neurocognitive alterations. The most distinctive feature found on the brain of patients with AD is the extensive

extracellular deposition of amyloid-β plaques and the intracellular presence of neurofibrillary tangles. Models of AD suggest that neurodegeneration and cognitive decline are caused by a pathophysiological cascade that begins with an abnormal increase in amyloid-β plaques that leads to an abnormal assembly of tau that spreads all through the cortex (Busche & Hyman, 2020).

AD has been described in three stages: preclinical in which cognitive ability is clinically normal, MCI and dementia. The first stage is characterized by the accumulation of amyloid, MCI can be amnestic and non-amnestic and dementia is characterized by severe problems in the memory process (Vermunt et al., 2019).

3.2. Resting State Networks and Brain Function

The human brain has been described as a complex dynamical system by many scientists (Bassett & Gazzaniga, 2011; Kabbara, EL Falou, Khalil, Wendling, & Hassan, 2017; Sporns, 2013; Zuo et al., 2010). Oscillatory waves generated by the brain have been associated with various neural processes including cognitive functions such as salience detection, emotional regulation, attention and memory (Knyazev, 2007) .

Temporal correlations between fMRI signals from brain regions were first reported by (B. Biswal et al., 1993) during an fMRI acquisition when subjects were not asked to perform a cognitive demanding task, which showed the maintenance of functional activity of the brain in the absence of active computations. The study of brain function at rest has revealed the presence of resting state networks; a result of functional connectivity between distinct areas of the brain that follows an intrinsic connectivity pattern (Azeez & Biswal, 2017). An example of these is the default mode network (DMN) that also has been reported in previous studies as a target region in the study of AD (Badhwar et al., 2017; Cha et al., 2013; Dai et al., 2019; Dillen et al., 2017; M. Habib et al., 2017).

3.3. Resting State Functional Magnetic Resonance Imaging

The interest in studying rs-fMRI relies on the fact that at low frequencies the brain oscillations captured by the scanner are linked to spontaneous neural activity (Damoiseaux et al., 2006; Zuo et al., 2010). In addition, fMRI BOLD signals acquired during rest are well known for revealing fully functional brain networks, instead of partial activation due to the isolation of brain function during task-based fMRI (B. B. Biswal, 2012; Khalili-Mahani et al., 2017; Mevel et al., 2011).

Functional neural behavior can be studied from two different approaches: functional segregation and functional integration (Lv et al., 2018). Functional segregation analysis is based on the local study of specific brain regions mapping according to metrics obtained from various approaches, some of them are: the Amplitude of Low Frequency Fluctuations (ALFF), fractional ALFF (fALFF), Regional Homogeneity (ReHo) (Lassonde et al., 2017) and Active Information Storage (AIS) (Lizier, Prokopenko, & Zomaya, 2012). On the other hand, functional integration methods refer to connectivity analysis, such as graph theory and independent component analysis.

The frequency of spontaneous neural oscillations has been described within the 0.01-0.08 Hz range (Zuo et al., 2010). This band can be decomposed into slow-5 (0.01–0.027 Hz) and slow-4 (0.027–0.073 Hz), in which different regions will reflect specific properties and physiological function (Penttonen & Buzsáki, 2003). For example, recent studies (An et al., 2013; Mao et al., 2017) found connectivity patterns mainly in the slow-5 and slow-4 and a decrement in connections related to long distance and an increase in short connections. Authors reported that changes found in the slow-5 and slow-4 bands could give a potential biomarker for AD.

3.4. Default Mode Network

The Default Mode Network is one of the well-defined resting state networks, it consists of a group of spatially segregated brain areas that are synchronously co-activated and deactivated over time (Randy L. Buckner, Andrews-Hanna, & Schacter, 2008). The core brain regions of the DMN are medial prefrontal cortex (MPFC), posterior cingulate cortex (PCC), left and right inferior parietal lobes (IPL), and bilateral hippocampus (Hipp) (R. L. Buckner et al., 2005). Several studies have revealed a dysfunction over the DMN during the progression of AD, mainly because this network has been reported to have susceptibility for the accumulation of β-amyloid in AD patients, which means that plaques associated with neural toxicity are located within the DMN regions (Dillen et al., 2017).

There is a link between its dysfunction and disturbances of brain oscillations (Sepulcre, Sabuncu, & Johnson, 2012; Uhlhaas & Singer, 2006) whose effect is observed not only AD but other neurodegenerative disorders (Agosta et al., 2012). Some studies have reported functional brain changes over the DMN during the progression of AD (Bayram et al., 2018), in addition, rs-fMRI studies have shown alterations and disruption in the integrity of this network (Cha et al., 2013). Therefore, the DMN has been highlighted by many scientists as a target region in the study of functional connectivity in AD in the look for biomarkers (Balthazar, Campos, Franco, Damasceno, & Cendes, 2013; Cha et al., 2013; Greicius, Srivastava, Reiss, & Menon, 2004). Additional findings around the study of the DMN in AD includes functional coupling disruption found in prodromal AD across regions (J. Zhou et al., 2010), as well as decreased functional connectivity across regions (Cha et al., 2013; Greicius et al., 2004; Koch et al., 2012; Lustig et al., 2003; H.-Y. Zhang et al., 2010).

3.5. Dynamic Brain Function

Contrary to the static approach, the study over short segments on time without assuming the stationary of brain functional connectivity (Schumacher et al., 2018) is often referred as dynamic functional connectivity or dynamic brain connectivity (Savva, Mitsis, & Matsopoulos, 2019). Although functional connectivity has been traditionally studied from a static approach, recent studies have shown the increasing interest in the measure, visualization and interpretation of dynamic functional connectivity (Hutchison, Womelsdorf, Gati, Everling, & Menon, 2013; Qiao, Lv, Cao, Wang, & Li, 2018; Xie et al., 2019) . The purpose of this analysis is to acquire additional information, instead of only working with the mean connectivity over the study (Qiao et al., 2018) due to the presence of fluctuations of the fMRI signal over short periods of time that has been associated with neurodegenerative disorders and other cognitive processes (Bahrami et al., 2019). We highlight the study in (Agosta et al., 2012), they argued that there exists a loss of relevant information when performing previously mentioned approaches given the inevitable collapse of data in space or time. Saggar et al. proposed a Topological Data Analysis (TDA) for studying brain connectivity from interactive relevant representations without collapsing space and time, contrary to the static analysis that is based on “average” functional connectivity. This new approach may be helpful in the recognition of the characteristics that constitute the healthy or altered brain.

Mapping brain dynamics into low-dimensional manifolds has been explored using methods that include embedding raw fMRI time series as well as dynamic brain states after independent component analysis and more recently, a method proposed by (Bahrami et al., 2019) described a direct methodological approach in which dynamic networks were embedded into a low-dimensional space preserving the information in high dimensional networks, it is suitable for large datasets and allows the use of various embedding techniques. Authors suggest this approach for

representing dynamic brain networks given its potential to provide a standard space for projecting brain networks and compare them between populations or various conditions, in addition they highlight the need to replicate the methodology in other populations. To date it has not yet been explored in ND.

3.6. Biomedical Signal Processing Methods

Biomedical signals are those transduced from a biological or medical source that is acquired for estimating a pathological or physiological state. The fMRI BOLD signals are obtained after a proper processing of functional images, they are characterized by its high spatial resolution and low temporal resolution (Cerutti & Marchesi, 2011).

The main goal of biomedical signal techniques is the accurate quantification of the relationships between events and measurements in a time series. The quantification of fMRI BOLD signal characteristics will be referred to as feature extraction, denoting function or dysfunction of brain regions.

3.6.1. Amplitude of Low Frequency Fluctuations

Spontaneous regional brain oscillations by fMRI have been previously studied using the ALFF and fALFF measures within a frequency range from 0.01 to 0.08 Hz (Giménez et al., 2016; Zang, Zuo, Milham, & Hallett, 2015; F. Zhou et al., 2016; Zou et al., 2008). Recent studies reported that a decreased ALFF was found in the left putamen in PD subjects (Pan et al., 2017; J. Wang et al., 2018). The use of ALFF and fALFF as features in machine learning algorithms improved the identification accuracy of subjects with subjective cognitive decline, amnestic MCI and dementia AD from normal controls (Yang et al., 2018), they highlighted that the ALFF and fALFF may be useful to detect the pathological mechanism in AD continuum.

For a timeseries of length N defined by equation 1, the ALFF is computed over a frequency range according to equation 2 and fALFF is computed over a frequency range according to equation 3.

$$x(t) = \sum_{k=1}^{N} [a_k \cos(2\pi f_k t) + b_k \sin(2\pi f_k t)] \quad (1)$$

$$ALFF = \sum_{k:\, f_k \in [0.01,0.08]} \sqrt{\frac{a_k^2(f_k) + b_k^2(f_k)}{N}} \quad (2)$$

$$fALFF = \frac{\sum_{k:\, f_k \in [0.01,0.08]} \sqrt{\frac{a_k^2(f_k) + b_k^2(f_k)}{N}}}{\sum_{k=1}^{N} \sqrt{\frac{a_k^2(f_k) + b_k^2(f_k)}{N}}} \quad (3)$$

3.6.2. Multitaper Spectral Estimation

The spectral estimation based on the periodogram is based on finite data length. This results in two problems: the bias and variance. In the analysis of neural signals, the problems previously mentioned can become a major limitation. However, bias limitation can be reduced by using data tapers for multiplying the data and variance limitations can be reduced by averaging overlapping segments of the signal.

Multitaper spectral estimation method was proposed by Thompson in 1982 in which signal is multiplied by several orthogonal tapers (equation 4) and posterior transformed by Fourier method. Multitaper estimation is defined by equation 5.

$$\text{[illegible]} = \sum_{t=1}^{N} w_t(k) x_t \exp(-2\pi i f t) \quad (4)$$

$$S_{MT}(f) = \frac{1}{k} \sum_{K=1}^{K} \left| \text{[illegible]}_k(f) \right|^2 \quad (5)$$

Multitaper analysis have been previously used for the analysis of neural signals, a study explored the relationship between the power spectral density and connectivity measures over task-based and rs-fMRI data, the analysis was performed using Multitaper spectral estimation for its advantage to reduce variance and bias. They used 13 tapers for rs-fMRI data and 5 for the task-based. The statistical analysis was performed over the 0.03, 0.10, and 0.23 Hz frequencies, it was found that this is a sensitive method for characterizing BOLD signal oscillations and results were promising to strengthen the analysis of network connectivity (Duff et al., 2008).

3.6.3. Graph Analysis

Graph theory is a mathematical approach used in the study of topological architectures; in the field of neuroscience, it provides a way to understand the complexity of brain function. In the analysis of human brain networks, it has revealed meaningful information concerning its modular organization, highly connected hubs and small-worldness property (Farahani, Karwowski, & Lighthall, 2019).

The analysis of brain networks using graph theory requires the construction of a connectivity matrix of NxN, where N is the number of nodes of the network and each element of the matrix represents the relationship between them. This relationship can be computed using any functional

connectivity metric such as correlation coefficient, mutual information and transfer entropy. Once the connectivity matrix is generated it is possible to extract the properties of the network using global and local metrics. Global properties of the network refer to the network-wide attributes, which includes efficiency, path length and clustering coefficient, on the other hand, local properties of the network refer to its nodal attributes such as degree and strength. Clustering Coefficient (CC) is a density metric that quantifies the connection between a node and its neighbors, the Degree (DD) refers to the number of connections a node has, Global Efficiency (GE) measures the ability to transmit information, Characteristic Path Length (PL) is the average distance between pairs of nodes and Small World Propensity (SWP), a metric that measures how much a network shows small-world properties by taking into account variations in the density of the network (Muldoon, Bridgeford, & Bassett, 2016).

Recent studies revealed that the small-worldness experiences topological alterations during neurologic and mental disorders in multiple sclerosis and AD patients compared to controls (Jalili, 2017; Miri Ashtiani et al., 2018). On the other hand, (Bachmann et al., 2018) used clustering coefficient, graph weight, weighted degree distribution, modularity and shortest path length using different techniques. They found that graph analysis properties did not produce significant differences between healthy subjects and mild cognitive impairment (MCI) patients, a prior stage of AD; therefore, they proposed a combination of statistical methods and machine learning classification techniques for increasing the power of prediction. It is important to consider that this study was performed with a small dataset of healthy subjects and people with mild cognitive impairment.

3.6.4. Information Theory

Information theory has been defined by the International Encyclopedia of the Social & Behavioral Sciences as *"the mathematical treatment of the concepts, parameters and rules governing the transmission of messages through communication systems"* (Smelser & Baltes, 2001). In neuroscience the brain is considered an interesting example of a communication and processing system (Timme & Lapish, 2018), in this case information theory is capable of quantifying the linear and nonlinear relationship within the neurophysiological data from a model independent approach. Information theory methods such as active information storage, transfer entropy and mutual information, has been previously used for the analysis of electroencephalography (EEG), magnetoencephalography (MEG) and fMRI data (Lizier, Heinzle, Horstmann, Haynes, & Prokopenko, 2011; Puche Sarmiento, Bocanegra García, & Ochoa Gómez, 2019; Timme & Lapish, 2018).

3.6.4.1. Permutation Entropy

Shannon's metric of entropy is a fundamental quantity in information theory, it is known as *h*. It measures uncertainty of a variable. Permutation Entropy (PE) is an approach proposed by (Bandt & Pompe, 2002) for the analysis of complex and chaotic time series, with the advantage of being capable of giving meaningful results in the presence of observational and dynamical noise. In addition, the method is simple, fast and robust. For a time series $\{x_t\}_{t=1,\dots,T}$, π permutations of order n, PE is denoted as H(n) and it is defined by equation 6, where $p(\pi)$ is defined by equation 7, the symbol # stands for 'number'.

$$H(n) = -\sum p(\pi)\log(p(\pi)) \quad (6)$$

$$p(\pi) = \frac{\#\left\{t \mid t \le T-n, (x_{t+1},...,x_{t+n}) has \;\; type \;\; \pi\right\}}{T-n+1} \quad (7)$$

PE has been tested on resting state fMRI signal of 30 normal controls, 33 early MCI, 32 late MCI and 29 AD subjects from the Alzheimer's disease Neuroimaging Initiative (ADNI) database, the quantification of PE complexity was carried out by voxel-based analysis. They found significant decreased complexity in the occipital, frontal and temporal lobes in AD patients than the MCI and controls (B. Wang et al., 2017).

3.6.4.2. Active Information Storage

Active information storage (AIS) is defined as the mutual information that exists between a past state of some variable and its next value. In other words, it allows the quantification of information storage that will be used for the computation of the next measure in the next action of a defined process. The AIS is the mutual information between the past state of a physical system $X_{t-1}^{k} = \{x_{t-1},...,x_{t-1-k}\}$ and its next value X_T. It is computed according to equation 8. X is a physical system that generates a time series $\{x_1, x_2,..., x_T\}$ by measurements at discrete times $t \in 1,2,...,T$ (Lizier et al., 2012).

$$A_X = \left\langle \log \frac{p(x_{t-1}^{k}, x_t)}{p(x_t)} \right\rangle \quad (8)$$

Nowadays the storage of active information in the dynamic of neural activity is available on neural activity related data such as rs-fMRI, which opens the possibility of studying this phenomenon in a cohort of interest (Schumacher et al., 2018). AIS has been previously explored, differences between subjects have been shown when using AIS in a brain disorder study (Siyah Mansoory,

Oghabian, Jafari, & Shahbabaie, 2017) and differences were found over motor regions of the brain cortex in PD compared to controls (Puche Sarmiento et al., 2019).

3.7. Machine Learning

Machine learning algorithms are of great interest in neuroscience, it allows classification, regression and clustering on data and provides tools to improve predictions on large datasets, which also represents a challenge concerning the integration of data from different sites. Machine learning algorithms are usually classified into two main categories: supervised and unsupervised learning. Supervised learning relies on previous knowledge of the labels, which usually are based on the ground truth of the field and are provided by a human, the learning process will be focused on the relationship between the data and the labels. On the other hand, unsupervised learning depends on finding the patterns within the data without human supervision (Vu et al., 2018). Regression and classification are supervised techniques, the goal of regression is to predict a quantity accurately for a new sample, classification is about selecting the correct class for a new input and clustering is an unsupervised learning technique in which data is grouped into clusters based on similarities between its elements.

One of the most common supervised machine learning technique is support vector machine (SVM), which has been reported in previous studies to be a powerful method for the classification of subjects from fMRI data given its better prediction accuracy and the insensitivity to small sample sizes in the training dataset (Al-Zubaidi, Mertins, Heldmann, Jauch-Chara, & Münte, 2019). Power spectral density metrics have been previously used to feed SVM, a recent study used this machine learning method for the classification of subjects with autism. The output was a diagnosis decision with 90% of sensitivity (Dekhil et al., 2018).

The purpose of using machine learning algorithms is to find a model capable of solving a problem with the lower error. For this purpose, it is suggested to consider some the following steps:

3.7.1. Data Collection, Preparation and Cleaning

One of the main problems in machine learning applications is the lack of data for training caused by not being available or its poor quality (Roh, Heo, & Euijong Whang, n.d.). Acquisition of neurophysiological data is known for being sensitive to artifacts, the most critical artifact in fMRI signals is head motion which depends on the cooperation of the individual during the procedure. Head motion can be reduced in data preprocessing, however too much motion causes alterations on the signal that could be considered inappropriate for further interpretation. Dealing with data from data-sharing initiatives does not involve data collection issues for the researcher, however information about the subjects and parameter of acquisition is needed.

3.7.2. Feature Engineering

Once raw data have been prepared and cleaned, data must be transformed into features so that they can be the inputs of the machine learning model. Features for the study of brain function from rs-fMRI are usually extracted from BOLD signals using the segregation and integration methods mentioned previously.

Features can be non-informative or redundant to get an accurate prediction from the model. There are two strategies for the selection of features in supervised machine learning algorithms:

Filter approach: it does not involve algorithms; it simply uses statistical dependencies such as correlation coefficient and chi-square test to select the best features. The disadvantage is that it usually selects a high number of features unless a threshold is used (Sánchez-Maroño, Alonso-Betanzos, & Tombilla-Sanromán, n.d.).

Wrapper approach: it involves a machine learning classifier to test the features and select an optimal subset, it can lead to overfitting due to the use of different sets of features to find the best combination. It takes high computational time (Kohavi & John, 1997). Examples of this approach are backward elimination and forward selection.

Embedded approach: it involves a learning algorithm that performs feature selection in the learning time, there is no risk of overfitting. Examples of this approach are the Ridge Regression and LASSO (Tang, Alelyani, & Liu, n.d.).

3.7.3. Model Selection

Different machine learning algorithms can be used according to the classification problem, some of them are logistic regression, decision trees, random forest, boosting and support-vector machines. As mentioned before, SVM is the most used technique for discriminating between patients and healthy controls in the field of neuroimaging and neurodegenerative diseases (Bi, Shu, Sun, & Xu, 2018; Dyrba, Grothe, Kirste, & Teipel, 2015; Hojjati, Ebrahimzadeh, Khazaee, & Babajani-Feremi, 2017, 2018; A. Khazaee, Ebrahimzadeh, & Babajani-Feremi, 2015; Mao et al., 2017; Shi & Liu, 2020; T. Zhang et al., 2019). One of these research papers (A. Khazaee et al., 2015) reported 100% accuracy using graph measures, the main limitation highlighted by the study is that it is necessary to test the proposed approach with other datasets. Although when using SVM it is important to test different kernels, the best results with SVM in bioinformatic applications with low number of subjects have been reached with linear kernel (Ben-Hur & Weston, 2010).

SVM technique relies on the definition of a decision boundary responsible of discriminating between classes, an important goal is the maximization of the decision boundary (support vectors) and the reduction of wrong classifications during training, for reaching these goals SVM algorithms requires the setting of two important hyperparameters ***C*** and ***gamma*** previous the

training step. ***C*** controls the misclassification of data points by setting restrictions to the model, also refer as penalization, for higher values of ***C*** on the other hand, ***gamma*** defines the influence of data points over the decision boundary, high values of gamma represent an increase in the flexibility of the decision boundary, therefore it is related with the kernel. Kernel functions are needed for transforming the data that is not linearly discriminated. A poor selection of these parameters can result in unsatisfactory performance as well as higher risk of overfitting (Ben-Hur & Weston, 2010). Figure 1 represents the effect of ***C*** and ***gamma,*** and figure 2 represents the effect of the *linear, Radial Basis Function (RBF) and polynomial* kernel on the classification.

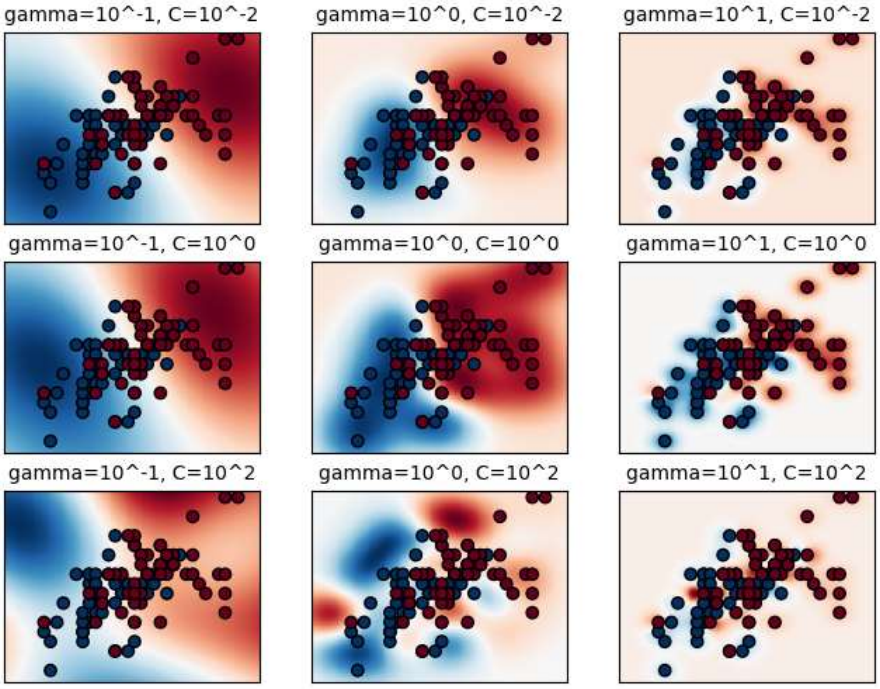

Figure 1. *Effect of gamma and c of the Radial Basis Function kernel. Each row represents the increase of gamma with c fixed, it shows that a higher gamma increases the flexibility of the decision boundary. Each column represents the increase of c with gamma fixed, it shows that higher values of c reduce the margins of the decision boundary. The figure was taken from scikit-learn.org.*

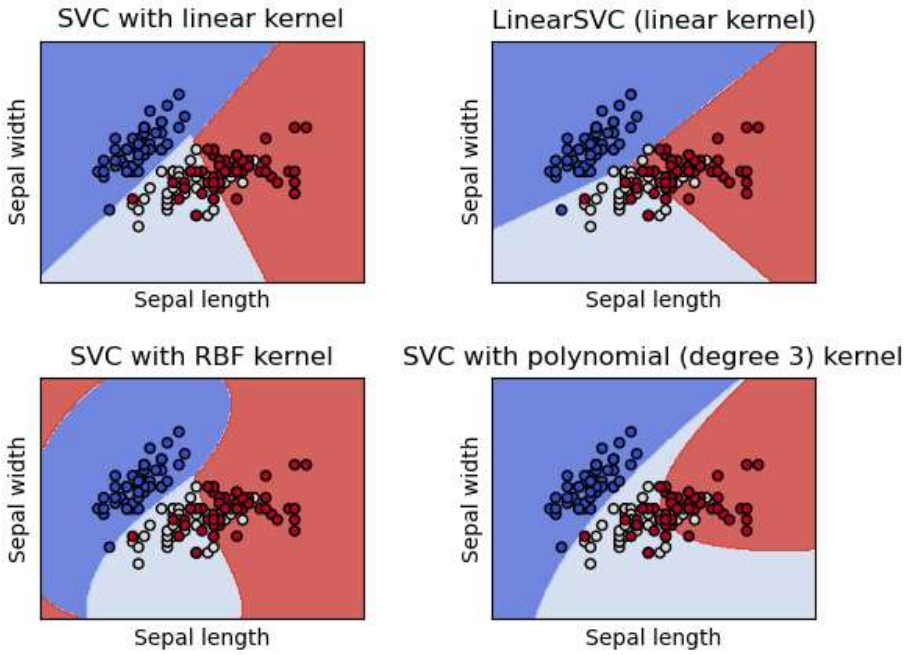

Figure 2. *Effect of the linear, polynomial and Radial Basis Function kernel on the multiclass classification problem of the well-known* Iris Dataset*, which consist of three types of irises that are represented in the figure with colors red, blue and white. The figure was taken from* scikit-learn.org.

3.7.4. Model Evaluation and Cross Validation

The purpose of the evaluation step is to test how well the model predicts the outcome of unseen data after the learning process. For this purpose, the dataset is split into two different subsets usually named training and test, the training dataset is used in the learning process and the test dataset will be used to evaluate the performance of the model. The use of metrics to quantify the performance of the model are needed, some of them are (Dalianis & Dalianis, 2018):

Confusion matrix: gives complete information of the performance of the model represented by the following matrix:

Table 1. *Confusion matrix representation for the evaluation of a classification model (Dalianis & Dalianis, 2018).*

		Predicted annotation	
		Positive	**Negative**
Gold annotation	**Positive**	True Positive (TP)	False Negative (FN)
	Negative	False Positive (FP)	True Negative (TN)

Accuracy: measures the number of correctly predicted observations to the total number of observations. It is defined by equation 9.

$$Accuracy = \frac{TP + TN}{TP + TN + FP + FN} \quad (9)$$

Precision: measures the number of correct positive results to the total of positive results predicted by the model. It is defined by equation 10.

$$Presicion = \frac{TP}{TP + FP} \quad (10)$$

Recall: measures the number of correct positive results to the total of correct results. It is defined by equation 11.

$$Recall = \frac{TP}{TP + FN} \quad (11)$$

F1: F1 score means the harmonic between precision and recall. Higher values of F1 (ranging from 0 to 1) stands for a better performance of the model. It is defined by equation 12.

$$F1 = 2 * \frac{1}{\frac{1}{presicion} + \frac{1}{recall}} \quad (12)$$

Area under the curve (AUC): this metric is widely use in binary classification problems, it is defined as the area under the false positive rate vs true positive rate, also known as the receiver operating characteristic (ROC) curve. It has a range between 0 and 1, higher values of the AUC denote a better performance of the model.

Cross Validation (CV) is an important step to prevent overfitting of the selected models after they have been trained and tested, it refers to the process of choosing the best model among various options with different parameters by considering the metrics explained before. The most common methods are the *leave-one-out cross-validation* and its extension *k-fold cross-validation*, the last is considered a standard validation method, it consist on taking k subsets of the same size (see figure 3) for computing the validation error k-1 times after training (Schnaubelt, Dovern, Fischer, Krauss, & Glas, 2019).

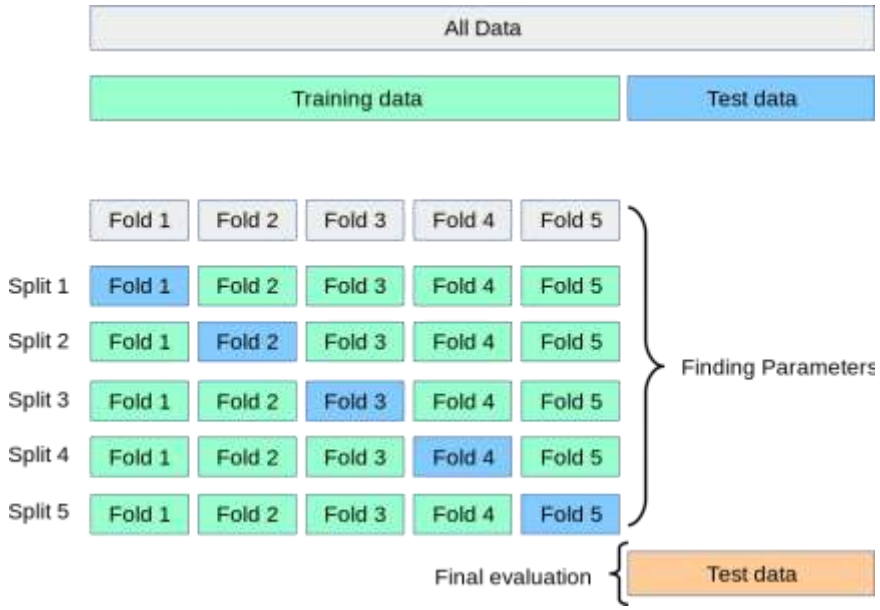

Figure 3. *Cross-validation process in which the data was split into 5 sets, each of them is used for training and testing the model. The figure was taken from* scikit-learn.org

4. Measures for the Estimation of Brain Function

4.1. Objective 1: To develop algorithms to compute features on static and dynamic brain networks using spectral estimation, information theory and graph theory.

The analysis of rs-fMRI data requires an initial stage to remove artifacts related to the acquisition, an election of regions of the brain to select the signals that will be studied, and the definition of methods for extracting meaningful information. Therefore, the purpose of this objective is to define preprocessing steps, the regions of interest and develop algorithms for the quantification of brain function from a static and dynamic approach. The use of spectral estimation, information theory and graph theory correspond to the static approach, the use of low-dimensional manifolds corresponds to the dynamic approach.

4.1.1. Materials and Methods

The computation of features began with raw rs-fMRI data, it was then followed by preprocessing steps, the extraction of BOLD signals according to the brain network of interest, finally the estimation of brain function using static and dynamic approaches. Algorithms were developed to perform the steps described in the following flowchart (figure 4).

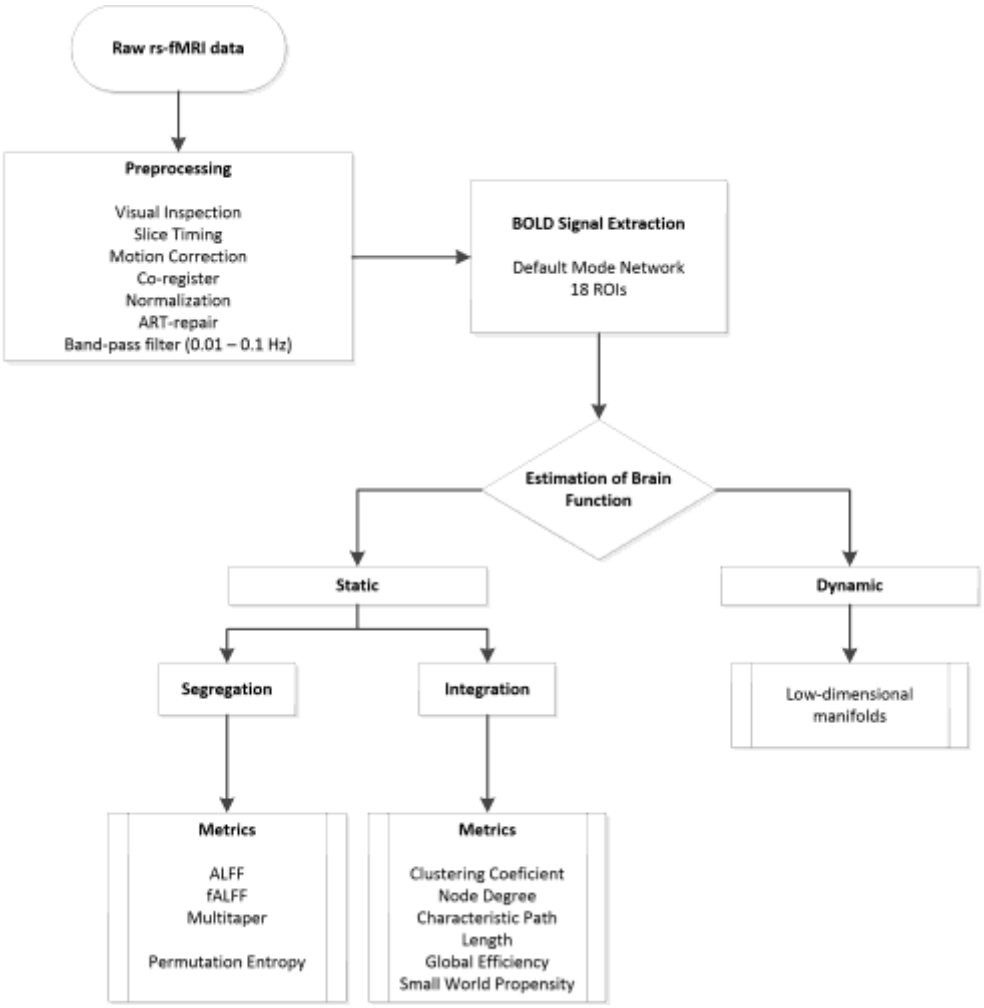

Figure 4. *flowchart representing the implemented approaches in objective 1.*

ALFF, fALFF and Multitaper metrics were computed for the slow-4, slow-5 and 0.01-0.1Hz frequency bands. Permutation entropy, integration metrics and the dynamic analysis were performed for the [0.01-0.1] Hz frequency band.

4.1.1.1.Subjects

Initially, 333 files labeled as AD and 1605 files labeled as Cognitively Normal were downloaded from the data available in the OASIS-3: Longitudinal Neuroimaging, Clinical, and Cognitive Dataset for Normal and Alzheimer's Disease (LaMontagne et al., 2019) after applying a filter to select subjects with MRI and rs-fMRI information. After this step, subjects with a second diagnosis

of any neurologic disorder were excluded, considering the small recruiting of left-handed and ambidextrous, only right-handed subjects were included. See the appendix 1a of the supplementary material for more information about the downloaded data.

OASIS-3 is a longitudinal project, therefore different subjects have more than one acquisition, subjects initially labeled as AD that in a posterior acquisition were labeled as CN or as uncertain dementia were excluded. As well as subjects that in a posterior acquisition had a neurologic disorder diagnosis different from AD. The selection of the subjects was made according to the clinical reports available at the database website (https://www.oasis-brains.org/). Only data with the same parameters of acquisition were included.

After checking the clinical inclusion criteria, data from 121 subjects were preprocessed, 23 subjects (AD:12, CN:11) were excluded for excessive head motion. Finally, 98 subjects with Alzheimer's disease (n = 40) and healthy righthanded subjects (n = 58) were taken for further analysis. The severity of the disease was assessed by the Clinical Dementia Rating Scale Sum of Boxes (CDR-SB) and the Mini-Mental State Examination (MMSE). Demographic information is shown in table 2. See the appendix 1b of the supplementary material for more information about the selected subjects.

Table 2. *Demographic and clinical characteristics*

Parameter	**AD** **Mean ± Standard Deviation**	**CN** **Mean ± Standard Deviation**	**P value**
n	40	58	-
Sex (female:male)	19:21	25:33	0.34
Age	74.57 ± 5.95	70.83 ± 6.54	<0.01
Years of education	15.30 ± 2.79	15.65 ± 2.69	0.72
MMSE	25.45 ± 3.13	28.93 ± 1.23	<0.01
CDR-SB	0.61 ± 0.21	-	-

MMSE: Mini-Mental State Examination
CDR-SB: Clinical Dementia Scale Sum of Boxes

4.1.1.2. Data Acquisition

For rs-fMRI acquisition, echo-planar images were collected at rest using a 3T SIEMENS Scanner (MAGNETOM Trio Tim, Siemens, Erlangen, Germany). The acquisition for each subject had 164 samples with parameters: echo time (TE) = 27 ms, repetition time (TR)= 2200 ms, flip angle (FA)= 90º, field of view (FoV)= 100 mm, 36 slices and voxel size= 4 mm x 4 mm x 4 mm. Additional details for the MRI acquisition in the OASIS project can be found elsewhere (https://www.oasis-brains.org/files/OASIS-3_Imaging_Data_Dictionary_v1.8.pdf).

4.1.1.3.Image Preprocessing

Preprocessing steps were performed in CONN (www.nitrc.org/projects/conn). Data were visually inspected to discard low-quality volumes. Volume realignment was performed taking the first volume as reference. Functional data was slice timing corrected and registered with the corresponding individual T1 image. Motion correction report was inspected to exclude subjects with excessive motion (translation > 2 mm and rotation > 2º in any direction). Data from the 121 subjects were preprocessed, after this stage, 23 subjects (AD:12, CN:11) were discarded from the posterior analysis given the excessive motion.

Selected data was normalized to the Montreal National Institute standard space, keeping the 2x2 x2 mm voxel size. Trends removal, movement correction, ART-repair, white matter and cerebrospinal fluid related signals, as well as temporal bandpass filtering, within the 0.01 to 0.1 Hz frequency band, were applied.

4.1.1.4.DMN Regions

BOLD signals were extracted based on the template proposed by (Shirer, Ryali, Rykhlevskaia, Menon, & Greicius, 2012) for each region of the DMN (figure 5), table 3 shows the name of each region. Labels shown in figure 5 from 1 to 9 for the ventral DMN are then referred as DMN from

10 to 18, the first 9 regions correspond to dorsal DMN. Masks of each region were taken for the extraction of the BOLD signals using the voxel-based and ROIs approach. Voxel-based approach was computed using image dimension of 91x109x91 and voxel dimension of 2x2x2 mm.

Table 3. *DMN regions of the template.*

Label	PCC / MPFC (Dorsal Default Mode Network)	Retrosplenial Cortex / Medial Temporal Lobe (Ventral Default Mode Network)
1	Medial Prefrontal Cortex	Left Retrosplenial Cortex, Posterior Cingulate Cortex
2	Left Angular Gyrus	Left Middle Frontal Gyrus
3	Right Superior Frontal Gyrus	Left Parahippocampal Gyrus
4	Posterior Cingulate Cortex, Precuneus	Left Middle Occipital Gyrus
5	Midcingulate Cortex	Right Retrosplenial Cortex, Posterior Cingulate Cortex
6	Right Angular Gyrus	Precuneus
7	Left and Right Thalamus	Right Superior Frontal Gyrus, Middle Frontal Gyrus
8	Left Hippocampus	Right Parahippocampal Gyrus
9	Right Hippocampus	Right Angular Gyrus, Middle Occipital Gyrus

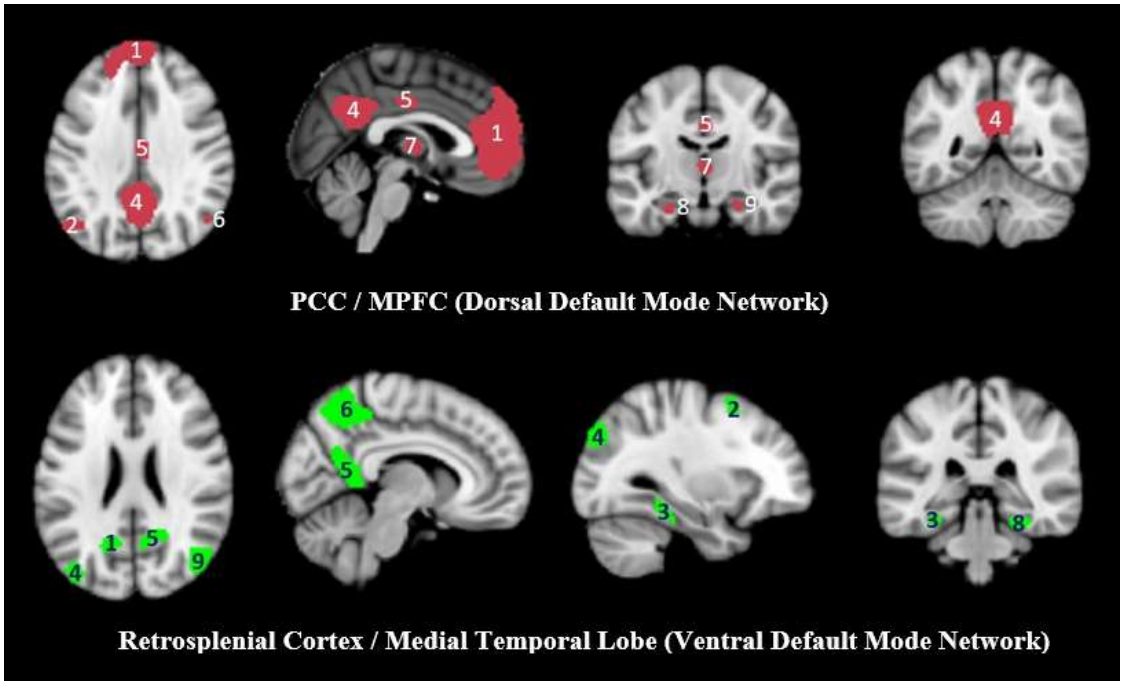

Figure 5. *Atlas of the DMN, 18 ROI masks were used for the extraction of the BOLD signals.*

4.1.1.5. Estimation of the Brain Function

For each region of the DMN, the ALFF, fALFF and Multitaper metrics on the slow-4, slow-5 and the [0.01-0.1] Hz frequency range; the SWP, CC, DG, PL and GE on the [0.01-0.1] Hz frequency range were computed and used as input features, 219 features were generated. Graph metrics were converted from fully connected functional brain networks to sparse brain networks using a proportional threshold function from [0.01 – 1] with an increment step of 0.01. This analysis was performed following the specifications described in section 4.1.1.

Low dimensional embedding maps are reported as the result of the dynamic approach described on section 4.1.2, the following section describe the details of the implemented methodology.

4.1.1.5.1. Static Approach

The static approach was designed for working with BOLD signals extracted by a voxel-based and a brain parcellation (ROIs) approach. Figure 6 represents the voxel-based approach used for the extraction of BOLD signals from the DMN, a network of interest in the study of ND.

The voxel-based approach consists of a selection of coordinates of voxels within a ROI mask with the same voxel size and image dimension. Coordinate indexes were used to extract BOLD signals from each fMRI image, it was obtained one signal for each voxel within a region. Brain parcellation approach, which consisted of averaging the BOLD signal within the ROIs was performed using the Data Processing Assistant for Resting-State fMRI: Advanced Edition (DPARSFA from DPABI_V4.1_190725, http://rfmri.org/dpabi). Each ROI mask from the DMN template was used to extract the average BOLD signal using the *extract ROI time courses* option available in the toolbox.

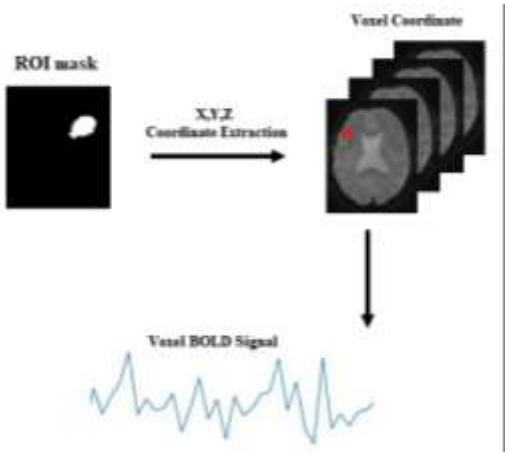

Figure 6. *Voxel-based approach implemented to extract BOLD time series.*

4.1.1.5.1.1.Segregation

Segregation metrics ALFF, fALFF, Multitaper and permutation entropy were performed according to equations 2, 3, 5 and 7. PE was computed for the ROI and voxel-based approach using an embedding delay of 1 to 2 and embedding dimension from 3 to 7 (Riedl, Müller, & Wessel, 2013; B. Wang et al., 2017). . Previous studies on EEG and fMRI data suggest a time delay of 1 or 2 and a dimension between 3 and 7 (Riedl et al., 2013; B. Wang et al., 2017). The selection of the dimension *m* and the delay *l* must satisfy the following condition $m! \leq N - (m - 1)l$ to avoid under sampling, where *N* is the length of the time series and *l* does not have much influence on the entropy of the time series (B. Wang et al., 2017). For *N=164*, a delay of 1 or 2 and dimensions 3 to 5 satisfy the previous condition.

BOLD signals obtained from the voxel-based approach were inputs for the segregation metrics algorithms, the voxel-based estimations were then averaged within each region. On the other hand, BOLD signals from the parcellation approach were directly inputs for each metric. The output of both approaches has the same dimension, which corresponds to estimations over ROIs of the network of interest.

4.1.1.5.1.2.Integration

Connectivity analysis was performed using graph theory, correlation matrices were obtained for the network of interest. A down-sampling step by a factor of 10 was required for the voxel-based approach given its high computational cost. The diagonal of the correlation matrix was set to zero, weights were kept and matrices were scaled to be within the 0 to 1 range. Graph metrics were computed using the Brain Connectivity Toolbox (https://github.com/aestrivex/bctpy/wiki), clustering coefficient as the average intensity of triangles around a node, node degree as the sum of weights of links connected to the node, characteristic path length as the average shortest path length in the network, the global efficiency as the average inverse shortest path length in the network. These graph metrics were computed following the search-based method proposed by (Ali Khazaee, Ebrahimzadeh, & Babajani-Feremi, 2015) to convert fully connected functional brain networks to sparse brain networks in which they reported accuracy of 100% for the classification of patients with AD using SVM and graph measures. The method consists of performing searches over the proportional threshold values in the range [0.05–0.7] with an increment step of 0.01. In this study it was used the proportional threshold function available in The Brain Connectivity Toolbox from [0.01 – 1] with an increment step of 0.01. The small propensity (ϕ), defined by equation 13, was computed for the fully connected matrix. Metrics were computed for symmetric and undirected matrixes.

$$\phi = 1 - \sqrt{\frac{\Delta_c^2 + \Delta_L^2}{2}} \quad (13)$$

Where,

$$\Delta_c = \frac{C_{latt} - C_{obs}}{C_{latt} - C_{rand}} \quad (14)$$

$$\Delta_L = \frac{L_{obs} - L_{rand}}{L_{latt} - L_{rand}} \quad (15)$$

Δ_C: the fractional deviation from the expected clustering coefficient of a random network.

Δ_L: the fractional deviation from the expected path length of a random network.

$latt$: lattice, $rand$: random, obs: observed.

Scripts for the computation of these metrics are available at: https://gitlab.com/neuro-tools/fmri/mlclassificationnd/-/tree/master/graph_measures/swp.

4.1.1.5.2. Dynamic Approach

The dynamic approach was implemented using the methodology proposed by (Bahrami et al., 2019). Figure 7 represents the methodology used for the representation of dynamic brain networks. The methodology requires BOLD signals from brain parcellations (ROIs), they are split into several segments using sliding window technique. The window selects a segment of the time series for each ROI, they are then used for computing the Pearson correlation coefficient between pairs which results in a correlation matrix for each shift of the window. The maximum number of dynamic networks is defined by equation 16, where *samples* is the number of data points of the time series, also known as the number of functional volumes, *wl* is the number of volumes that define the length of the window and *step* is the shift size, which defines how many volumes should move the window over the time series.

$$w = \frac{samples - wl}{step} \quad (16)$$

Once correlation matrices are generated, values from the lower triangular part of the matrix are taken and reshaped into a one-dimensional vector. Vectors are then used to create a 2D matrix called *vectorized dynamic correlation* with N x T rows and *(n x (n - 1))/2* columns, where N is the number of subjects, T is the number of windows of one subject and n is the number of ROIs.

The dimension of the vectorized dynamic correlation matrix is reduced using Principal Component Analysis (PCA), components explaining the 99% of the variability are stored as well as the two principal components. The components obtained from the previous step are embedded using Multidimensional Scaling (MDS) and t-Distributed Stochastic Neighbor Embedding (TSNE) algorithms available in *scikit learn* (Pedregosa et al., 2011).

The dynamic approach was designed to choose the values from the lower triangular part of the correlation matrices assuming that the correlation matrices are symmetric and undirected (Bahrami et al., 2019). The split of the BOLD signal into several segments on voxel BOLD signals required high computational resources. Therefore, the dynamic approach was just implemented for the parcellation analysis. Computational resources used for the computation of these metrics was provided by Google Collaboratory with the backend of Google Compute Engine, RAM of 12.72 Gb and 107.77 Gb of disk memory. Local resources included an intel core i5 processor 8^{th} generation, RAM of 8 Gb and 400 Gb of disk memory.

The embedded dimension and embedded delay for the estimation of the permutation entropy are chosen by the user to get the best representation of the dynamic of the system. In addition, the user can define the window size and the step from the dynamic approach. Scripts for the computation of these metrics are available at: https://gitlab.com/neuro-tools/fmri/mlclassificationnd/.

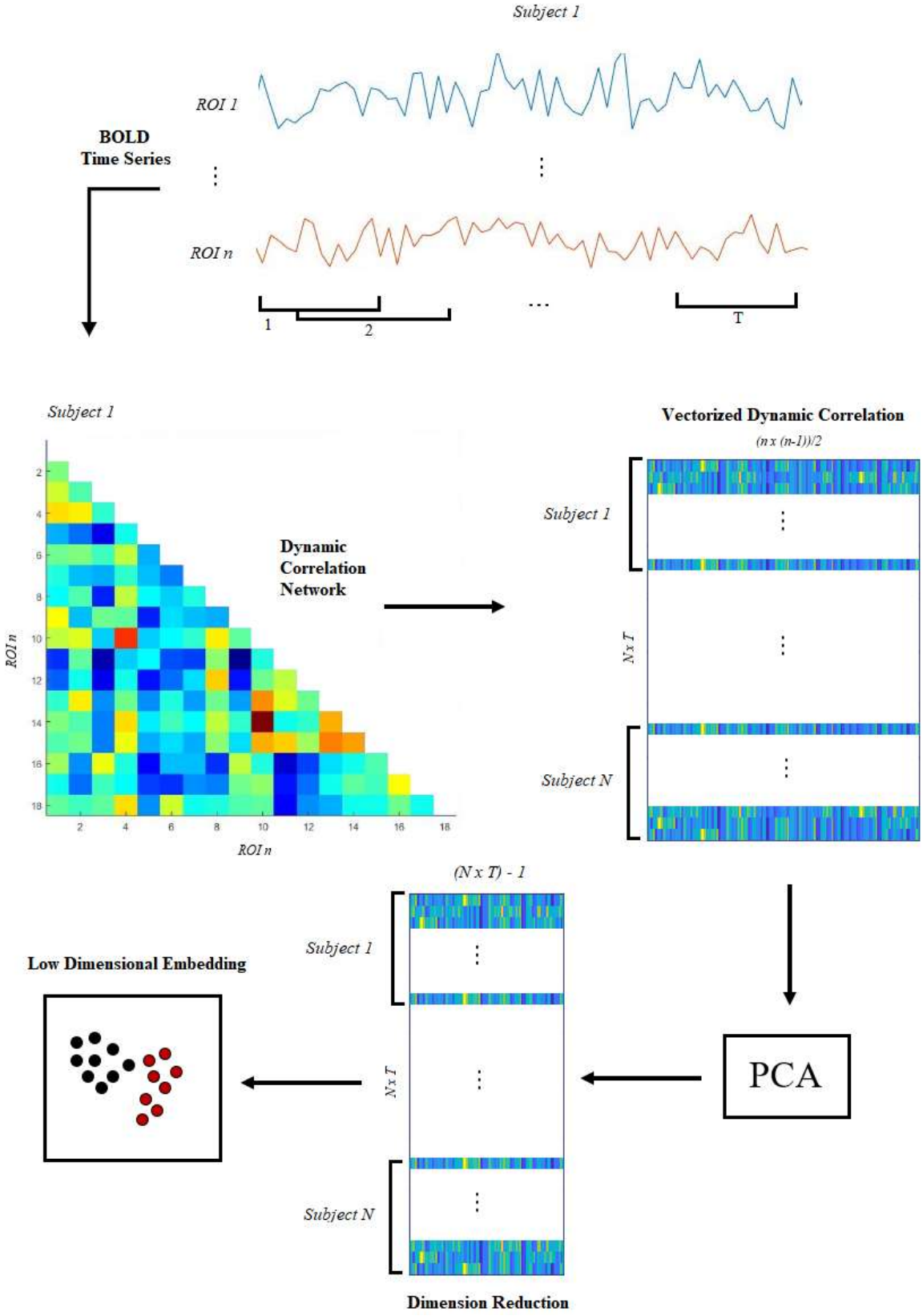

Figure 7. *Dynamic brain function analysis using low-dimensional manifolds (Bahrami et al., 2019).*

BOLD signals from the 18 DMN regions were used to generate dynamic networks using the sliding window technique with rectangular windows of 54 volumes, corresponding to 118.8 seconds and shift size from 16 to 27 volumes, that is equals to 30 to 50% of overlapping. For *n=18,* the dimension of the vectorized dynamic correlation for each window is *(n x (n - 1))/2 = 153.* Table 6 shows the dimensions of the dynamic vectorized network for the different shift sizes and the number of components that explained 99% of the variance after PCA. The components generated on the previous step were used for the low dimension embedding representation using the *T-distributed Stochastic Neighbor Embedding* (t-SNE) algorithm available at *scikit-learn*. t-SNE is a supervised non-linear algorithm to visualize high dimensional data, it converts Euclidean distances between data points into conditional probabilities that represent similarities, the t-SNE minimize the Kullback-Leibler divergence between the joint probabilities of the high-dimensional space and the low-dimensional space (Nl & Hinton, 2008).

4.1.2. Results

Figure 8 represents the 18 preprocessed BOLD signals from the DMN for one subject with AD using the ROI approach, the 219 metrics generated for this subject are shown in table 4. Figure 9 represents the 1328 down-sampled and preprocessed BOLD signals from the DMN for one subject with AD using the voxel-based approach, the 219 metrics generated for this subject are shown in table 5. The x axis represents the 160 time points of the signals and the y axis represents its amplitude. When comparing the approaches, all metrics had a similar result except for the node degree. In addition, the visual representation of the signals revealed that BOLD signals obtained from the voxel-based approach have more abrupt fluctuations than signals from the ROI approach.

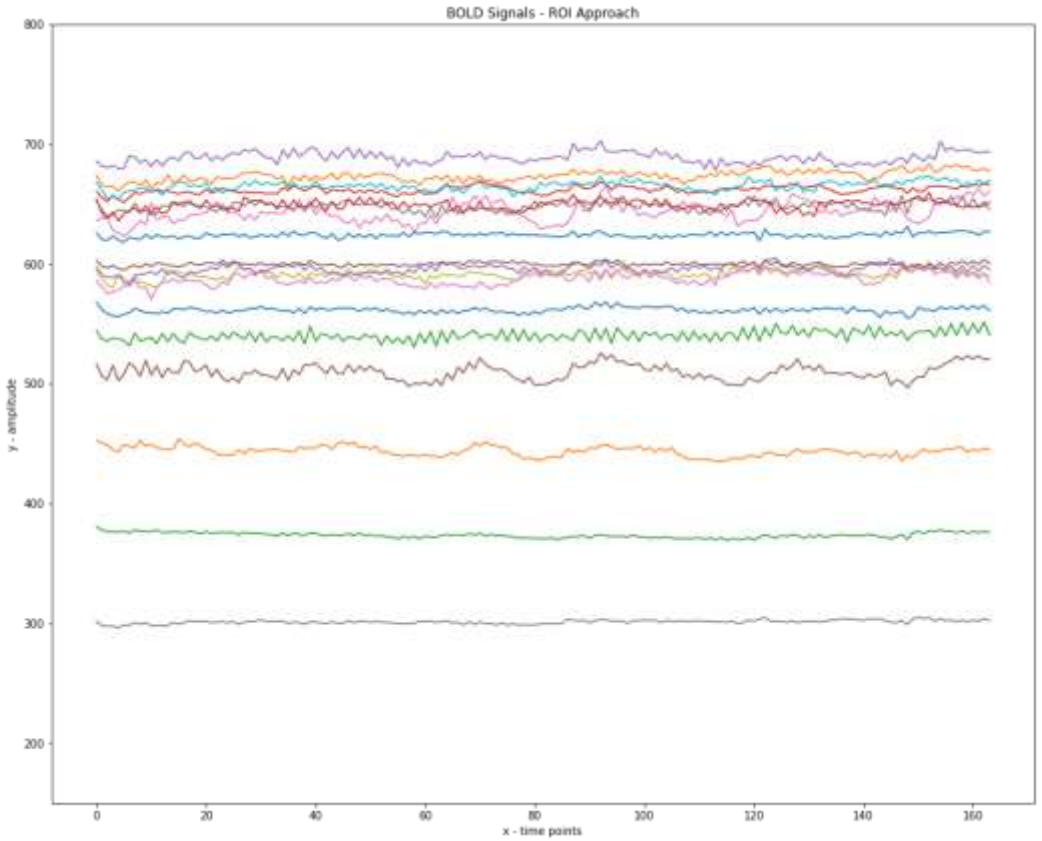

Figure 8. *Representation of the 18 preprocessed BOLD signals from the DMN for one subject with AD using the ROI approach.*

Table 4. *Quantification of brain function using segregation and integration metrics for the DMN BOLD signals for the ROI approach. 219 metrics are generated.*

Metric	1	2	3	4	5	6	7	8	9	10	11	12	13	14	15	16	17	18
ALFF-4	13.37	10.62	12.89	15.72	16.25	12.23	15.55	15.34	13.98	15.81	14.79	15.95	8.95	15.38	14.13	14.27	13.84	7.15
ALFF-5	36.18	29.02	34.94	42.50	44.52	33.87	41.82	41.68	37.77	42.60	39.99	43.28	24.34	41.28	37.93	38.48	37.51	19.26
ALFF	15.98	12.76	15.39	18.77	19.54	14.78	18.55	18.35	16.69	18.87	17.67	19.10	10.71	18.33	16.80	17.02	16.57	8.53
fALFF-4	0.19	0.19	0.19	0.19	0.19	0.19	0.20	0.19	0.19	0.19	0.19	0.19	0.19	0.19	0.19	0.20	0.19	0.19
fALFF-5	0.19	0.19	0.19	0.19	0.19	0.19	0.19	0.19	0.19	0.19	0.19	0.19	0.19	0.19	0.19	0.19	0.19	0.19
fALFF	0.48	0.48	0.48	0.48	0.48	0.48	0.48	0.47	0.47	0.47	0.47	0.47	0.48	0.47	0.47	0.48	0.48	0.47
MTM-4	9.27E-03	9.68E-03	9.41E-03	9.21E-03	9.42E-03	1.03E-02	1.04E-02	9.24E-03	9.21E-03	9.14E-03	9.26E-03	9.24E-03	9.40E-03	8.98E-03	9.21E-03	9.29E-03	9.19E-03	9.17E-03
MTM-5	9.91E-01	9.90E-01	9.91E-01	9.91E-01	9.91E-01	9.90E-01	9.90E-01	9.91E-01	9.91E-01	9.91E-01	9.91E-01	9.91E-01	9.91E-01	9.91E-01	9.91E-01	9.91E-01	9.91E-01	9.91E-01
MTM	1.00	1.00	1.00	1.00	1.00	1.00	1.00	1.00	1.00	1.00	1.00	1.00	1.00	1.00	1.00	1.00	1.00	1.00
CC	0.56	0.36	0.52	0.58	0.56	0.51	0.51	0.56	0.54	0.55	0.48	0.56	0.38	0.51	0.52	0.53	0.53	0.57
ND	10.36	5.81	9.35	10.92	10.19	9.29	8.98	10.26	10.01	10.06	8.65	10.51	6.20	9.12	8.77	9.53	9.92	10.52
PE	0.93	0.97	0.86	0.97	0.97	0.96	0.95	0.92	0.96	0.95	0.95	0.95	0.96	0.93	0.93	0.92	0.94	0.96

PL: 1.01E+00 **GE:**9.97E-01 **SWP:**0.49

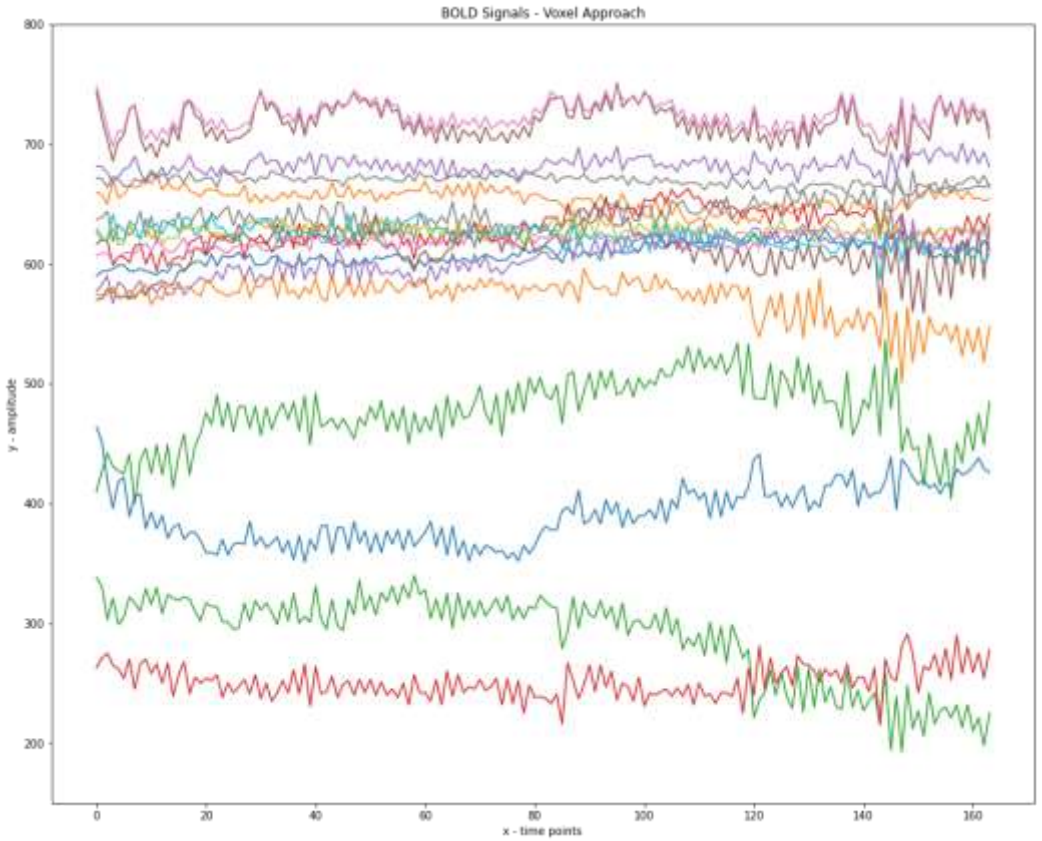

Figure 9. *Representation of 18 from the 1328 preprocessed BOLD signals from the DMN for one subject with AD using the voxel-based approach.*

Table 5. *Quantification of brain function using segregation and integration metrics for the DMN BOLD signals for the voxel-based approach. 219 metrics are generated.*

Metric	1	2	3	4	5	6	7	8	9	10	11	12	13	14	15	16	17	18
ALFF-4	13.44	12.36	11.83	15.74	16.13	13.38	15.39	15.40	14.16	15.79	14.98	16.25	8.97	15.32	14.05	14.22	13.88	8.15
ALFF-5	36.24	33.53	32.44	42.55	44.20	37.30	41.55	41.78	38.17	42.56	40.44	44.19	24.34	41.06	37.81	38.28	37.39	21.86
ALFF	16.03	14.81	14.19	18.79	19.39	16.27	18.40	18.41	16.89	18.85	17.89	19.49	10.73	18.24	16.73	16.95	16.58	9.71
fALFF-4	0.20	0.20	0.20	0.20	0.20	0.20	0.20	0.20	0.20	0.20	0.20	0.20	0.19	0.20	0.20	0.20	0.20	0.19
fALFF-5	0.19	0.20	0.19	0.19	0.20	0.20	0.19	0.19	0.19	0.19	0.19	0.19	0.19	0.19	0.19	0.19	0.19	0.18
fALFF	0.47	0.48	0.47	0.48	0.48	0.48	0.47	0.47	0.47	0.47	0.47	0.47	0.46	0.47	0.47	0.48	0.48	0.45
MTM-4	0,03	0,03	0,03	0,03	0,03	0,03	0,05	0,03	0,03	0,03	0,03	0,03	0,04	0,03	0,03	0,03	0,03	0,05
MTM-5	0.97	0.97	0.97	0.97	0.97	0.97	0.95	0.97	0.97	0.97	0.97	0.97	0.96	0.97	0.97	0.97	0.97	0.95
MTM	1.00	1.00	1.00	1.00	1.00	1.00	1.00	1.00	1.00	1.00	1.00	1.00	1.00	1.00	1.00	1.00	1.00	1.00
CC	0.49	0.49	0.49	0.51	0.51	0.52	0.50	0.50	0.49	0.50	0.49	0.50	0.48	0.50	0.50	0.49	0.50	0.49
ND	670.15	666.83	672.23	699.16	704.66	711.98	684.17	681.36	660.36	684.06	670.60	688.72	656.51	677.42	687.17	673.04	685.48	672.36
PE	0,95	0,96	0,92	0,95	0,96	0,96	0,95	0,94	0,93	0,95	0,94	0,93	0,95	0,95	0,94	0,96	0,94	0,95

PL:1.01E+00 **GE:**1.01E+00 **SWP:**0.51

Brain function estimations for a proportional threshold of 0.81 obtained by the integration approach are represented in figures 10 to 12, except for the SWP which was computed on a fully connected network. Static approach estimations are represented in figures 13 to 22. This visual representation of the metrics obtained by the developed algorithms was only made for the ROI approach. Boxplots for the voxel approach are available in the supplementary material, appendix 2.

There is a greater variability of the clustering coefficient in the CN group compared to AD, however there are larger outliers in the AD group compared to CN (figure 10). Figure 11 shows big variability in both groups, a slightly higher median node degree is observed on regions 1, 2, 4, 5, 8, 9, 11, 12, 14, 16, 17 and 18 in the CN group compared to AD. Slightly lower median node degree is observed on the Right Superior Frontal Gyrus, Right Angular Gyrus, Left and Right Thalamus, Left Middle Occipital Gyrus and Precuneus in the AD group compared to CN.

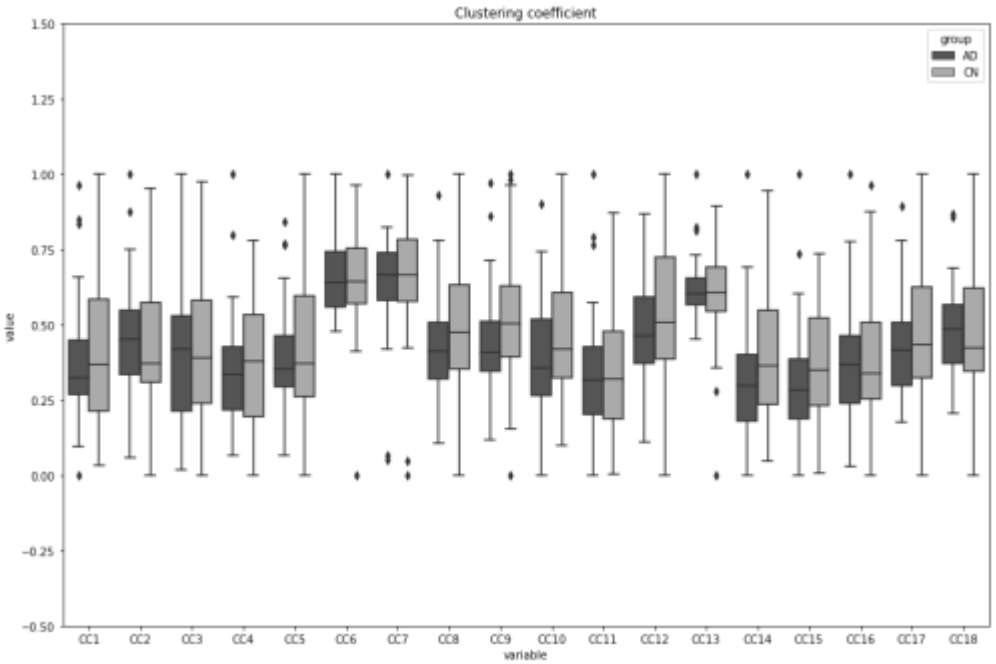

Figure 10. *Clustering coefficient for AD and CN subjects, proportional threshold of 0.81. CC1 notation stands for the clustering coefficient in region 1.*

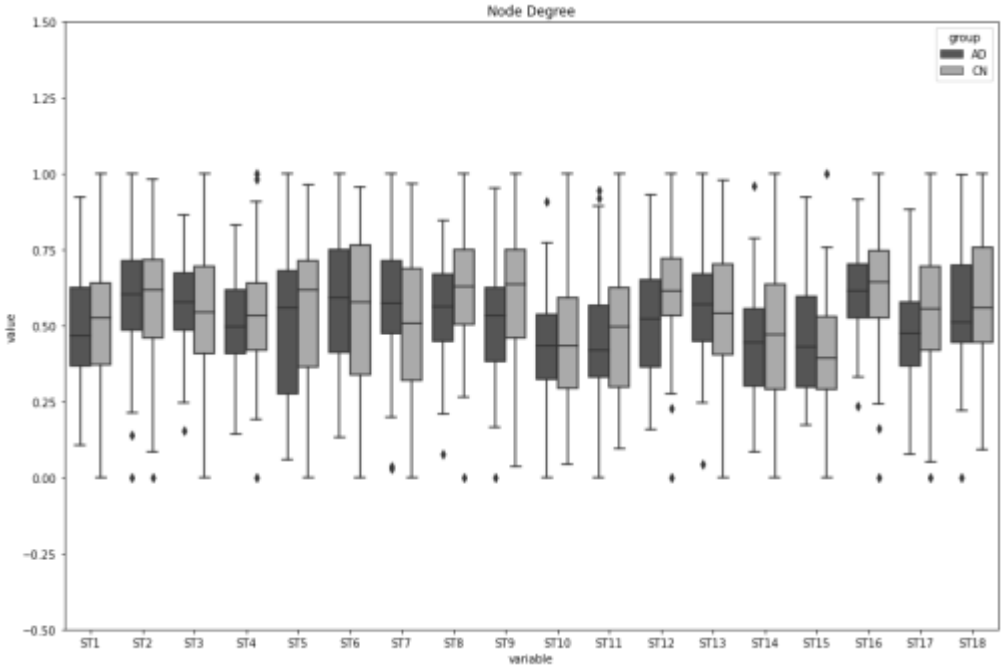

Figure 11. *Node Degree for AD and CN subjects, proportional threshold of 0.81. ST stands for "strength" given that the computation is performed on a weighted network. ST1 notation stands for "strength" in region 1.*

Bigger variability in PL and GE is observed in CN compared to AD, SWP in CN is slightly bigger in CN compared to AD (figure 12).

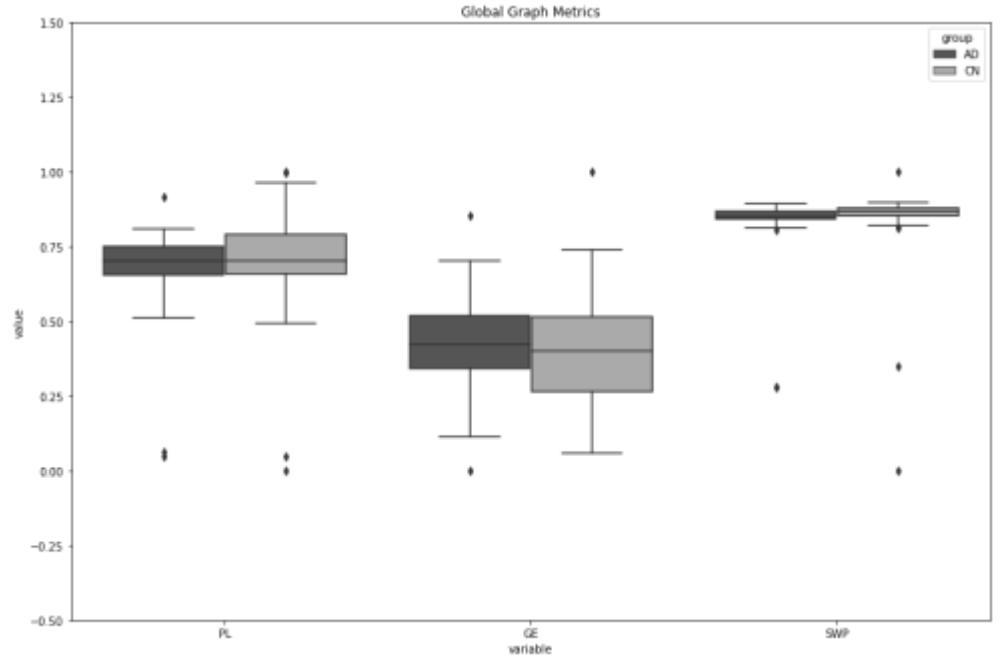

Figure 12. *Global connectivity properties of the DMN in AD and CN subjects. Characteristic path length (PL) and global efficiency (GE) property of the network with proportional threshold of 0.81. The small world propensity of the fully connected network is denoted as SWP.*

Figure 13 shows a slightly higher median ALFF in the slow-4 band on the Left Parahippocampal Gyrus and Right Parahippocampal Gyrus in AD compared to CN. Slightly higher ALFF in the slow-4 band on the Right Superior Frontal Gyrus, Posterior Cingulate Cortex, Precuneus, Midcingulate Cortex, Left Retrosplenial Cortex, Posterior Cingulate Cortex, Left Middle Frontal Gyrus, Precuneus, Right Superior Frontal Gyrus, Middle Frontal Gyrus and Right Angular Gyrus, Middle Occipital Gyrus in CN compared to AD.

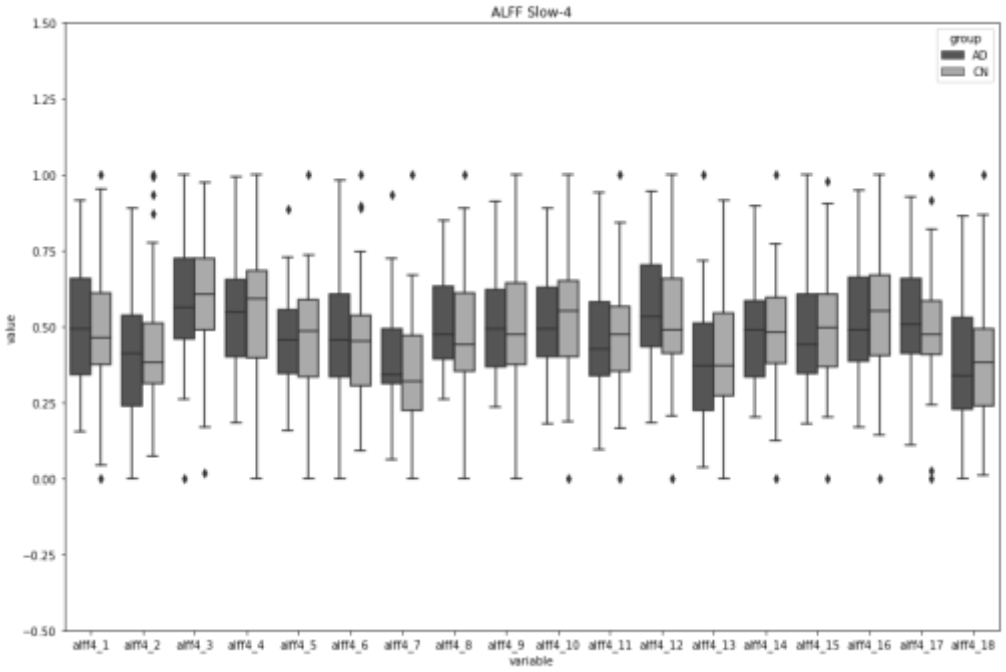

Figure 13. *ALFF in the slow-4 band for AD and CN subjects in the 18 regions of the DMN. alff4_1 notation stands for the ALFF metric, slow-4 band in region 1.*

Figure 14 shows a slightly higher median ALFF in the slow-5 band on the Left Retrosplenial Cortex, Posterior Cingulate Cortex, Left Middle Frontal Gyrus, Precuneus, Right Superior Frontal Gyrus, Middle Frontal Gyrus, Right Angular Gyrus, Middle Occipital Gyrus in CN compared to AD. Previously mentioned regions showed a slightly higher median ALFF in the 0.01-0.1 Hz frequency band in CN compared to AD (figure 15).

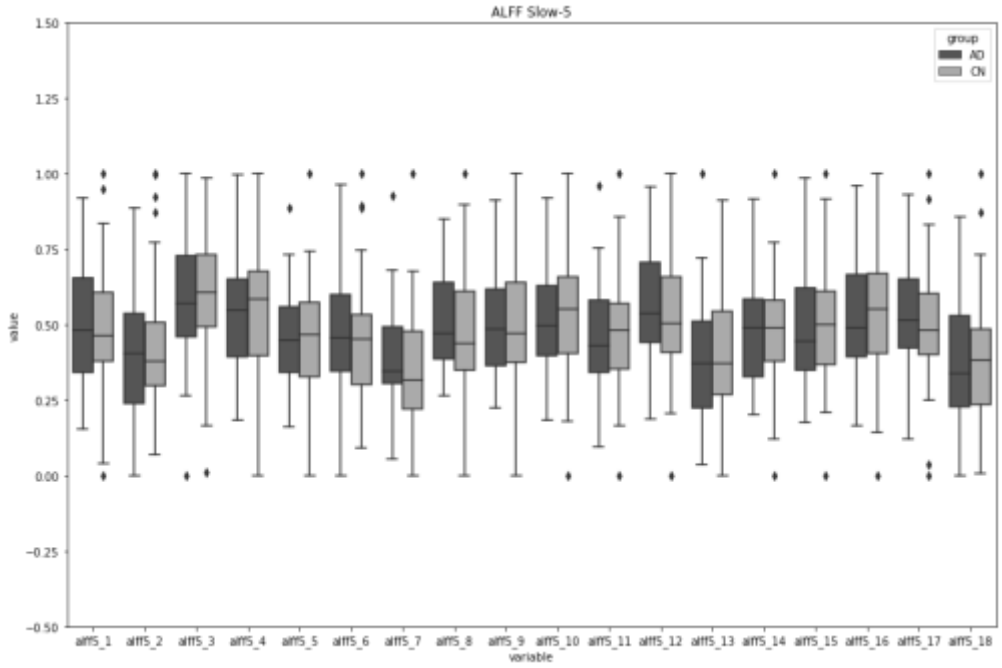

Figure 14. *ALFF in the slow-5 band for AD and CN subjects in the 18 regions of the DMN. alff5_1 notation stands for the ALFF metric, slow-5 band in region 1.*

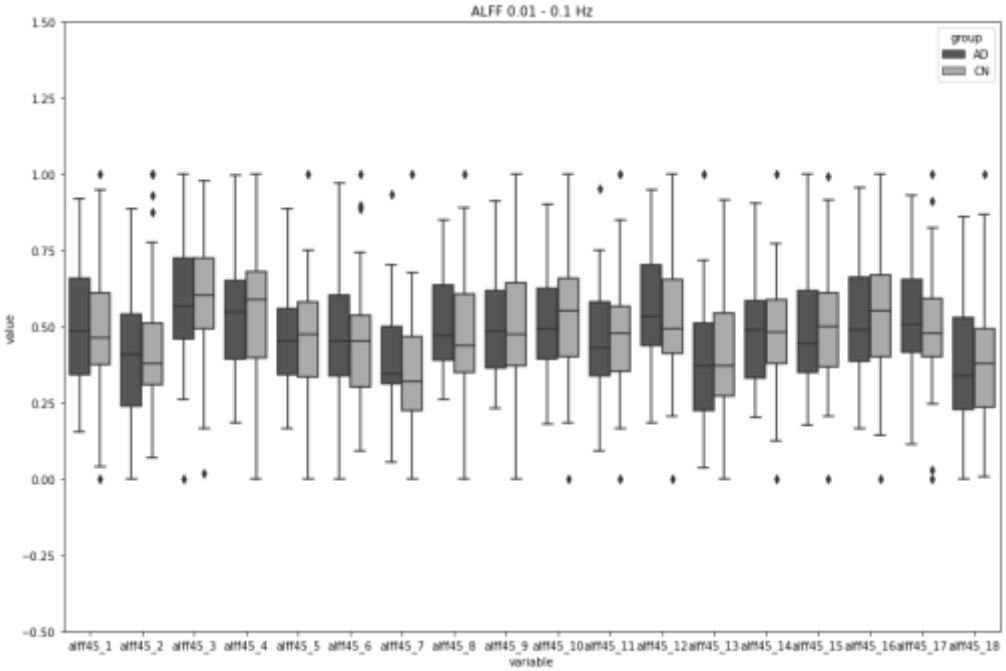

Figure 15. *ALFF in the 0.01 to 0.1 Hz frequency band for AD and CN subjects in the 18 regions of the DMN. alff45_1 notation stands for the ALFF metric, 0.01-0.1Hz band in region 1.*

Bigger variability in the fALFF slow-4 band is observed in CN compared to AD, small differences between medians of the two groups are shown in figure 16. On the other hand, slightly higher median fALFF in the slow-5 band is observed in all regions in AD compared to CN (figure 17).

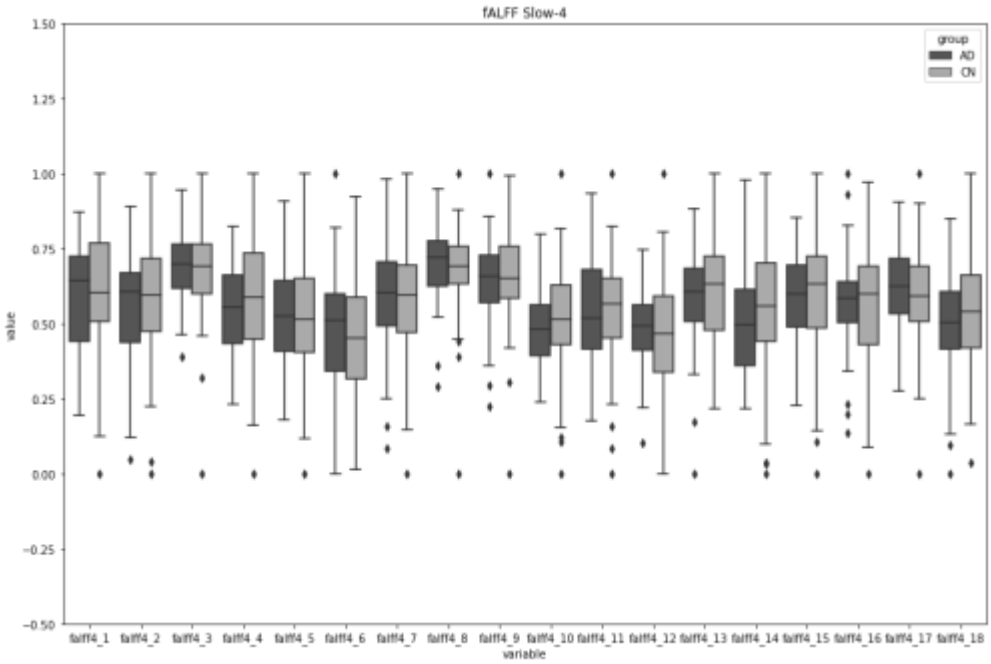

Figure 16. *fALFF in the slow-4 band for AD and CN subjects in the 18 regions of the DMN. falff4_1 notation stands for the fALFF metric, slow-4 band in region 1.*

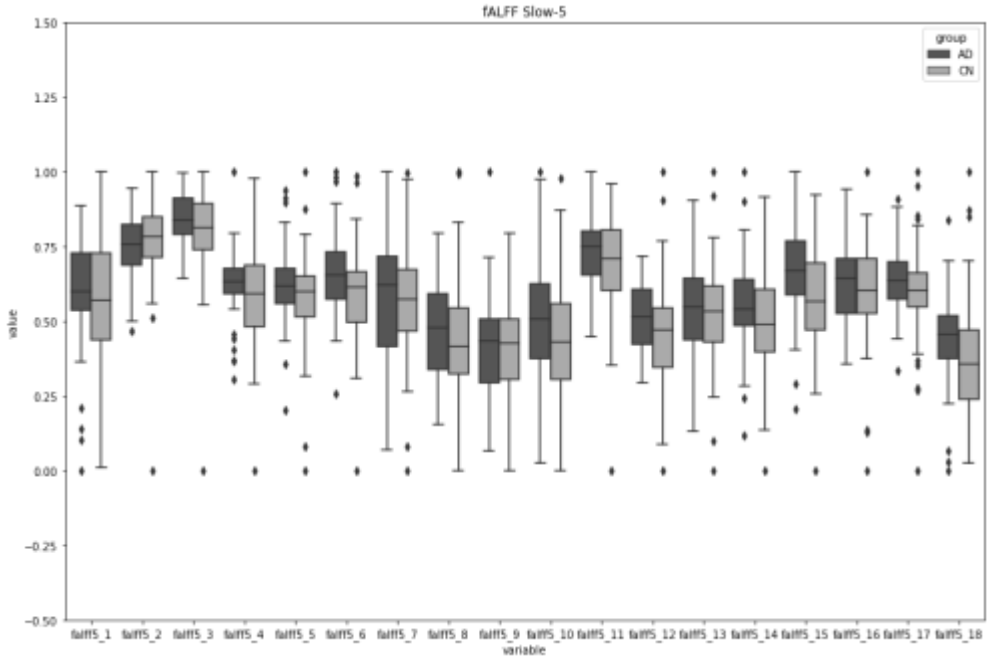

Figure 17. *fALFF in the slow-5 band for AD and CN subjects in the 18 regions of the DMN. falff5_1 notation stands for the fALFF metric, slow-5 band in region 1.*

Slightly higher median fALFF in the 0.01 to 0.1 Hz band is observed in the Midcingulate Cortex, Right Angular Gyrus, Right Parahippocampal Gyrus and Right Angular Gyrus, Middle Occipital Gyrus in AD compared to CN. On the other hand, slightly higher median fALFF in the 0.01 to 0.1 Hz band is observed in the Medial Prefrontal Cortex, Left Angular Gyrus, Left Hippocampus, Right Hippocampus in CN compared to AD.

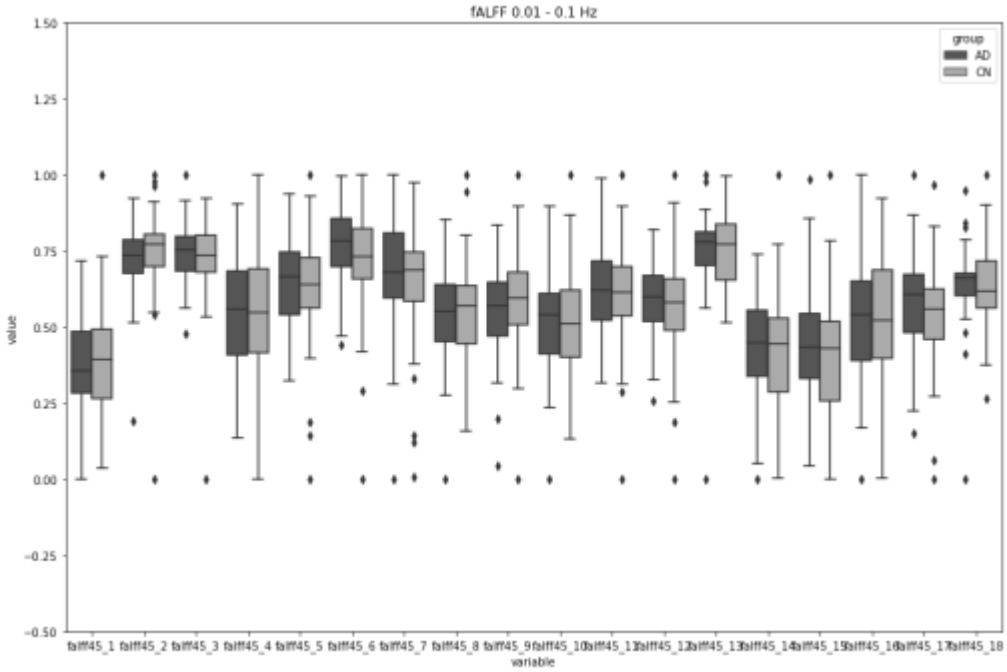

Figure 18. *fALFF in the 0.01 to 0.1 Hz frequency band for AD and CN subjects in the 18 regions of the DMN. falff45_1 notation stands for the fALFF metric, 0.01-0.1Hz band in region 1.*

Slightly higher median Multitaper in the slow-4 band is observed in the Left and Right Thalamus, Left Retrosplenial Cortex, Posterior Cingulate Cortex, Left Middle Frontal Gyrus, Left Parahippocampal Gyrus, Right Superior Frontal Gyrus, Middle Frontal Gyrus in CN compared to AD (figure 19). Non-relevant differences are observed for median Multitaper in the slow-5 (figure 20).

Slightly higher median Multitaper in the 0.01 to 0.1 Hz band is observed in the Left Hippocampus, Left Parahippocampal Gyrus, Left Middle Occipital Gyrus, Right Retrosplenial Cortex, Posterior

Cingulate Cortex, Right Superior Frontal Gyrus, Middle Frontal Gyrus, Right Angular Gyrus, Middle Occipital Gyrus in AD compared to CN. Slightly higher median Multitaper in the 0.01 to 0.1 Hz band is observed in the Right Superior Frontal Gyrus and Posterior Cingulate Cortex, Precuneus in CN compared to AD.

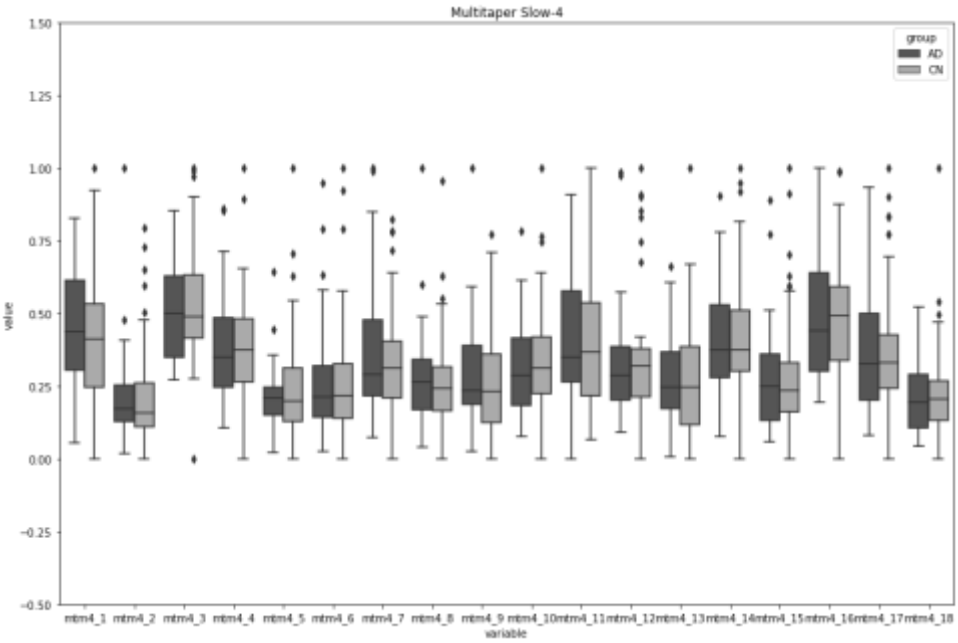

Figure 19*. Multitaper in the slow-4 band for AD and CN subjects in the 18 regions of the DMN. mtm4_1 notation stands for the multitaper metric, slow-4 band in region 1.*

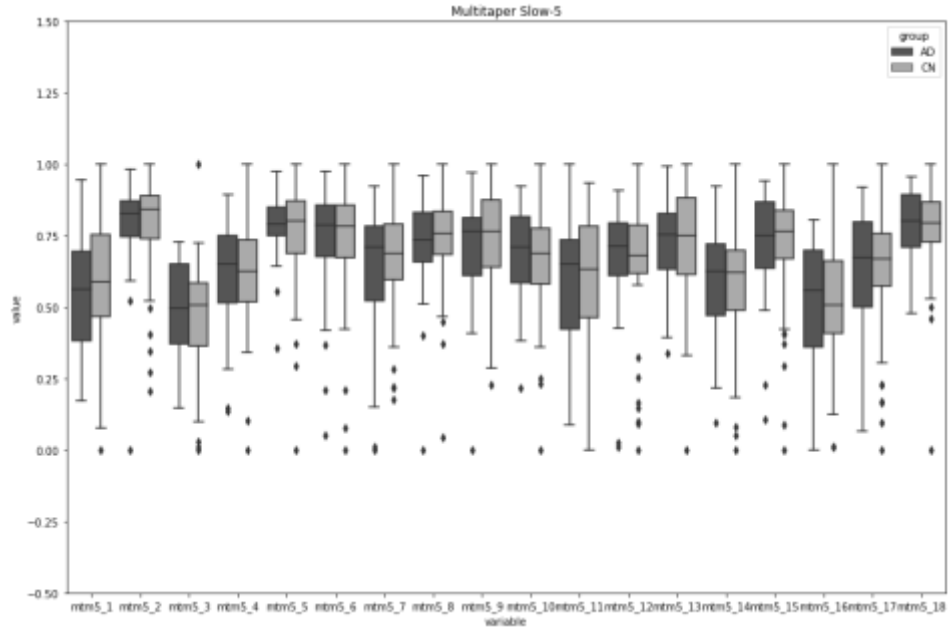

Figure 20. *Multitaper in the slow-5 band for AD and CN subjects in the 18 regions of the DMN. mtm5_1 notation stands for the multitaper metric, slow-5 band in region 1.*

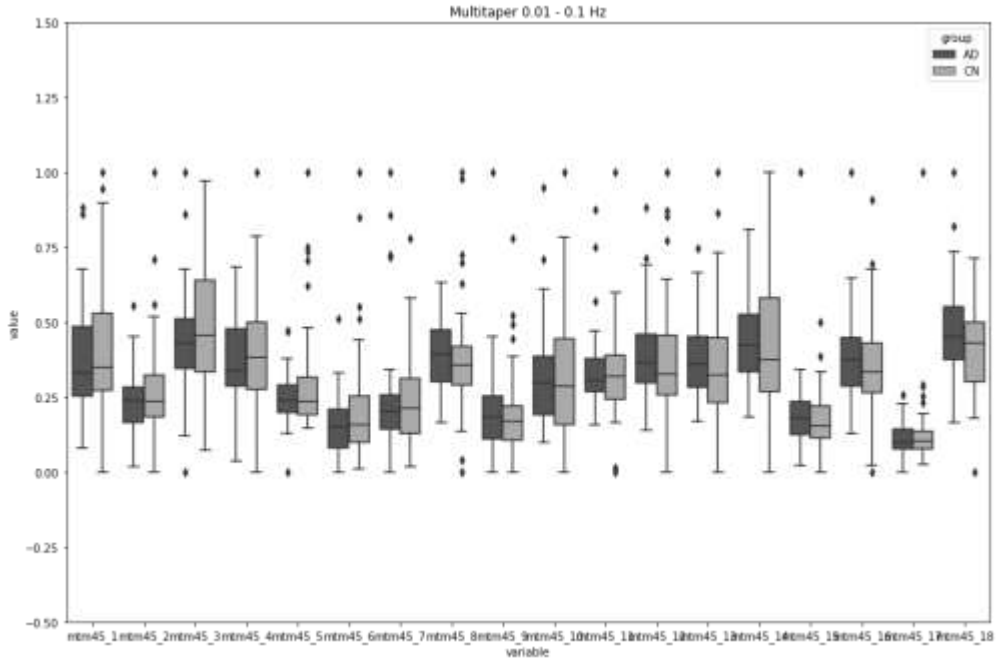

Figure 21. *Multitaper in the 0.01 to 0.1 Hz frequency band for AD and CN subjects in the 18 regions of the DMN. mtm45_1 notation stands for the multitaper metric, 0.01-0.1Hz band in region 1.*

Slightly higher median Permutation Entropy in the 0.01 to 0.1 Hz band is observed in all regions except for the Midcingulate Cortex, Right Angular Gyrus, Left Hippocampus, Right Hippocampus, Left Middle Occipital Gyrus in AD compared to CN.

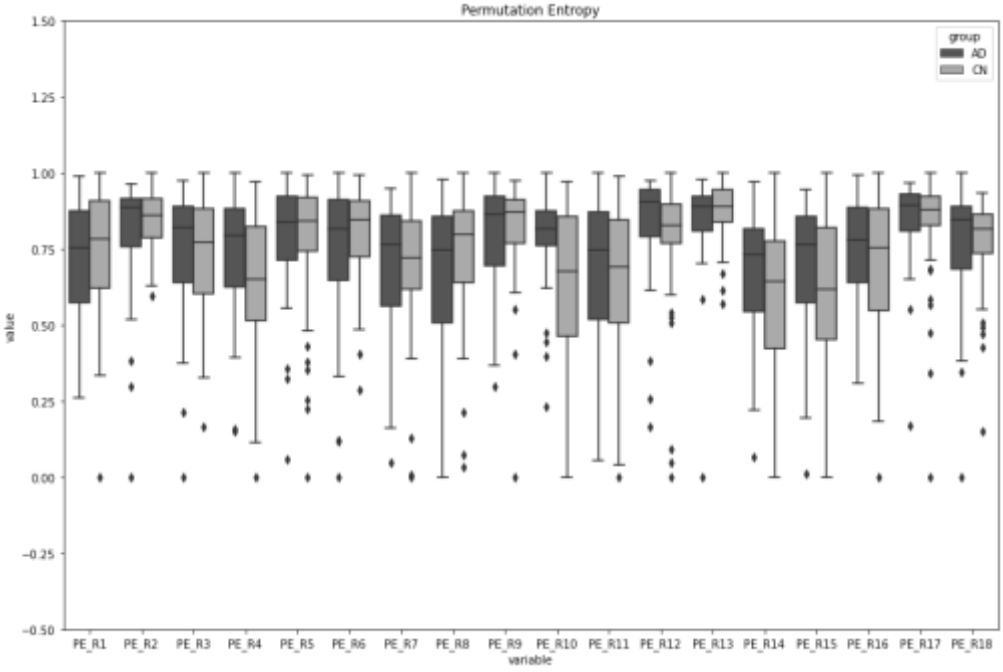

Figure 22. *Permutation entropy for AD and CN subjects in the 18 regions of the DMN. Embedding dimension of 4 and embedding delay of 2. PE_R1 notation stands for the permutation entropy metric, 0.01-0.1Hz band in region 1.*

Figures 23 to 25 shows the embedded dynamic brain networks for AD and CN subjects using two methods of representation: the two principal components and all components that explain the 99% of the variance. The pattern of the two top principal components embedded networks differs from the pattern of the components that explain 99% of variability. However, in both methods the pattern of embedded networks has a bigger separation between data points in CN than in AD. Embedded networks from CN subjects showed more variability in the spatial distribution than the pattern of AD subjects. No big differences were found between the embedded networks as well as the few differences found using the other segregation and integration methods implemented in this study. As mentioned before, this analysis was performed only for the ROIs approach given the high computational resources required by the voxel-based approach.

Table 6. *Dynamic network generated using the sliding window technique, rectangular window of 54 volumes and different shift sizes from 16 to 27 volumes.*

Shift Size	**Dynamic Networks AD:CN**	**Components 99% AD:CN**
16	280:406	90:100
17	240:348	86:98
18	240:348	88:98
19	240:348	89:98
20	240:348	90:99
21	200:290	85:96
22	200:290	86:97
23	200:290	87:97
24	200:290	88:98
25	160:232	81:94
26	160:232	82:94
27	160:232	82:95

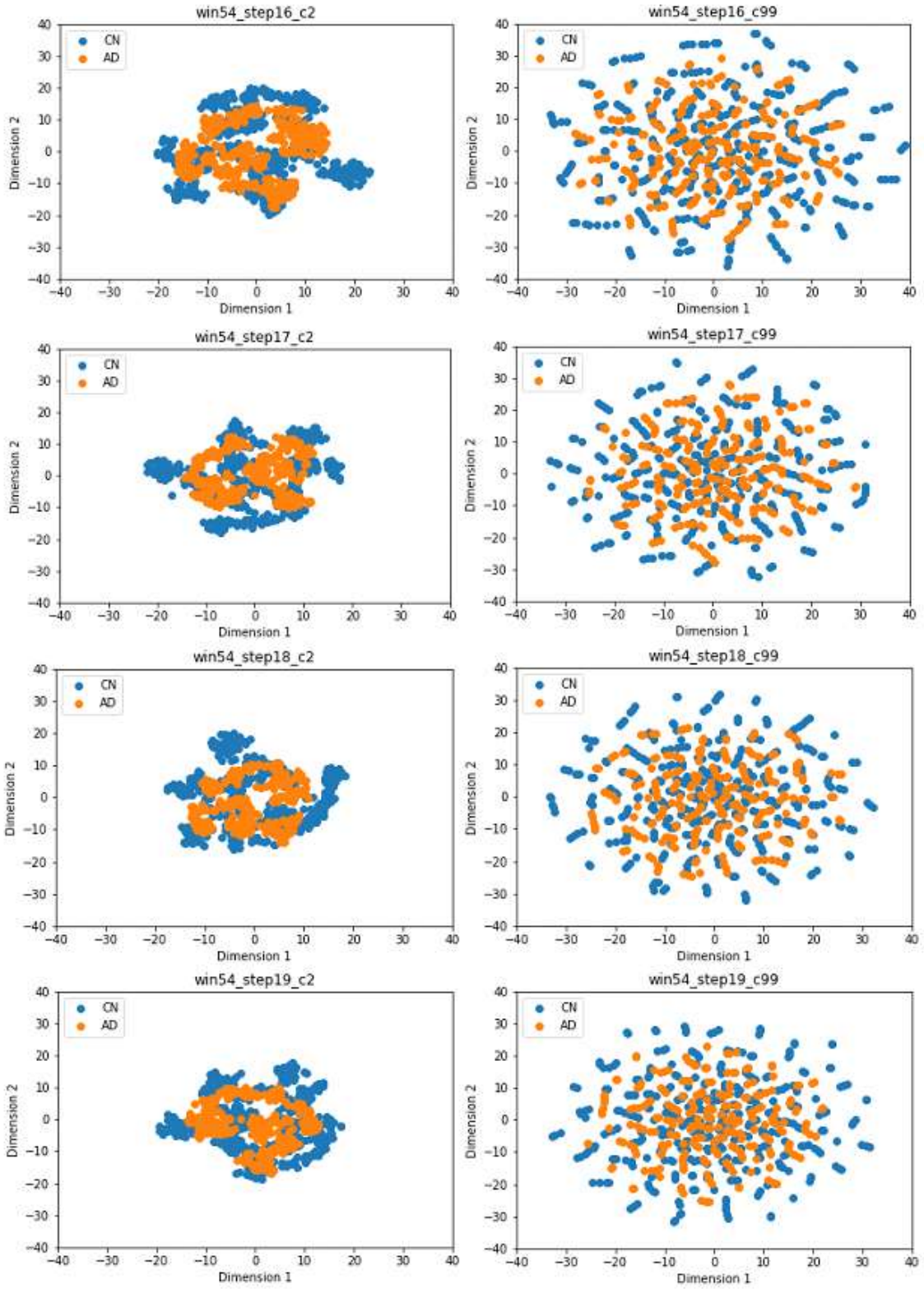

Figure 23. *Embedded dynamic brain networks for AD and CN subjects with rectangular windows of 54 volumes and shift size from 16 to 19 volumes.*

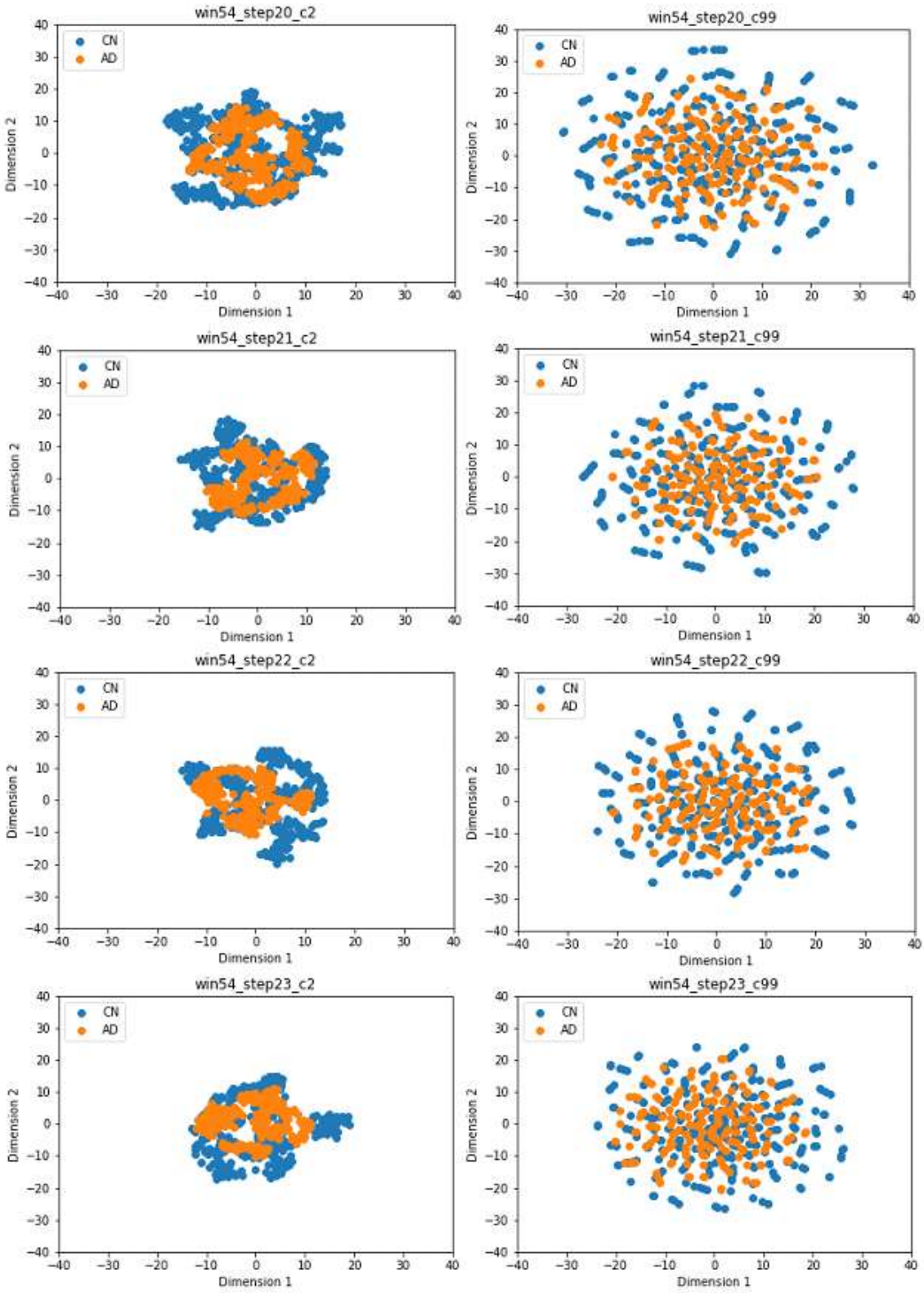

Figure 24. *Embedded dynamic brain networks for AD and CN subjects with rectangular windows of 54 volumes and shift size from 20 to 23 volumes.*

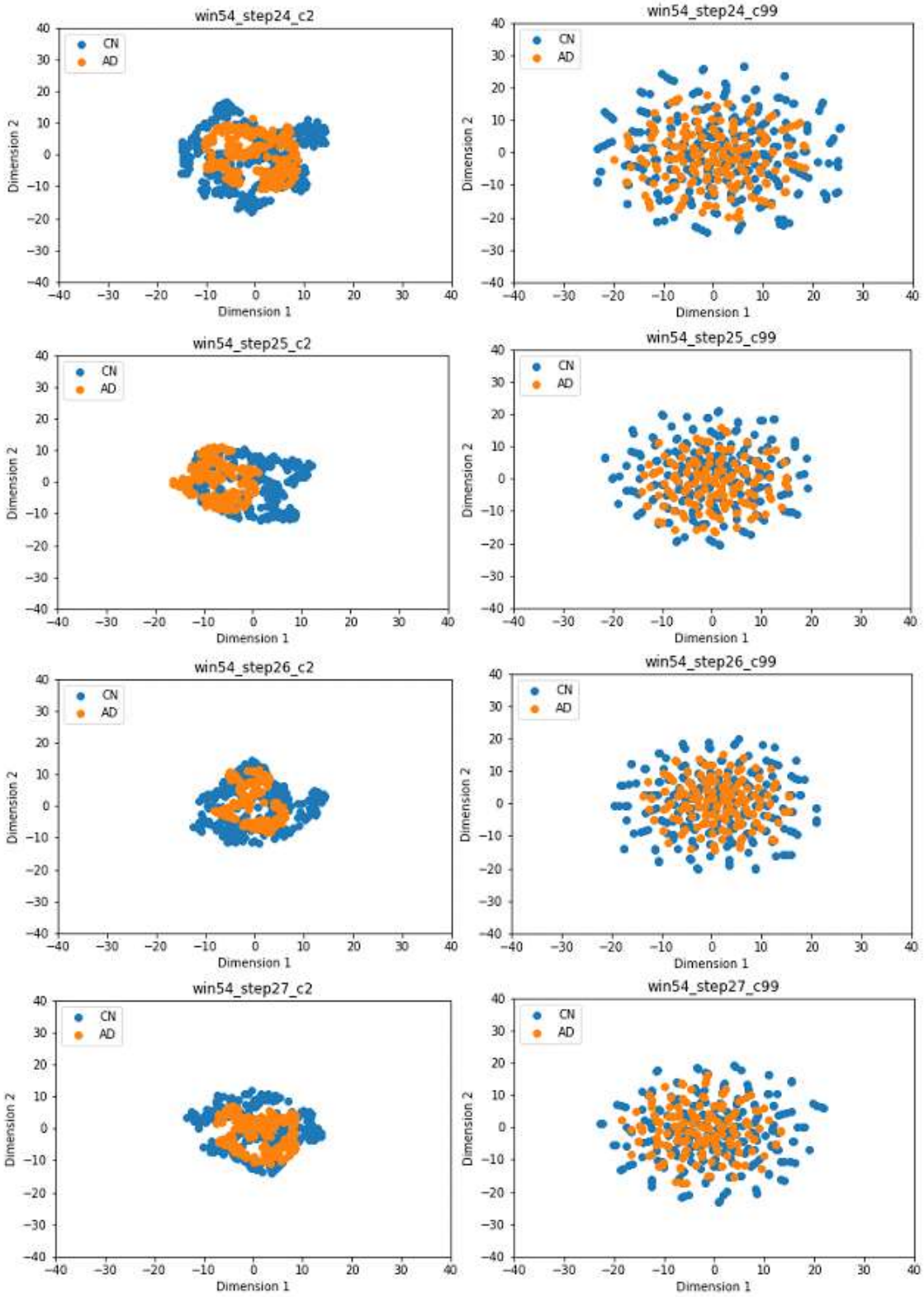

Figure 25. *Embedded dynamic brain networks for AD and CN subjects with rectangular windows of 54 volumes and shift size from 24 to 27 volumes.*

4.1.3. Discussion and Conclusions

Metrics described in the current section have been previously used for the analysis of neural signals. In this study, the algorithms developed for its computation were designed to be used on BOLD signals derived from the ROIs approach as well as the voxel-based approach. The need to test the voxel-based approach relies on its potential for developing tools that would allow the visualization of activation maps for metrics that are not included in neuroimaging packages.

The computation of the segregation metrics does not require highly computational resources for both ROIs and voxel-based approaches, the computation of the PE requires more computational resources for big embedding dimensions as well as big embedding delays. It is important to highlight that the embedding parameters for the estimation of PE should be selected carefully to avoid under sampling due to the short length of BOLD signals (B. Wang et al., 2017). On the other hand, the computation of graph metrics for voxel-based signals requires high computational resources.

The estimations of global connectivity metrics, PL and GE described a higher differential pattern between AD and CN than the SWP (figure 12). Compared to ALFF, a higher differential pattern between the groups is described by fALFF in all frequency bands (figures 16 to 18). However, more atypical values are presented in this metric, as well as in the Multitaper estimation (figures 20 to 21). Permutation entropy on the Posterior Cingulate Cortex, Precuneus and the Left Retrosplenial Cortex, Posterior Cingulate Cortex showed a higher differential pattern between the groups than the other metrics, a bigger entropy was observed in AD compared to CN on those regions.

The dynamic analysis approach increases the amount of data, given the generation of several segments for each BOLD signal and the computation of a connectivity matrix. The performance

of this approach is highly dependent on the number of subjects, the data points of the signals, the size of the window, the overlapping factor and the number of regions of interest. Therefore, the dynamic analysis was not performed in this study for the voxel-based approach.

Low dimensional manifolds have been used to map the dynamic of the brain function. The methodology used in this study has been used to map working memory task-based networks in a population of young and older adults. The results of this study showed a clear separation between the dynamic network during the execution of a 2-back working memory task, with high cognitive demand, and the dynamic network of the rest condition (Bahrami et al., 2019). An overlapping pattern between the 1-back working memory task and the rest condition was also reported (Bahrami et al., 2019). It suggested that the closer the cognitive demand is between condition; it will be more difficult to find a clear separation between the embedded dynamic networks. The results of our study show that the dynamic brain networks between AD and CN are not clearly distinguishable, which suggest that the differences between them are yet small at rest. The capacity of this approach to show the dynamic pattern of brain networks would be useful for longitudinal tracking in different networks not only to follow the changes related to the severity of the disease but to identify changes from a clinical healthy brain to a disease one.

5. Classification Capacity of Brain Function Features

5.1. Objective 2: Evaluate the classification potential of the obtained features from the brain networks using machine learning techniques.

Once the metrics for the estimation of brain function are defined, it is necessary to evaluate how well do those metrics discriminate between cognitively normal subjects and individuals with neurodegenerative diseases. For this purpose, statistical and machine learning approaches were used. The statistical analysis using the non-parametric two-sample t-test and the effect size was used to evaluate the performance of the metrics, the machine learning approach was used for data cleaning and feature selection using thresholds for the effect size and mutual information to select the most discriminant features.

5.1.1. Materials and Methods

The discriminative power of the brain function features from the static approach was tested using a dataset from a data-sharing initiative. Segregation and integration metrics were computed for the ROIs and voxel-based approaches. A statistical analysis was performed before the implementation of machine learning techniques to identify the metrics with more discriminative power. Machine learning techniques commonly used in feature selection often require a previous dimensionality reduction step to decrease the dimensionality of the dataset. Details of the rs-fMRI dataset, preprocessing steps, DMN template and statistical analysis are described in the following sections: Figure 26 shows a brief introduction of the methodology implemented in this section.

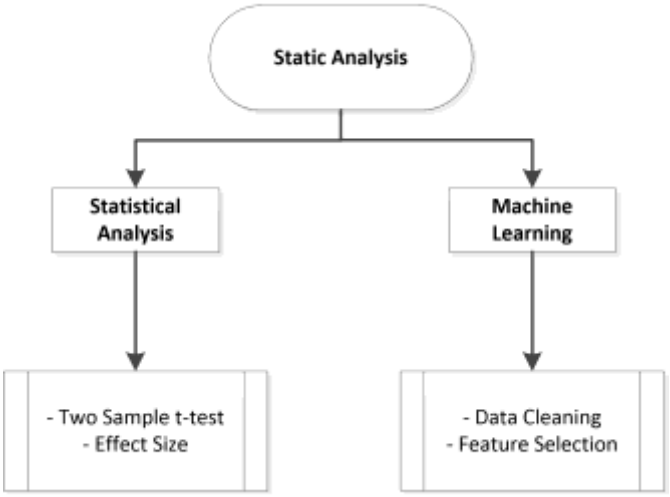

Figure 26. *flowchart representing a brief introduction to the methodology implemented in objective 2.*

5.1.1.1.Statistical Comparison

Statistical analysis was performed using a non-parametric two-sample T-test released by (Glerean et al., 2016), code is available at https://github.com/eglerean/hfASDmodules/blob/master/ABIDE/bramila_ttest2_np.m. The test does not rely on the t-distribution, an alternative null distribution is estimated using permutation of group labels without assumption of same distribution for each data-point. All p values were corrected using false discovery rate (FDR) (Benjamini & Hochberg, 1995) and the effect size was calculated with the Hedges'g, using The Measures of Effect Size (MES) Toolbox (Hentschke & Stüttgen, 2011). To avoid any possible effect of the age differences, all measures were regressed by age to remove its effect before the statistical comparison analysis. Statistically significant results after the non-parametric two-sample T-test and the MES values above ±0.5 are written with bold font.

5.1.1.2. Machine Learning Techniques

ALFF, fALFF and Multitaper metrics on the slow-4, slow-5 and the [0.01-0.1] Hz frequency range; the SWP, CC, DG, PL and GE on the [0.01-0.1] Hz frequency range were used as input features. The computation of all measures over the 18 regions of the DMN described by figure 5 generated 219 features. As mentioned before, graph metrics were converted from fully connected functional brain networks to sparse brain networks using a proportional threshold function from [0.01 – 1] with an increment step of 0.01.

5.1.1.2.1. Data Cleaning

Preprocessed data from subjects described on table 2 was used. Data was inspected to detect atypical values, in addition, a dimensionality reduction step was performed previous feature selection to reduce the 219 features into a smaller and meaningful dataset. PCA was performed to keep the components that explained the variance in the range of [80 - 99] % with step of 1%.

5.1.1.2.2. Feature Selection

The union of the Mutual information (MI) and the effect size (ES) was used for the selection of the most discriminant features. MI was used to measure the dependency between the features and the label, it computes the probability distribution of the features using non-parametric methods based on entropy estimation from k-nearest neighbors distances (Kraskov, Stoegbauer, & Grassberger, 2003), the computation was performed using *scikit-learn* mutual information for classification (*mutual_info_classif*). ES was used to measure the magnitude of the difference between features of the two targets, it was computed using cohen's *d* approach, which is defined as $d = \frac{U1 - U2}{S}$, where $U1$ and $U2$ are the mean of the first and the second sample, S is the pooled standard deviation.

5.1.2. Results

The statistical analysis for the static approach is reported for both the ROIs and voxel-based approach.

5.1.2.1.Static Approach

The static analysis from the segregation and integration measures are detailed in the following sections.

5.1.2.1.1. Segregation Measures

Spectral metrics, ALFF, fALFF and Multitaper were computed for three frequency bands slow 4, slow 5 and for the 0.01 to 0.1 Hz frequency range. Information theory metric, Permutation Entropy was computed for the 0.01 to 0.1 Hz frequency range.

5.1.2.1.1.1. ALFF

Statistical comparison between AD and CN subjects did not show differences either corrected (table 6) or uncorrected (table S1, supplementary material appendix 3) p-values. Low MES values were found for the three frequency bands, the bigger value -0.23 was found on region 7 (Left and Right Thalamus) in the slow-4 and 0.01-0.1 Hz bands, ROI approach (table 7).

Table 7. *Permutation t-test between CN and AD subjects. The test was performed for ALFF values computed with the ROI and voxel-based approach. Non-significant differences were found.*

	ROI Corrected p values						**Voxel-based Corrected p values**					
ROI	**Slow 4**		**Slow 5**		**0.01 – 0.1 Hz**		**Slow 4**		**Slow 5**		**0.01 – 0.1 Hz**	
	P1	**P2**	**P1**	**P2**	**P1**	**P2**	**P1**	**P2**	**P1**	**P2**	**P1**	**P2**
1	0.73	0.70	0.76	0.71	0.74	0.70	0.71	0.72	0.75	0.72	0.72	0.72
2	0.73	0.70	0.76	0.71	0.74	0.70	0.71	0.79	0.75	0.80	0.72	0.80
3	0.73	0.70	0.76	0.71	0.74	0.70	0.71	0.72	0.75	0.72	0.72	0.72
4	0.73	0.70	0.76	0.71	0.74	0.70	0.71	0.72	0.75	0.72	0.72	0.72

5	0.73	0.70	0.76	0.71	0.74	0.70	0.71	0.72	0.75	0.72	0.72	0.72
6	0.73	0.70	0.76	0.71	0.74	0.70	0.78	0.72	0.80	0.72	0.81	0.72
7	0.87	0.70	0.86	0.71	0.87	0.70	0.86	0.72	0.86	0.72	0.86	0.72
8	0.87	0.70	0.86	0.71	0.87	0.70	0.86	0.72	0.86	0.72	0.86	0.72
9	0.73	0.70	0.76	0.71	0.74	0.70	0.71	0.72	0.75	0.72	0.72	0.72
10	0.73	0.70	0.76	0.71	0.74	0.70	0.71	0.72	0.75	0.72	0.72	0.72
11	0.73	0.70	0.76	0.71	0.74	0.70	0.71	0.72	0.75	0.72	0.72	0.72
12	0.87	0.70	0.86	0.71	0.87	0.70	0.86	0.72	0.86	0.72	0.86	0.72
13	0.73	0.70	0.76	0.71	0.74	0.70	0.71	0.72	0.75	0.72	0.72	0.72
14	0.73	0.70	0.76	0.71	0.74	0.70	0.71	0.72	0.75	0.72	0.72	0.72
15	0.73	0.70	0.76	0.71	0.74	0.70	0.71	0.72	0.75	0.72	0.72	0.72
16	0.73	0.70	0.76	0.71	0.74	0.70	0.71	0.72	0.75	0.72	0.72	0.72
17	0.87	0.70	0.86	0.71	0.87	0.70	0.86	0.72	0.86	0.72	0.86	0.72
18	0.73	0.70	0.76	0.71	0.74	0.70	0.71	0.72	0.75	0.72	0.72	0.72

P1: p-value corrected for multiple comparisons for tail CN > AD
P2: p-value corrected for multiple comparisons for tail CN < AD
*: statistically significant result

Table 8. *MES between CN and AD subjects. The test was performed for ALFF values computed with the ROI and voxel approach. Low MES were found.*

	ROIs			**Voxel-based**		
ROI	**Slow 4**	**Slow 5**	**0.01–0.1 Hz**	**Slow 4**	**Slow 5**	**0.01–0.1 Hz**
1	0.04	0.04	0.04	0.04	0.03	0.04
2	0.11	0.11	0.11	0.17	0.18	0.17
3	0.02	0.02	0.02	0.04	0.03	0.04
4	0.02	0.01	0.02	0.02	0.00	0.01
5	-0.01	-0.02	-0.01	-0.01	-0.02	-0.01
6	-0.04	-0.04	-0.04	-0.06	-0.07	-0.06
7	-0.23	-0.22	-0.23	-0.22	-0.20	-0.21
8	-0.18	-0.18	-0.17	-0.18	-0.18	-0.17
9	0.01	0.00	0.01	0.00	0.00	0.01
10	0.04	0.03	0.04	0.04	0.02	0.03
11	0.07	0.06	0.07	0.07	0.07	0.07
12	-0.19	-0.19	-0.19	-0.21	-0.22	-0.21
13	0.10	0.10	0.10	0.09	0.10	0.09
14	-0.02	-0.04	-0.03	-0.01	-0.02	-0.01
15	0.10	0.08	0.09	0.09	0.08	0.09
16	0.03	0.02	0.03	0.04	0.04	0.04
17	-0.17	-0.17	-0.17	-0.16	-0.16	-0.16
18	0.06	0.06	0.06	0.08	0.07	0.07

5.1.2.1.1.2.fALFF

Statistical comparison between AD and CN subjects did not show differences with corrected p-values in any frequency band (table 8), uncorrected p-values showed differences in the slow-5 band for the ROI and voxel-based approach (table S2, supplementary material appendix 3). Low MES values were found for the three frequency bands, the bigger value -0.48 was found on region 10 (Left Retrosplenial Cortex, Posterior Cingulate Cortex) in the slow-5 band, voxel-based approach (table 9).

Table 9. *Permutation t-test between CN and AD subjects. The test was performed for fALFF values computed with the ROI and voxel-based approach. Non-significant differences were found.*

	ROI Corrected p values						**Voxel-based Corrected p values**					
ROI	**Slow 4**		**Slow 5**		**0.01 – 0.1 Hz**		**Slow 4**		**Slow 5**		**0.01 – 0.1 Hz**	
	P1	**P2**	**P1**	**P2**	**P1**	**P2**	**P1**	**P2**	**P1**	**P2**	**P1**	**P2**
1	0.79	0.86	0.98	0.42	0.88	0.72	0.91	0.75	0.99	0.46	0.93	0.68
2	0.77	0.86	0.98	0.77	0.88	0.89	0.91	0.56	0.99	0.69	0.93	0.68
3	0.79	0.86	0.98	0.18	0.88	0.70	0.91	0.64	0.99	0.28	0.93	0.68
4	0.77	0.86	0.98	0.26	0.88	0.70	0.91	0.81	0.99	0.25	0.93	0.68
5	0.79	0.86	0.98	0.22	0.88	0.70	0.91	0.75	0.99	0.29	0.93	0.68
6	0.79	0.86	0.98	0.18	0.90	0.70	0.91	0.75	0.99	0.46	0.93	0.68
7	0.79	0.86	0.98	0.54	0.88	0.70	0.91	0.56	0.99	0.69	0.93	0.68
8	0.79	0.86	0.98	0.28	0.88	0.70	0.91	0.56	0.99	0.39	0.93	0.68
9	0.79	0.86	0.98	0.48	0.88	0.89	0.91	0.81	0.99	0.69	0.93	0.93
10	0.77	0.86	0.98	0.18	0.88	0.70	0.91	0.75	0.99	0.16	0.93	0.68
11	0.79	0.86	0.98	0.26	0.88	0.70	0.91	0.56	0.99	0.25	0.93	0.61
12	0.79	0.86	0.98	0.19	0.88	0.70	0.91	0.56	0.99	0.25	0.93	0.61
13	0.79	0.86	0.98	0.47	0.88	0.72	0.91	0.56	0.99	0.59	0.93	0.68
14	0.77	0.86	0.98	0.18	0.88	0.70	0.91	0.86	0.99	0.25	0.93	0.73
15	0.79	0.86	0.98	0.18	0.88	0.70	0.91	0.81	0.99	0.29	0.93	0.73
16	0.79	0.86	0.98	0.31	0.88	0.70	0.91	0.56	0.99	0.25	0.93	0.68
17	0.79	0.86	0.98	0.18	0.89	0.70	0.99	0.24	0.99	0.16	0.98	0.44
18	0.77	0.87	0.98	0.18	0.88	0.70	0.91	0.56	0.99	0.25	0.93	0.61

P1: p-value corrected for multiple comparisons for tail CN > AD
P2: p-value corrected for multiple comparisons for tail CN < AD
*: statistically significant result

Table 10. *MES between CN and AD subjects. The test was performed for fALFF values computed with the ROI and voxel approach. Low MES were found.*

	ROIs			**Voxel-based**		
ROI	**Slow 4**	**Slow 5**	**0.01–0.1 Hz**	**Slow 4**	**Slow 5**	**0.01–0.1 Hz**
1	0.09	-0.10	0.07	0.01	-0.08	-0.01
2	0.18	0.14	0.24	-0.23	0.10	-0.07
3	-0.07	-0.35	-0.12	-0.10	-0.24	-0.14
4	0.17	-0.21	0.01	0.14	-0.27	0.01
5	-0.10	-0.25	-0.16	-0.02	-0.20	-0.05
6	-0.10	-0.41	-0.27	0.03	-0.13	-0.02
7	-0.13	0.00	-0.10	-0.13	0.07	0.01
8	-0.17	-0.18	0.02	-0.13	-0.13	0.04
9	0.03	-0.04	0.21	0.12	0.10	0.31
10	0.15	-0.34	0.00	0.04	-0.48	-0.15
11	0.00	-0.21	-0.13	-0.20	-0.28	-0.26
12	-0.15	-0.27	-0.15	-0.20	-0.33	-0.24
13	0.11	-0.06	0.08	-0.13	0.00	-0.03
14	0.18	-0.31	0.02	0.21	-0.25	0.10
15	0.06	-0.42	-0.16	0.12	-0.20	0.09
16	0.00	-0.15	-0.01	-0.16	-0.26	-0.20
17	-0.13	-0.30	-0.21	-0.43	-0.41	-0.40
18	0.23	-0.31	-0.06	-0.20	-0.28	-0.24

5.1.2.1.1.3.Multitaper

Statistical comparison between AD and CN subjects did not show differences with corrected p-values in any frequency band (table 10), uncorrected p-values showed differences in slow-4 and slow-5 band for the voxel-based approach on region 16 (Right Superior Frontal Gyrus, Middle Frontal Gyrus) see table S3, supplementary material appendix 3. Low MES values were found for the three frequency bands, the bigger value 0.39 was found on region 8 (Left Hippocampus) in the 0.01-0.1Hz band, voxel-based approach (table 11).

Table 11. *Permutation t-test between CN and AD subjects. The test was performed for Multitaper values computed with the ROI approach. Non-significant differences were found.*

ROI	ROI Corrected p values						Voxel-based Corrected p values					
	Slow 4		Slow 5		0.01 – 0.1 Hz		Slow 4		Slow 5		0.01 – 0.1 Hz	
	P1	P2	P1	P2	P1	P2	P1	P2	P1	P2	P1	P2
1	0.84	0.83	0.83	0.84	0.84	0.94	0.72	0.94	0.95	0.72	0.57	0.97
2	0.78	0.83	0.83	0.77	0.57	0.94	0.84	0.94	0.95	0.85	0.57	0.97
3	0.78	0.83	0.83	0.77	0.57	0.94	0.72	0.94	0.95	0.72	0.50	0.97
4	0.78	0.83	0.83	0.77	0.84	0.94	0.58	0.94	0.95	0.59	0.33	0.97
5	0.78	0.83	0.83	0.77	0.57	0.94	0.60	0.94	0.95	0.59	0.33	0.97
6	0.78	0.83	0.83	0.77	0.57	0.94	0.92	0.94	0.95	0.93	0.63	0.97
7	0.84	0.83	0.83	0.84	0.84	0.75	0.93	0.94	0.95	0.93	0.63	0.97
8	0.78	0.83	0.83	0.77	0.84	0.75	0.72	0.94	0.95	0.72	0.33	0.98
9	0.84	0.83	0.83	0.84	0.84	0.75	0.72	0.94	0.95	0.72	0.35	0.97
10	0.78	0.83	0.83	0.77	0.84	0.89	0.58	0.94	0.95	0.59	0.33	0.97
11	0.78	0.83	0.83	0.77	0.84	0.75	0.72	0.94	0.95	0.72	0.47	0.97
12	0.78	0.83	0.83	0.77	0.84	0.75	0.72	0.94	0.95	0.72	0.41	0.97
13	0.78	0.83	0.83	0.77	0.84	0.75	0.84	0.94	0.95	0.85	0.47	0.97
14	0.78	0.83	0.83	0.77	0.84	0.75	0.58	0.94	0.95	0.59	0.33	0.97
15	0.78	0.83	0.83	0.77	0.87	0.75	0.72	0.94	0.95	0.72	0.47	0.97
16	0.78	0.83	0.83	0.77	0.84	0.75	0.58	0.96	0.95	0.59	0.33	0.97
17	0.78	0.83	0.83	0.77	0.84	0.94	0.58	0.94	0.95	0.59	0.33	0.97
18	0.78	0.83	0.83	0.77	0.95	0.75	0.72	0.94	0.95	0.72	0.33	0.97

P1: p-value corrected for multiple comparisons for tail CN > AD
P2: p-value corrected for multiple comparisons for tail CN < AD
*: statistically significant result

Table 12. *MES between CN and AD subjects. The test was performed for Multitaper values computed with the ROI and voxel approach. Low MES were found.*

	ROIs			Voxel-based		
ROI	**Slow 4**	**Slow 5**	**0.01–0.1 Hz**	**Slow 4**	**Slow 5**	**0.01–0.1 Hz**
1	-0.17	0.17	0.10	-0.03	0.03	0.01
2	-0.01	0.01	0.25	-0.13	0.13	0.00
3	0.19	-0.19	0.23	0.14	-0.14	0.07
4	-0.02	0.02	0.08	0.22	-0.22	0.26
5	0.17	-0.17	0.31	0.17	-0.17	0.28
6	-0.01	0.01	0.29	-0.24	0.24	-0.06
7	-0.17	0.17	-0.05	-0.32	0.32	-0.07

8	-0.06	0.06	-0.09	-0.01	0.01	0.39
9	-0.20	0.20	-0.14	0.01	-0.01	0.20
10	0.11	-0.11	0.03	0.20	-0.20	0.22
11	-0.05	0.05	-0.06	0.07	-0.07	0.08
12	0.11	-0.11	-0.13	0.04	-0.04	0.15
13	-0.07	0.07	-0.05	-0.14	0.14	0.10
14	0.09	-0.09	-0.04	0.25	-0.25	0.26
15	0.08	-0.08	-0.21	0.05	-0.05	0.10
16	-0.05	0.05	-0.14	0.30	-0.30	0.23
17	0.12	-0.12	0.17	0.25	-0.25	0.27
18	0.16	-0.16	-0.34	0.08	-0.08	0.23

5.1.2.1.1.4. Permutation Entropy

For a delay of 1, statistically significant differences were found on region 10 (Left Retrosplenial Cortex, Posterior Cingulate Cortex) using the ROI approach (table 12) independent of the embedding dimension, no statistically significant difference was found for the voxel-based approach, results are available on the supplementary material appendix 3, table S4 and S6. MES values above 0.5 were found for all the embedding dimensions that were tested, the bigger value -0.59 was found for a dimension of 7 (table 14).

For a delay of 2, statistically significant differences were also found on region 10 (Left Retrosplenial Cortex, Posterior Cingulate Cortex) using the ROI approach (table 13) independent of the embedding dimension, no statistically significant difference was found for the voxel-based approach, results are available on the supplementary material appendix 3, table S5 and S6. MES values above 0.5 were found for all the embedding dimensions that were tested, the bigger value -0.67 was found for a dimension of 7 (table 15).

According to table 15, the bigger MES was accomplished for a time delay of 2 and dimension of 4. Therefore, these parameters were used for the upcoming analysis that involves permutation entropy.

Table 13. *Permutation t-test between CN and AD subjects. The test was performed for PE values computed with the ROI approach, an embedding delay of 1 and embedding dimension from 3 to 7 were used. Statistically significant differences were found in region 10 (Left Retrosplenial Cortex, Posterior Cingulate Cortex).*

	Corrected p values, delay:1									
ROI	**dim: 3**		**dim: 4**		**dim: 5**		**dim: 6**		**dim: 7**	
	P1	**P2**	**P1**	**P2**	**P1**	**P2**	**P1**	**P2**	**P1**	**P2**
1	0.43	0.99	0.59	0.96	0.56	0.98	0.65	0.94	0.97	0.93
2	0.43	0.99	0.35	0.96	0.37	0.98	0.18	0.98	0.24	0.98
3	0.62	0.99	0.98	0.80	1.00	0.66	1.00	0.50	0.97	0.71
4	1.00	0.22	1.00	0.11	1.00	0.09	1.00	0.30	0.97	0.65
5	0.84	0.99	0.98	0.80	1.00	0.78	1.00	0.68	0.97	0.72
6	0.26	0.99	0.35	0.96	0.37	0.98	0.18	0.98	0.24	0.98
7	0.62	0.99	0.75	0.96	0.57	0.98	0.65	0.94	0.74	0.98
8	0.17	0.99	0.35	0.96	0.57	0.98	0.89	0.94	0.97	0.90
9	0.62	0.99	0.59	0.96	0.56	0.98	0.67	0.94	0.97	0.79
10	1.00	**0.04***	1.00	**0.02***	1.00	**0.04***	1.00	**0.03***	1.00	**0.02***
11	0.74	0.99	1.00	0.80	1.00	0.46	1.00	0.50	0.97	0.65
12	0.86	0.99	1.00	0.59	1.00	0.62	1.00	0.54	0.97	0.65
13	0.43	0.99	0.59	0.96	0.56	0.98	0.65	0.94	0.97	0.93
14	0.86	0.99	1.00	0.59	1.00	0.41	1.00	0.50	0.97	0.72
15	0.86	0.99	1.00	0.59	1.00	0.41	1.00	0.50	0.97	0.65
16	0.86	0.99	1.00	0.59	1.00	0.41	1.00	0.54	0.97	0.79
17	0.84	0.99	0.98	0.80	1.00	0.66	1.00	0.62	0.97	0.72
18	0.43	0.99	0.98	0.93	1.00	0.78	1.00	0.70	0.97	0.79

P1: p-value corrected for multiple comparisons for tail CN > AD
P2: p-value corrected for multiple comparisons for tail CN < AD
*****: statistically significant result

Table 14. *Permutation t-test between CN and AD subjects. The test was performed for PE values computed with the ROI approach, an embedding delay of 2 and embedding dimension from 3 to 7 were used. Statistically significant differences were found in region 10 (Left Retrosplenial Cortex, Posterior Cingulate Cortex).*

	Corrected p values, delay:2									
ROI	**dim: 3**		**dim: 4**		**dim: 5**		**dim: 6**		**dim: 7**	
	P1	**P2**	**P1**	**P2**	**P1**	**P2**	**P1**	**P2**	**P1**	**P2**
1	0.44	0.99	0.64	0.96	0.59	0.97	0.75	0.93	0.95	0.87
2	0.44	0.99	0.43	0.96	0.55	0.98	0.19	0.98	0.26	0.98
3	0.68	0.99	1.00	0.78	1.00	0.62	1.00	0.41	0.95	0.63
4	1.00	0.22	1.00	0.15	1.00	0.1	1.00	0.34	0.95	0.53

5	0.87	0.99	1.00	0.78	1.00	0.78	1.00	0.66	0.95	0.63
6	0.31	0.99	0.43	0.96	0.41	0.98	0.19	0.98	0.26	0.98
7	0.67	0.99	0.85	0.96	0.74	0.97	0.75	0.93	0.95	0.88
8	0.13	0.99	0.43	0.96	0.62	0.97	0.82	0.93	0.95	0.87
9	0.68	0.99	0.64	0.96	0.59	0.97	0.75	0.93	0.95	0.78
10	1.00	**0.04***	1.00	**0.02***	1.00	**0.03***	1.00	**0.04***	1.00	**0.01***
11	0.75	0.99	1.00	0.72	1.00	0.37	1.00	0.41	0.95	0.53
12	0.88	0.99	1.00	0.60	1.00	0.62	1.00	0.57	0.95	0.53
13	0.44	0.99	0.64	0.96	0.59	0.97	0.75	0.93	0.95	0.87
14	0.87	0.99	1.00	0.60	1.00	0.34	1.00	0.41	0.95	0.63
15	0.87	0.99	1.00	0.60	1.00	0.37	1.00	0.41	0.95	0.53
16	0.87	0.99	1.00	0.60	1.00	0.34	1.00	0.57	0.95	0.79
17	0.87	0.99	1.00	0.78	1.00	0.65	1.00	0.57	0.95	0.63
18	0.63	0.99	1.00	0.85	1.00	0.78	1.00	0.66	0.95	0.78

P1: p-value corrected for multiple comparisons for tail CN > AD
P2: p-value corrected for multiple comparisons for tail CN < AD
*****: statistically significant result

Table 15. *MES between CN and AD subjects for embedding delay of 1 and 2 across embedding dimensions from 3 to 7 for the ROI approach.*

	delay:1					**delay:2**				
ROI	**dim: 3**	**dim: 4**	**dim: 5**	**dim: 6**	**dim: 7**	**dim: 3**	**dim: 4**	**dim: 5**	**dim: 6**	**dim: 7**
1	0.19	0.16	0.22	0.21	0.18	0.23	0.19	0.22	0.19	0.10
2	0.35	0.38	0.41	0.47	0.44	0.32	0.33	0.34	0.44	0.44
3	0.13	0.00	-0.10	-0.23	-0.14	0.08	-0.05	-0.12	-0.23	-0.12
4	-0.43	-0.49	-0.49	-0.35	-0.21	-0.41	-0.45	-0.48	-0.38	-0.25
5	-0.05	-0.02	0.03	0.02	0.01	-0.02	-0.04	-0.01	-0.06	-0.11
6	0.43	0.44	**0.50**	**0.53**	**0.51**	0.40	0.39	0.45	0.45	0.43
7	0.01	0.01	0.09	0.16	0.23	0.13	0.09	0.12	0.15	0.17
8	**0.54**	0.37	0.20	0.12	0.12	**0.52**	0.32	0.17	0.09	0.10
9	0.19	0.25	0.24	0.24	0.06	0.11	0.16	0.20	0.14	-0.04
10	**-0.59**	**-0.58**	**-0.54**	**-0.52**	**-0.52**	**-0.59**	**-0.63**	**-0.62**	**-0.62**	**-0.67**
11	0.06	-0.12	-0.21	-0.17	-0.18	0.04	-0.12	-0.26	-0.27	-0.23
12	-0.12	-0.16	-0.12	-0.12	-0.13	-0.17	-0.21	-0.15	-0.16	-0.24
13	0.30	0.24	0.25	0.30	0.26	0.28	0.20	0.22	0.17	0.13
14	-0.08	-0.13	-0.21	-0.12	0.00	-0.11	-0.22	-0.31	-0.24	-0.11
15	-0.16	-0.20	-0.24	-0.25	-0.25	-0.13	-0.18	-0.25	-0.28	-0.28
16	-0.07	-0.23	-0.31	-0.13	0.05	-0.07	-0.25	-0.29	-0.12	0.01
17	-0.02	-0.01	-0.04	-0.04	-0.03	-0.06	-0.08	-0.10	-0.12	-0.14
18	0.34	0.15	0.09	0.06	0.06	0.17	0.01	-0.02	-0.06	-0.02

5.1.2.1.2. Integration Measures

Clustering coefficient (CC), node degree (ND), characteristic path length (PL), global efficiency (GE) and small world propensity (SWP) metrics were computed over the correlation matrices for the voxel-based and ROI approaches. Down-sampled BOLD signals extracted from the remaining 1328 voxels within the DMN were used to compute the connectivity measures, they were then averaged into the 18 DMN ROIs.

Statistically significant differences were found when comparing the characteristic path length between AD and CN subjects using the ROI approach. No statistically significant differences were found for the other local and global metrics, however differences between the groups on region 17 (Right Parahippocampal Gyrus) with both approaches are shown on table 15 and 16 with uncorrected p-values.

Table 16. *Permutation t-test between CN and AD subjects. The test was performed for CC values computed with the ROI and voxel-based approach. Uncorrected statistically significant differences were found on region 8 (Left Hippocampus), 9 (Right Hippocampus), 12 (Left Parahippocampal Gyrus) and 17 (Right Parahippocampal Gyrus) for the ROI approach and regions 10 (Left Retrosplenial Cortex, Posterior Cingulate Cortex) and 17 (Right Parahippocampal Gyrus) for the voxel-based approach.*

ROI	**ROI**				**Effect Size**	**Voxel-based**				**Effect Size**
	Corrected p values		**Uncorrected p values**			**Corrected p values**		**Uncorrected p values**		
	P1	**P2**	**P1**	**P2**		**P1**	**P2**	**P1**	**P2**	
1	0.41	0.98	0.25	0.75	0.14	0.18	0.96	0.10	0.90	0.27
2	0.41	0.98	0.27	0.73	0.12	0.14	0.96	0.06	0.94	0.32
3	0.59	0.98	0.56	0.44	-0.03	0.18	0.96	0.14	0.86	0.22
4	0.41	0.98	0.25	0.75	0.13	0.14	0.96	0.07	0.93	0.30
5	0.40	0.98	0.17	0.83	0.20	0.18	0.96	0.11	0.89	0.25
6	0.43	0.98	0.31	0.69	0.10	0.27	0.96	0.27	0.73	0.13
7	0.61	0.98	0.61	0.39	-0.06	0.21	0.96	0.20	0.80	0.17
8	0.20	0.98	**0.04***	0.96	0.35	0.14	0.96	0.07	0.93	0.30
9	0.20	0.98	0.04*	0.96	0.36	0.14	0.96	0.06	0.94	0.31
10	0.41	0.98	0.23	0.77	0.15	0.14	0.96	**0.05***	0.95	0.33
11	0.40	0.98	0.17	0.83	0.19	0.18	0.96	0.15	0.85	0.22

12	0.20	0.98	**0.02***	0.98	0.44	0.14	0.96	0.06	0.94	0.32
13	0.59	0.98	0.53	0.47	-0.01	0.18	0.96	0.16	0.84	0.21
14	0.40	0.98	0.18	0.82	0.19	0.14	0.96	0.06	0.94	0.32
15	0.59	0.98	0.50	0.50	0.00	0.18	0.96	0.16	0.84	0.21
16	0.52	0.98	0.41	0.59	0.05	0.18	0.96	0.12	0.88	0.24
17	0.20	0.98	**0.04***	0.96	0.36	0.14	0.96	**0.04***	0.96	0.35
18	0.40	0.98	0.12	0.88	0.24	0.14	0.96	0.07	0.93	0.29

P1: p-value corrected for multiple comparisons for tail CN > AD
P2: p-value corrected for multiple comparisons for tail CN < AD
*: statistically significant result

Table 17. *Permutation t-test between CN and AD subjects. The test was performed for ND values computed with the ROI and voxel-based approach. Uncorrected statistically significant differences were found on region 8 (Left Hippocampus), 9 (Right Hippocampus), 12 (Left Parahippocampal Gyrus) and 17 (Right Parahippocampal Gyrus) for the ROI approach and regions 10 (Left Retrosplenial Cortex, Posterior Cingulate Cortex), 12 (Left Parahippocampal Gyrus) and 17 (Right Parahippocampal Gyrus) for the voxel-based approach.*

ROI	**ROI**				**Effect Size**	**Voxel-based**				**Effect Size**
	Corrected p values		**Uncorrected p values**			**Corrected p values**		**Uncorrected p values**		
	P1	**P2**	**P1**	**P2**		**P1**	**P2**	**P1**	**P2**	
1	0.58	0.99	0.35	0.65	0.08	0.28	0.96	0.19	0.81	0.24
2	0.58	0.99	0.39	0.61	0.06	0.23	0.96	0.13	0.87	0.13
3	0.78	0.99	0.75	0.25	-0.13	0.31	0.96	0.28	0.72	0.32
4	0.58	0.99	0.34	0.66	0.08	0.17	0.96	0.06	0.94	0.25
5	0.52	0.99	0.17	0.83	0.20	0.23	0.96	0.11	0.89	0.01
6	0.58	0.99	0.42	0.58	0.04	0.48	0.96	0.48	0.52	0.13
7	0.78	0.99	0.78	0.22	-0.15	0.31	0.96	0.27	0.73	0.30
8	0.20	0.99	**0.02***	0.98	0.39	0.17	0.96	0.07	0.93	0.32
9	0.20	0.99	**0.05***	0.95	0.35	0.17	0.96	0.06	0.94	0.35
10	0.58	0.99	0.30	0.70	0.10	0.17	0.96	**0.04***	0.96	0.18
11	0.54	0.99	0.24	0.76	0.15	0.29	0.96	0.21	0.79	0.33
12	0.18	0.99	**0.01***	0.99	0.48	0.17	0.96	**0.05***	0.95	0.06
13	0.78	0.99	0.72	0.28	-0.12	0.41	0.96	0.39	0.61	0.33
14	0.52	0.99	0.20	0.80	0.17	0.17	0.96	0.05	0.95	0.16
15	0.78	0.99	0.72	0.28	-0.12	0.29	0.96	0.23	0.77	0.20
16	0.60	0.99	0.46	0.54	0.02	0.28	0.96	0.17	0.83	0.36
17	0.20	0.99	**0.03***	0.97	0.38	0.17	0.96	**0.04***	0.96	0.24
18	0.49	0.99	0.14	0.86	0.23	0.23	0.96	0.12	0.88	0.24

P1: p-value corrected for multiple comparisons for tail CN > AD
P2: p-value corrected for multiple comparisons for tail CN < AD
*****: statistically significant result

Table 18. *Statistical comparison p-values and MES between AD and CN subjects. The test was performed for PL, GE and SWP. Statistically significant differences were found for the characteristic path length with the ROI approach, low MES were found.*

Approach	Metric	Corrected p values		Uncorrected p values		Effect Size
		P1	P2	P1	P2	
Voxel-based	PL	0.56	0.44	0.56	0.44	-0,04
	GE	0.86	0.13	0.86	0.13	-0.26
	SWP	0.81	0.18	0.81	0.18	-0.18
ROI	PL	**0.03***	0.96	**0.03***	0.96	0.24
	GE	0.51	0.48	0.51	0.48	0.01
	SWP	0.23	0.76	0.23	0.76	0.13

P1: p-value corrected for multiple comparisons for tail CN > AD
P2: p-value corrected for multiple comparisons for tail CN < AD
*****: statistically significant result

5.1.2.2. Machine Learning Techniques

Statistical analysis over metrics for the quantification of brain function revealed that the permutation entropy and the characteristic path length have a statistically significant power to discriminate between the groups, however its effect size was not big. In this study all the metrics described above were used as features for the design of a classification model using machine learning techniques.

5.1.2.2.1. Feature Selection

Results of the dimensionality reduction step applied to the 219 features are described for two proportional thresholds: for a proportional threshold of 0.58, ALFF metrics in the slow 4 for almost all the DMN regions had a high contribution on the first component. In addition, permutation entropy in regions 4 (Posterior Cingulate Cortex, Precuneus) and 7 (Left and Right Thalamus), path length and global efficiency had a high contribution to the second principal component. Figure 27 shows the loadings after a PCA reduction keeping the components with the 99% of the variance.

The amount of variance explained by the first two components was 28%, 77 components were selected (see figure 28).

For a proportional threshold of 0.81, ALFF metrics in the slow 4 for almost all the DMN regions had a high contribution on the first component. In addition, permutation entropy in regions 4 (Posterior Cingulate Cortex, Precuneus) and global efficiency had a high contribution to the second principal component. Figures 29 shows the loadings after a PCA reduction keeping the components with the 99% of the variance. The amount of variance explained by the first two components is 31%, 76 components were selected (see figure 30).

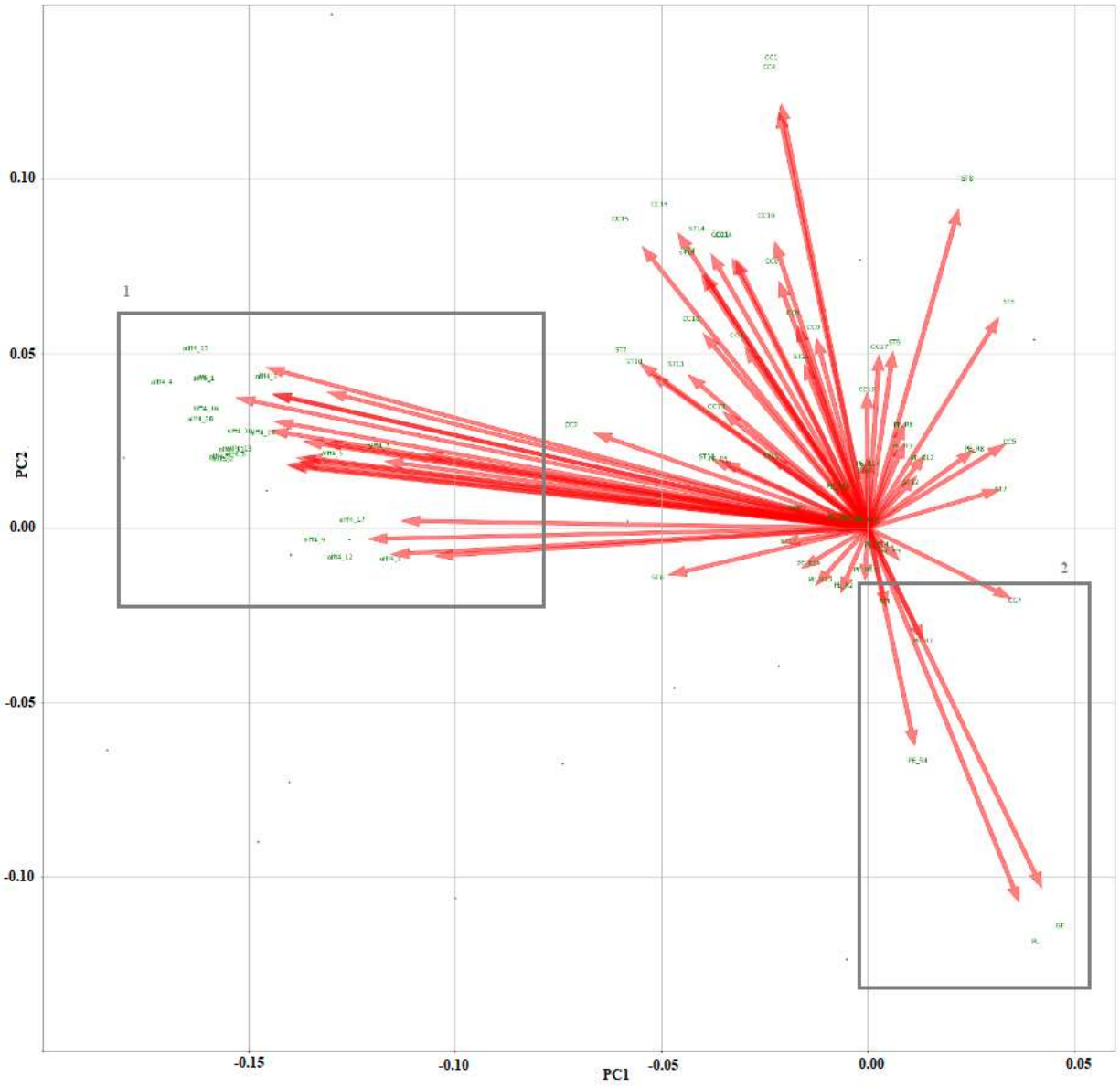

Figure 27. *PCA loadings for a threshold of 0.58.*

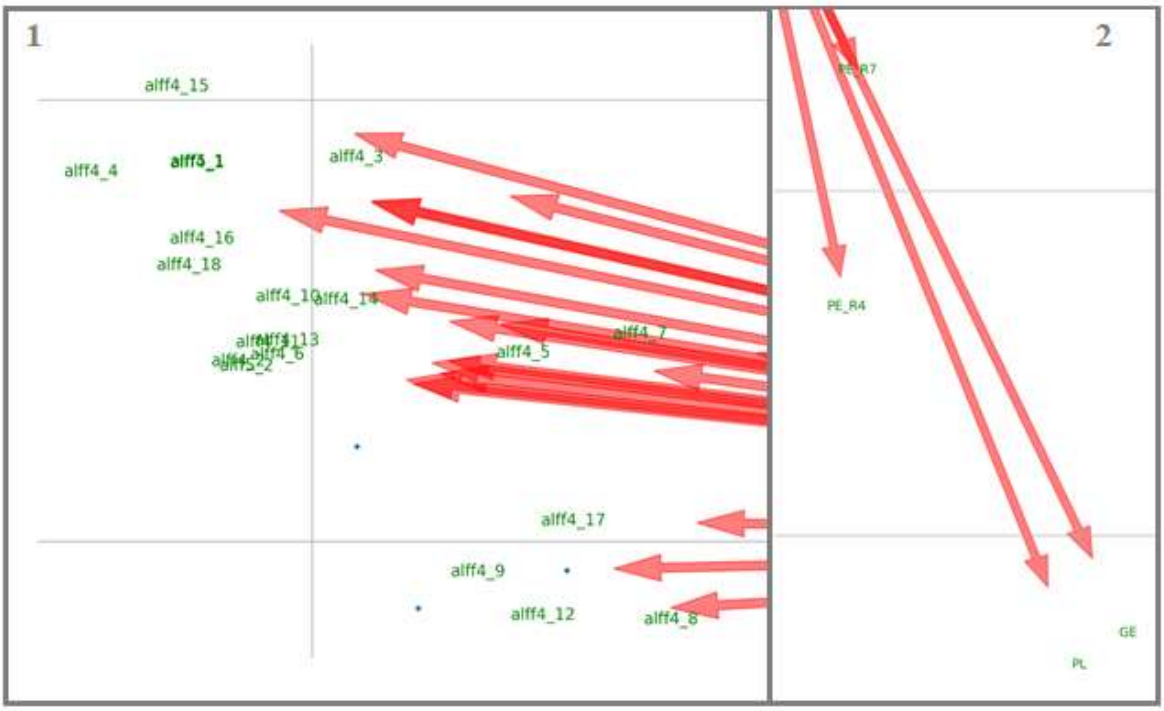

Figure 28. *Zoom of figure 27.* ***1:*** *features with bigger contributions to the first principal component. ALFF in the slow 4 for almost all regions.* ***2:*** *features with bigger contributions to the second principal component. Permutation entropy in regions 4 and 7, path length and global efficiency.*

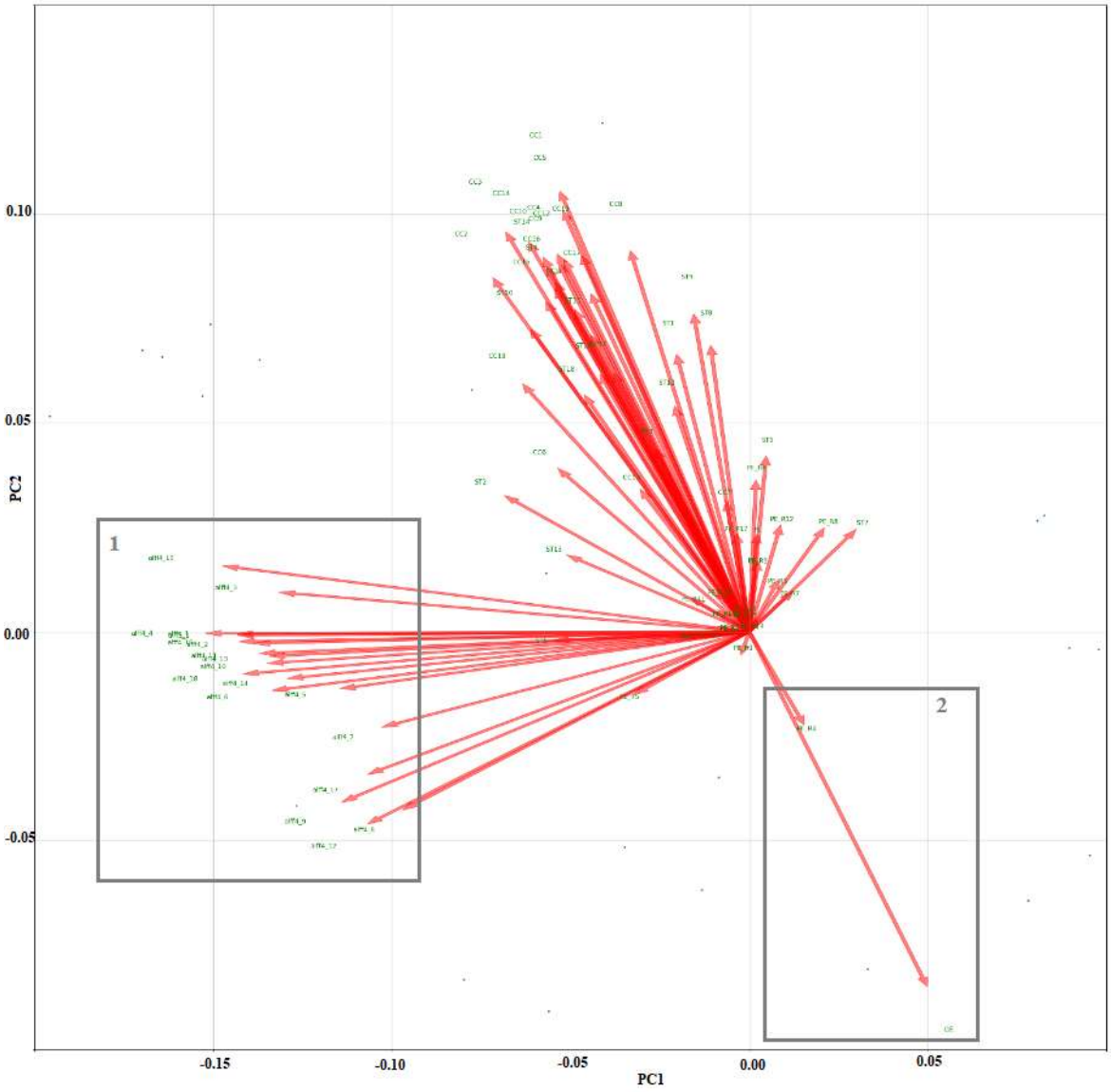

Figure 29. *PCA loadings for a threshold of 0.81.*

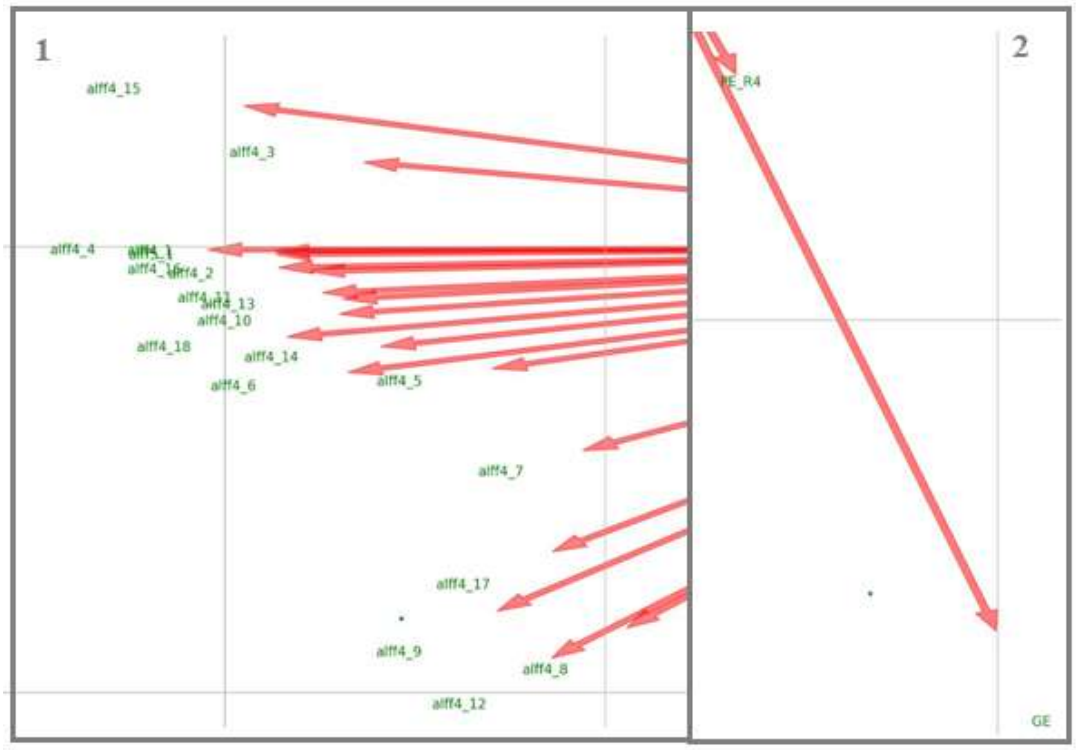

Figure 30. *Zoom of figure 29.* ***1:*** *features with bigger contributions to the first principal component. ALFF in the slow 4 for almost all regions.* ***2:*** *features with bigger contributions to the second principal component. Permutation entropy in regions 4 and global efficiency.*

5.1.2.3.Discussion and conclusions

The few differences and the low MES values found on the segregation and integration analysis suggest that there are not big differences between the groups that could be captured by those measures. PE was the only metric that revealed statistically significant difference and an effect size above |0.5|, also known as a medium effect, on the Left Retrosplenial Cortex, Posterior Cingulate Cortex. The negative MES and the statistically significant difference on the tail CN < AD suggest that there is more entropy on AD BOLD signals compared to CN.

Voxel-based results did not have statistically significant differences in any comparison, differences found with this approach were not statistically significant (supplementary material, appendix 3 table S2 and S3), which suggest low capacity to discriminate between these AD and CN subjects. Therefore, this approach was not used in the implementation of a machine learning model.

The explained variance of the first principal components for the proportional thresholds 0.58 and 0.81 had a high contribution of the ALFF in the slow 4. Global efficiency and permutation entropy in region 4 also contributed to the second principal component in both thresholds. The characteristic path length had a high weight to the second component for threshold 0.58, however that contribution was not present for threshold 81. This result shows the impact that the application of different proportional thresholds has on graph metrics. The dependence on a threshold would affect the performance of this methodology with other datasets.

Although visual inspection of the results from section 4 (*Measures for the Estimation of Brain Function*) showed differential pattern between groups in fALFF, a higher contribution is made by the ALFF to the first principal component. Visual inspection of section 4 results showed that PE in regions 4, 7 and 10 described a differential pattern between the groups, the differences was confirmed for region 10 by the statistical analysis performed on section 5. However, figure 30 shows that the feature that contributes the most to the second principal component is the PE in the region 4. This comparison was made because both analyses were performed with the same proportional threshold, 0.81.

The posterior cingulate cortex is considered a key region of the DMN that has shown changes of functional connectivity in AD (Dillen et al., 2016), with a high diagnostic power for discriminating AD from healthy subjects (Koch et al., 2012). Decreased complexity has been previously reported in AD compared to healthy subjects in rs-fMRI studies (B. Wang et al., 2017; Zheng, Onoda, Nagai, & Yamaguchi, 2020) and (Grieder, Wang, Dierks, Wahlund, & Jann, 2018) reporting that the decreased signal complexity in DMN nodes reflects the cognitive decline in AD, including the posterior cingulate cortex. In addition, a previous study (Boccardi, Comanducci, Baroni, & Mecocci, 2017) concerning the impact of aging in old age dementia reported that the late onset

AD can be seen as a manifestation of reduced energy production, therefore an increase in entropy. Authors suggest that accumulation of modifications related with age as well as exhausted mitochondria might be responsible for the poor capacity of the brain to adapt its brain structures and cerebral functions. It is important to highlight that OASIS-3 is a database that includes subjects ranging in age from 42-95 years that were recruited over the course of 30 years. Some of the subjects included in this study were initially labeled as cognitively normal that developed Alzheimer over time.

The ALFF is a metric that has been used in studies of AD as a feature in classification algorithms obtaining good performance (Yang et al., 2018). Researchers from a previous study (Kundu et al., 2019) found an increase in the median of GE over the DMN in AD subjects compared to CN, in line with our results (figure 12). They also found a reduction in the mean of PL in AD compared to CN, in our results the median is the same for both groups (figure 12). They also reported that the biggest differences between AD and CN described by in PL and GE is present in the right frontoparietal network (Kundu et al., 2019). Further studies using this pipeline should be performed over this network.

6. Pipeline for the classification of subjects with neurodegenerative diseases from rs-fMRI

6.1. Objective 3: To develop a pipeline that integrates the measures for feature extraction and the classifier using open-source software.

For the design of the classifier, features and labels of the two classes are required. Model selection and model evaluation steps are also necessary to identify the best model to discriminate between the two classes. Therefore, developments from previous objectives were integrated with the model selection and model evaluation steps defined in this section.

6.1.1. Materials and Methods

The selected features, after the feature selection step, were used as inputs to the machine learning models. As mentioned before, SVM have been widely used for the classification of neurological disorder. In this step, different models were tested using SVM random search for hyperparameter tuning, a data scientist assistant tool known as TPOT was used to automate the process of model selection. TPOT is a tool built by automated machine learning researches to be used in supervised classification problems with the purpose of maximizing the classification accuracy of the models (Olson, Edu, & Moore, 2016). Finally, the Synthetic Minority Oversampling Technique (SMOTE) was used as an oversampling method for the imbalanced data. Figure 31 shows a brief introduction to the methodology implemented in this objective.

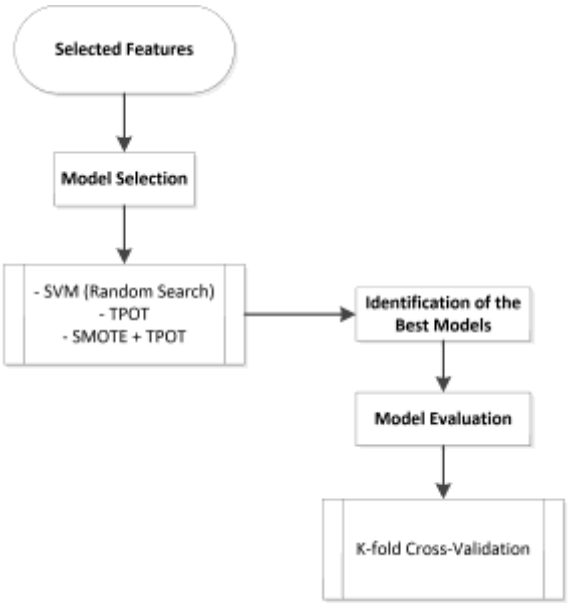

Figure 31. *flowchart representing a brief introduction to the methodology implemented in objective 3.*

6.1.2. Model Selection and Model Evaluation

The best models were selected according to the AUC, recall and specificity, without ignoring the other metrics. Specificity is needed to know how well the model classifies cognitively normal subjects, recall is necessary to know the ratio of AD subjects correctly classified from all AD subjects, ROC-AUC is also important to know the discriminatory ability of the model.

6.1.2.1. SVM (random search)

A randomized search was performed to find the best parameters (*c, gamma* and *kernel*) for the classification. The search of *c* was carried out from 2 to 100, *gamma* from 0.1 to 1, the linear and RBF kernels were also tested. The 75% of the dataset was split into the training set and the remaining 25% was selected for testing the model. The best models for the ROI approach after keeping the components that explained the 99% of the variability are described on table 19. Table 18 shows the results of the k-fold cross-validation, figures 33 to 35 shows the boxplot of the performance of each model from table 19 after performing k-fold cross-validation with k=5. The performance of all models obtained from the components that explained [80 - 99] % of the

variability are available in the supplementary material, appendix 4. Best metrics were found keeping the components with the 99% of the variance.

Table 19. *Best SVM models after feature selection with components that explained the 99% of the variability. Th: proportional threshold applied to the graph metrics for the ROI approach.*

Th	Model Parameters	Performance precision-recall-f1-score-support	Features selected
0.06	SVC(C=12.837689046425513, break_ties=False, cache_size=200, class_weight=None, coef0=0.0, decision_function_shape='ovr', degree=3, gamma=0.31969749262499214, kernel='linear', max_iter=-1, probability=False, random_state=None, shrinking=True, tol=0.001, verbose=False)	0 0.78 – 0.93 – 0.85 – 15 1 0.86 – 0.60 – 0.71 – 10	16
0.14	SVC(C=86.47761323199036, break_ties=False, cache_size=200, class_weight=None, coef0=0.0, decision_function_shape='ovr', degree=3, gamma=0.10471885619097257, kernel='linear', max_iter=-1, probability=False, random_state=None, shrinking=True, tol=0.001, verbose=False)	0 0.80 - 0.80 - 0.80 - 15 1 0.70 - 0.70 - 0.70 - 10	14
0.25	SVC(C=86.47761323199036, break_ties=False, cache_size=200, class_weight=None, coef0=0.0, decision_function_shape='ovr', degree=3, gamma=0.10471885619097257, kernel='linear', max_iter=-1, probability=False, random_state=None, shrinking=True, tol=0.001, verbose=False)	0 0.83 – 1.00 - 0.91 – 15 1 1.00 – 0.70 – 0.82 – 10	12
0.47	SVC(C=12.837689046425513, break_ties=False, cache_size=200, class_weight=None, coef0=0.0, decision_function_shape='ovr', degree=3, gamma=0.31969749262499214, kernel='linear', max_iter=-1, probability=False, random_state=None, shrinking=True, tol=0.001, verbose=False)	0 0.81 – 0.87 – 0.84 – 15 1 0.78 – 0.70 – 0.74 – 10	16
0.48	SVC(C=49.91899368450383, break_ties=False, cache_size=200, class_weight=None, coef0=0.0, decision_function_shape='ovr', degree=3, gamma=0.4864191107835447, kernel='linear', max_iter=-1, probability=False, random_state=None, shrinking=True, tol=0.001, verbose=False)	0 0.88 – 0.93 – 0.90 – 15 1 0.89 – 0.80 – 0.84 – 10	15
0.53	SVC(C=19.862432454294343, break_ties=False, cache_size=200, class_weight=None, coef0=0.0, decision_function_shape='ovr', degree=3, gamma=0.6325737018318947, kernel='linear', max_iter=-1, probability=False, random_state=None, shrinking=True, tol=0.001, verbose=False)	0 0.88 – 1.00 – 0.94 – 15 1 1.00 – 0.80 – 0.89 – 10	15
0.54	SVC(C=86.47761323199036, break_ties=False, cache_size=200, class_weight=None, coef0=0.0, decision_function_shape='ovr', degree=3, gamma=0.10471885619097257, kernel='linear', max_iter=-1, probability=False, random_state=None, shrinking=True, tol=0.001, verbose=False)	0 1.00 – 0.80 – 0.89 – 15 1 0.77 – 1.00 – 0.87 – 10	15
0.58	SVC(C=35.611195012089865, break_ties=False, cache_size=200, class_weight=None, coef0=0.0, decision_function_shape='ovr', degree=3, gamma=0.27541045374233664, kernel='linear', max_iter=-1, probability=False, random_state=None, shrinking=True, tol=0.001, verbose=False)	0 0.80 – 0.80 – 0.80 – 15 1 0.70 – 0.70 – 0.70 – 10	17
0.59	SVC(C=19.862432454294343, break_ties=False, cache_size=200, class_weight=None, coef0=0.0, decision_function_shape='ovr', degree=3, gamma=0.6325737018318947, kernel='linear', max_iter=-1, probability=False,	0 0.85 - 0.73 - 0.79 - 15 1 0.67 - 0.80 - 0.73 - 10	17

	random_state=None, shrinking=True, tol=0.001, verbose=False)		
0.60	SVC(C=12.837689046425513, break_ties=False, cache_size=200, class_weight=None, coef0=0.0, decision_function_shape='ovr', degree=3, gamma=0.31969749262499214, kernel='linear', max_iter=-1, probability=False, random_state=None, shrinking=True, tol=0.001, verbose=False)	0 0.81 – 0.87 – 0.84 – 15 1 0.78 – 0.70 – 0.74 – 10	13
0.65	SVC(C=4.043913202692316, break_ties=False, cache_size=200, class_weight=None, coef0=0.0, decision_function_shape='ovr', degree=3, gamma=0.31002657767286057, kernel='rbf', max_iter=-1, probability=False, random_state=None, shrinking=True, tol=0.001, verbose=False)	0 0.86 - 0.80 - 0.83 - 15 1 0.73 - 0.80 - 0.76 - 10	19
0.89	SVC(C=86.47761323199036, break_ties=False, cache_size=200, class_weight=None, coef0=0.0, decision_function_shape='ovr', degree=3, gamma=0.10471885619097257, kernel='linear', max_iter=-1, probability=False, random_state=None, shrinking=True, tol=0.001, verbose=False)	0 0.86 - 0.80 - 0.83 - 15 1 0.73 - 0.80 - 0.76 - 10	14
0.91	SVC(C=20.646718316338273, break_ties=False, cache_size=200, class_weight=None, coef0=0.0, decision_function_shape='ovr', degree=3, gamma=0.31010774244258366, kernel='rbf', max_iter=-1, probability=False, random_state=None, shrinking=True, tol=0.001, verbose=False)	0 0.78 - 0.93 - 0.85 - 15 1 0.86 - 0.60 - 0.71 - 10	14
0.97	SVC(C=20.646718316338273, break_ties=False, cache_size=200, class_weight=None, coef0=0.0, decision_function_shape='ovr', degree=3, gamma=0.31010774244258366, kernel='rbf', max_iter=-1, probability=False, random_state=None, shrinking=True, tol=0.001, verbose=False)	0 0.78 - 0.93 - 0.85 - 15 1 0.86 - 0.60 - 0.71 - 10	14

Table 20. *Performance of each model from table 19 after k-fold cross-validation for the ROI approach.*

Th	Metric	Performance k-fold Cross-validation Mean±Standard Deviation	Th	Metric	Performance k-fold Cross-validation Mean±Standard Deviation
0.06	**accuracy**	0.73 ± 0.04	0.58	**accuracy**	0.76 ± 0.11
	F1	0.65 ± 0.06		**F1**	0.71 ± 0.15
	recall	0.64 ± 0.13		**recall**	0.73 ± 0.11
	precision	0.72 ± 0.14		**precision**	0.73 ± 0.23
	roc_auc	0.80 ± 0.10		**roc_auc**	0.82 ± 0.12
	specificity	0.65 ± 0.06		**specificity**	0.60 ± 0.10
0.14	**accuracy**	0.68 ± 0.04	0.59	**accuracy**	0.79 ± 0.09
	F1	0.57 ± 0.13		**F1**	0.72 ± 0.11
	recall	0.56 ± 0.16		**recall**	0.68 ± 0.15
	precision	0.65 ± 0.21		**precision**	0.79 ± 0.18
	roc_auc	0.69 ± 0.06		**roc_auc**	0.81 ± 0.10
	specificity	0.66 ± 0.12		**specificity**	0.65 ± 0.08
0.25	**accuracy**	0.69 ± 0.12	0.60	**accuracy**	0.70 ± 0.08
	F1	0.57 ± 0.21		**F1**	0.59 ± 0.15
	recall	0.57 ± 0.23		**recall**	0.56 ± 0.14
	precision	0.64 ± 0.24		**precision**	0.65 ± 0.19
	roc_auc	0.76 ± 0.15		**roc_auc**	0.76 ± 0.04
	specificity	0.66 ± 0.14		**specificity**	0.67 ± 0.10
	accuracy	0.74 ± 0.05	0.65	**accuracy**	0.76 ± 0.07
	F1	0.66 ± 0.09		**F1**	0.68 ± 0.10
	recall	0.65 ± 0.10		**recall**	0.64 ± 0.12

0.47	**precision**	0.70 ± 0.12		**precision**	0.73 ± 0.10
	roc_auc	0.80 ± 0.11		**roc_auc**	0.78 ± 0.09
	specificity	0.64 ± 0.07		**specificity**	0.66 ± 0.09
0.48	**accuracy**	0.77 ± 0.07	0.89	**accuracy**	0.75 ± 0.09
	F1	0.70 ± 0.11		**F1**	0.69 ± 0.12
	recall	0.67 ± 0.09		**recall**	0.70 ± 0.21
	precision	0.75 ± 0.17		**precision**	0.70 ± 0.03
	roc_auc	0.80 ± 0.09		**roc_auc**	0.80 ± 0.10
	specificity	0.64 ± 0.08		**specificity**	0.64 ± 0.08
0.53	**accuracy**	0.78 ± 0.09	0.91	**accuracy**	0.65 ± 0.11
	F1	0.73 ± 0.12		**F1**	0.52 ± 0.19
	recall	0.77 ± 0.21		**recall**	0.51 ± 0.19
	precision	0.71 ± 0.08		**precision**	0.56 ± 0.19
	roc_auc	0.83 ± 0.12		**roc_auc**	0.65 ± 0.11
	specificity	0.61 ± 0.09		**specificity**	0.68 ± 0.12
0.54	**accuracy**	0.70 ± 0.06	0.97	**accuracy**	0.66 ± 0.07
	F1	0.63 ± 0.07		**F1**	0.55 ± 0.12
	recall	0.64 ± 0.09		**recall**	0.55 ± 0.20
	precision	0.66 ± 0.15		**precision**	0.61 ± 0.10
	roc_auc	0.84 ± 0.04		**roc_auc**	0.73 ± 0.10
	specificity	0.64 ± 0.03		**specificity**	0.68 ± 0.10

The best model for classifying AD subjects from Cognitively normal subjects was found for a proportional threshold of 0.59. The model had a good performance: the rate for predicting false positives and false negatives described by the F1 score (0.72 ± 0.11) with a minimum of 0.61, recall (0.68 ± 0.15) with a minimum of 0.53 and precision (0.79 ± 0.18) with a minimum of 0.61; the rate of correct predictions defined by the accuracy (0.79 ± 0.09) with a minimum of 0.70, an AUC score of 0.81 ± 0.10 with a minimum of 0.71 and specificity 0.65 ± 0.08 with a minimum of 0.57.

In addition to SVM, XGBoost classifier was also tested. No models with good performance were found.

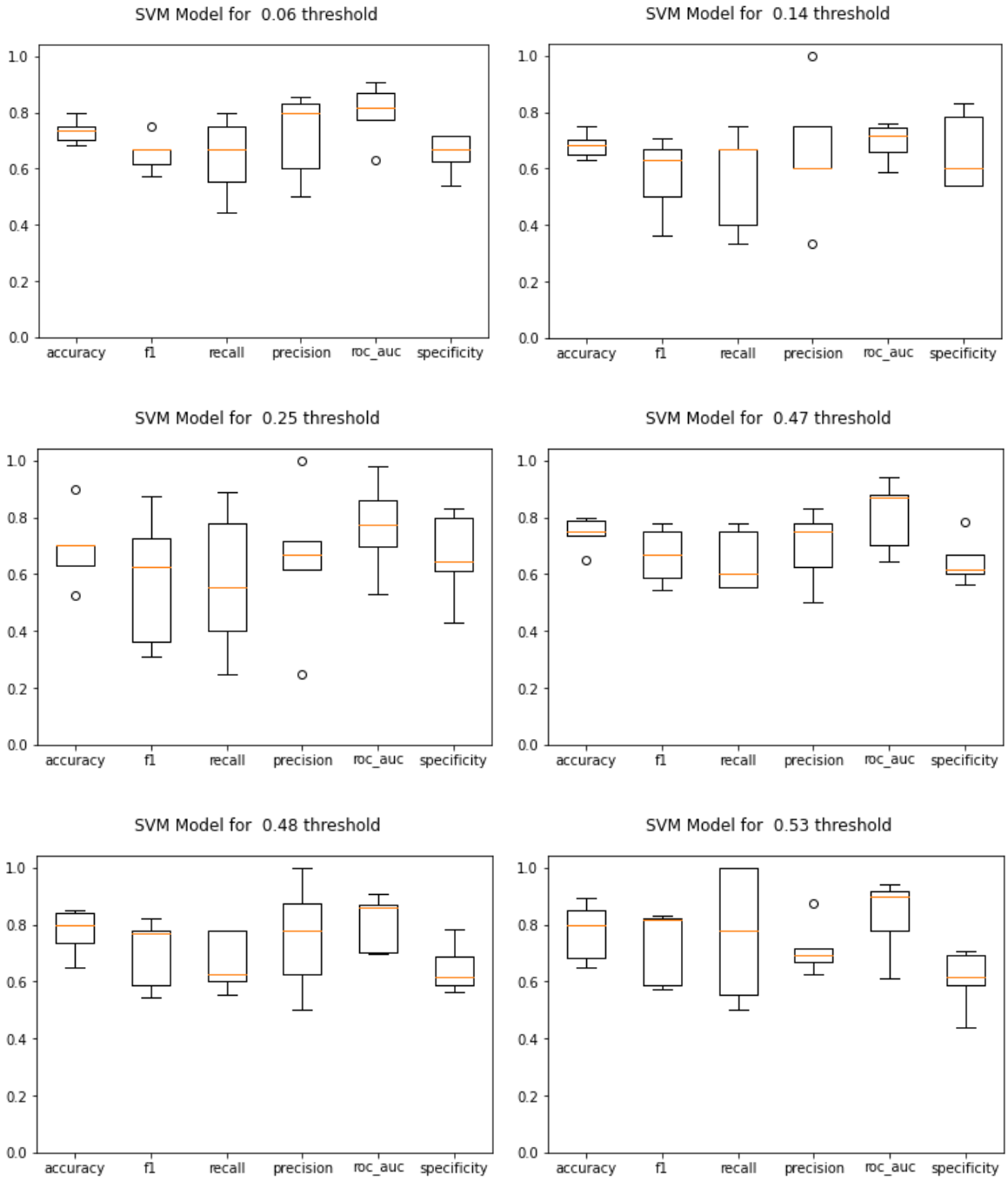

Figure 32. *Boxplot of the evaluation metrics after k-fold cross-validation for graph metrics with proportional threshold of 0.06 to 0.53.*

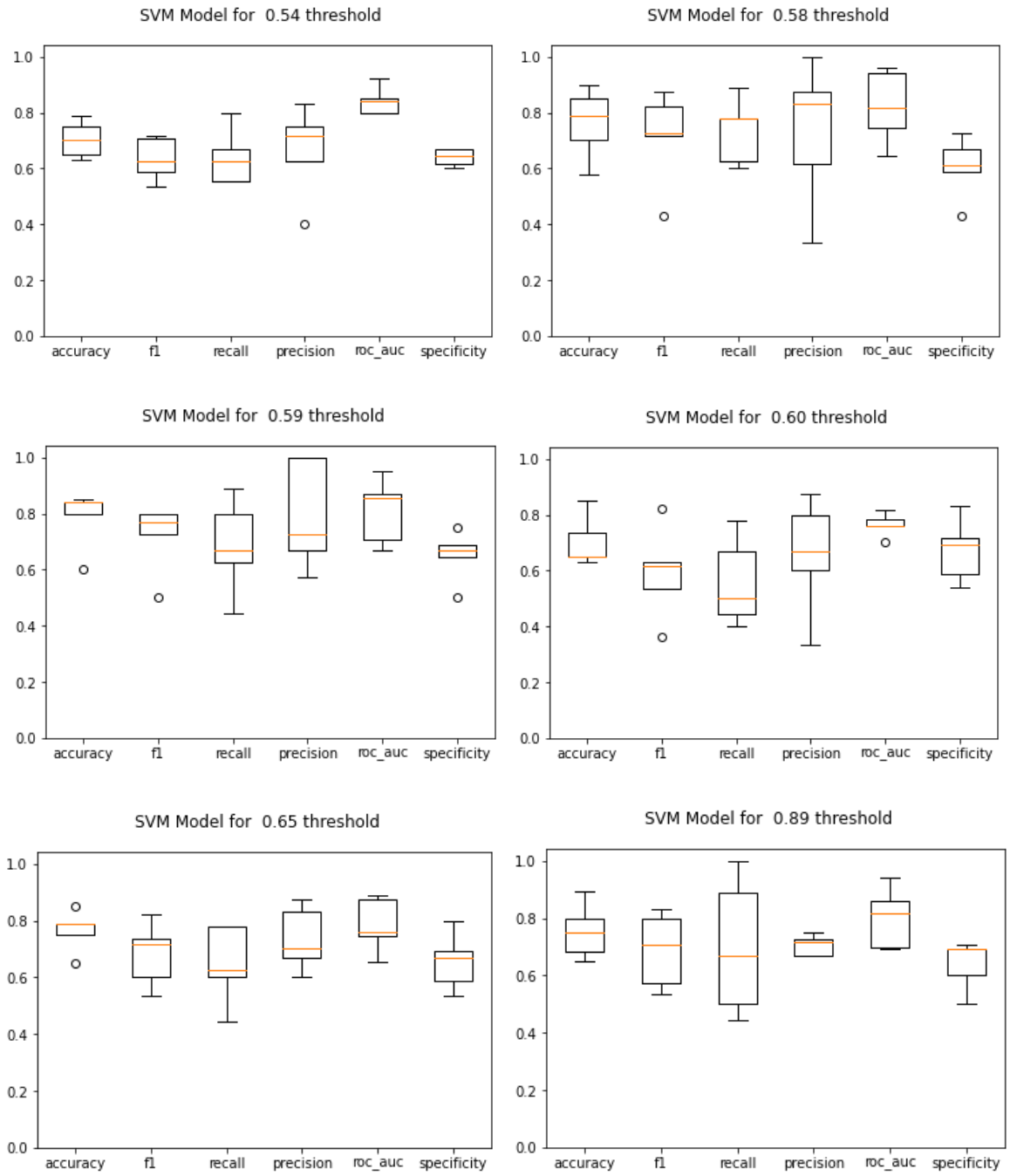

Figure 33. *Boxplot of the evaluation metrics after k-fold cross-validation for graph metrics with proportional threshold of 0.54 to 0.89.*

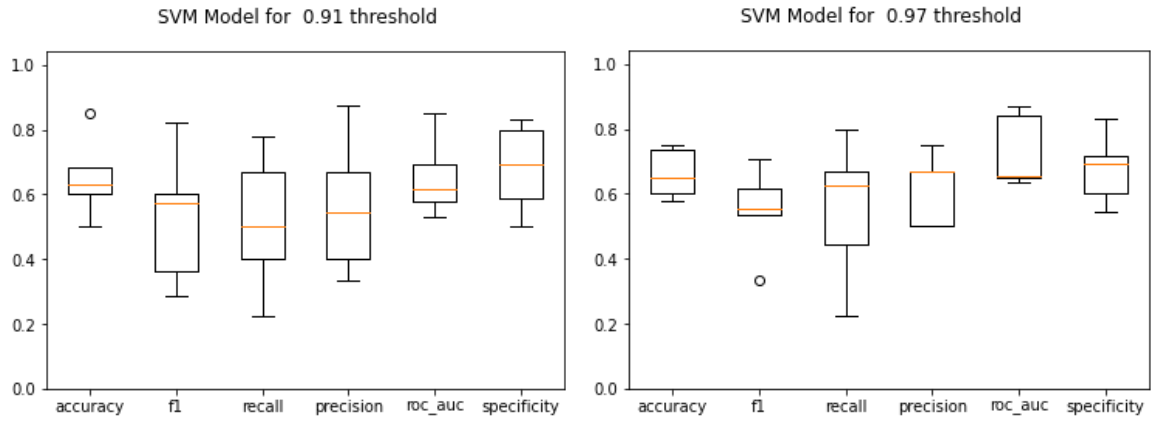

Figure 34. *Boxplot of the evaluation metrics after k-fold cross-validation for graph metrics with proportional threshold of 0.91 and 0.97.*

6.1.2.2. TPOT

The TPOTClassifier function from the TPOT python library (http://epistasislab.github.io/tpot/) was used to estimate the best pipeline. Parameters were set to 50 generations, population size of 50 and k-fold cross-validation of 5, it evaluated 2500 pipelines and used 5 folds to evaluate the pipeline using cross-validation during the optimization process. The best pipeline had an average cross-validation score on the training set of 0.93, it was found for a proportional threshold of 0.81. This pipeline was tested to check its performance, results are shown on table 21. k-fold cross-validation results are shown on figure 35. All pipelines generated by TPOT are available on the supplementary material appendix 5.

Table 21. *Best pipeline after running TPOT with components that explained the 99% of the variance for each proportional threshold applied to the graph metrics for the ROI approach.*

Th	Pipeline Parameters	Performance precision-recall-f1-score-support	Features selected

0.81	exported_pipeline = make_pipeline(
	make_union(
	MinMaxScaler(),
	FunctionTransformer(copy)
	),
	LinearSVC(C=10.0, dual=True, loss="hinge", penalty="l2", tol=0.0001)
	)
	# Fix random state for all the steps in exported pipeline
	set_param_recursive(exported_pipeline.steps, 'random_state', 42)
		0 0.87 - 0.87 - 0.87 - 15
		1 0.80 - 0.80 - 0.80 - 10
			15

Table 22. *Performance of the best model from table 20 after k-fold cross-validation for the ROI approach.*

Th	Metric	Performance k-fold cross-validation Mean ± Standard Deviation
0.81	**accuracy**	0.79 ± 0.04
	F1	0.73 ± 0.06
	recall	0.74 ± 0.34
	precision	0.73 ± 0.07
	roc_auc	0.83 ± 0.07
	specificity	0.62 ± 0.05

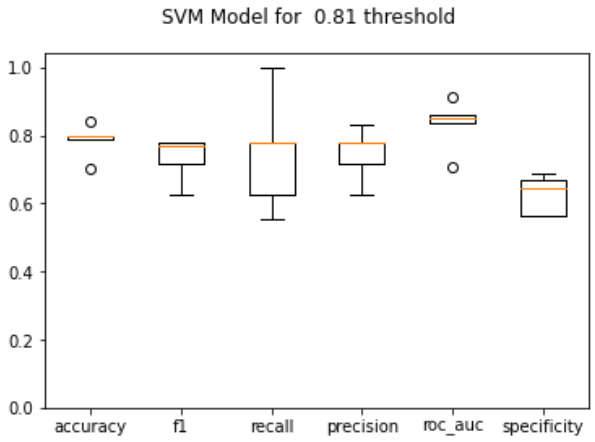

Figure 35. *Boxplot of the evaluation metrics after k-fold cross-validation for graph metrics with proportional threshold of 0.81 for the best pipeline generated by TPOT.*

6.1.2.3. SMOTE

The training features and training target datasets were split using the train_test_split function available in sklearn with the parameters defined in the best pipeline generated by TPOT, see supplementary material appendix 5. The training features and training target datasets were oversampled using SMOTE. Before SMOTE, the training dataset had 30 subjects for label 1 (AD) and 43 subjects for label 0 (CN), after SMOTE the training dataset had 43 subjects for label 1 and 43 subjects for label 0. The performance of the pipeline is shown in table 22. The code is available on the supplementary material appendix 6. The TPOT model was also validated using k-fold cross-validation (k=5) in which the training dataset for each fold was oversampled using SMOTE. Table

24 shows the average score that describe the performance of the best TPOT model k-fold cross-validation, figure 36 shows the boxplot.

Table 23. *Best pipeline after running TPOT with components that explained the 99% of the variance for each proportional threshold applied to the graph metrics for the ROI approach.*

Th	Pipeline Parameters	Performance precision-recall-f1-score-support	Features selected

0.81	sm = SMOTE(random_state = 2)
	X_train_res, y_train_res = sm.fit_sample(training_features, training_target)
	exported_pipeline = make_pipeline(
	make_union(
	MinMaxScaler(),
	FunctionTransformer(copy)
	),
	LinearSVC(C=10.0, dual=True, loss="hinge", penalty="l2", tol=0.0001)
	)
	# Fix random state for all the steps in exported pipeline
	set_param_recursive(exported_pipeline.steps, 'random_state', 42)
		0 0.93 - 0.93 - 0.93 - 15
		1 0.90 - 0.90 - 0.90 - 10
			15

Table 24. *k-fold cross-validation performance of the best TPOT model from table 23 after SMOTE for the ROI approach.*

Th	Metric	Performance k-fold cross-validation Mean ± Standard Deviation
0.81	**accuracy**	0.74 ± 0.05
	F1	0.69 ± 0.06
	recall	0.72 ± 0.15
	precision	069 ± 0.12
	roc_auc	0.75 ± 0.06
	specificity	0.60 ± 0.01

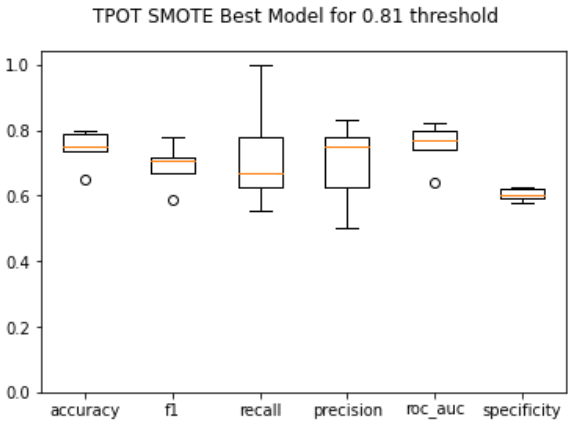

Figure 36. *Boxplot of the evaluation metrics after k-fold cross-validation for graph metrics with proportional threshold of 0.81 for the best pipeline generated by TPOT after SMOTE.*

6.1.3. Discussion and conclusions

It was possible to find a model with good performance using SVM and random search. The classification improved slightly after using TPOT, however k-fold cross-validation revealed that the use of SMOTE did not represent an improvement in the performance.

It is also important to highlight that it was possible to find models with good performance for almost any proportional threshold, contrary as described in a previous study (A. Khazaee et al., 2015) that reported 100% of accuracy for the classification of AD subjects using rs-fMRI and graph theory. They got the best classification for a proportional threshold of 0.19, in this study the best classification was found for a proportional threshold of 0.81. Further analysis is required to avoid working with sparse brain networks due to the high dependence between the threshold and the model performance. The variability in the performance of the models across each proportional threshold suggest that graph metrics are relevant features and should be considered for subsequent analysis. Further analysis is required to test the effect of each metric in the performance of each model, mainly because the PCA reduction does not allow to track the relevance of each individual feature or which combination of features improved the model performance. Only one metric showed a big capacity to capture changes between AD and CN, statistical analysis results suggest that the PE should be considered for future improvements of this pipeline. The good performance of PE to capture complexity of the BOLD signals will be beneficial to study other neurodegenerative disorder such as PD through this pipeline.

Limitations of this analysis also include: the unbalanced sample size, the clinical information available at the web-page of the data sharing initiative was not extensively detailed; many excluded subjects with longitudinal registers were diagnosed with AD but in the following acquisition were diagnosed as CN. An important aspect in the classification process is the ground truth of the field

to assign a label to the data, which in this case is related to the diagnosis made by clinicians. A recent systematic review (Ansart et al., 2020) highlighted this concern and suggest that machine learning approaches are not likely to have good performance outside research studies with well controlled conditions

7. Validation of the pipeline on rs-fMRI data from subjects with MCI

7.1. Objective 4: Validate the pipeline with rs-fMRI data from healthy and AD subjects.

The pipeline for the classification of subjects with neurodegenerative diseases was tested with data from subjects with Alzheimer's disease and cognitively normal individuals. It is necessary to implement the pipeline with another dataset to evaluate if the pipeline can be successfully implemented on data with a different data acquisition protocol and to detect its limitations.

As mentioned before, the methodology was developed and tested with a rs-fMRI dataset from OASIS-3: Longitudinal Neuroimaging, Clinical, and Cognitive Dataset for Normal and Alzheimer's Disease. One motivation of this study was to validate the pipeline on rs-fMRI data from subjects with pre-clinical AD from the research project *"Identificación de biomarcadores preclínicos en Enfermedad de Alzheimer a través de un seguimiento longitudinal de la actividad eléctrica cerebral en poblaciones con riesgo genético"* funded by the Departamento Administrativo de Ciencia, Tecnología e Innovación (COLCIENCIAS). However, rs-fMRI data from this project have not yet been collected.

7.1.1. Materials and Methods

The proposed pipeline starts with raw resting state fMRI signals from two groups, signals are preprocessed (visual inspection, slice timing, motion correction, co-register, normalization, ART-repair and band pass filter), BOLD signals are extracted according to the template of a network using the ROI approach, metrics for quantifying the static brain function are computed for the 0.01-0.1 Hz frequency band (Permutation Entropy, Clustering Coefficient, Node Degree, Characteristic Path Length, Global Efficiency and the Small World Propensity) and for the slow-4, slow-5 and the 0.01-0.1 Hz frequency bands (ALFF, fALFF and Multitaper). Those 219 metrics

are used as features, steps for data cleaning and feature selection are performed to select the most relevant features, model selection is carried out with the SVM random search and TPOT, the best model was identified according to its performance, finally the best model was validated using leave-one-out cross-validation.

Figure 37 shows a brief introduction to the methodology implemented in this objective.

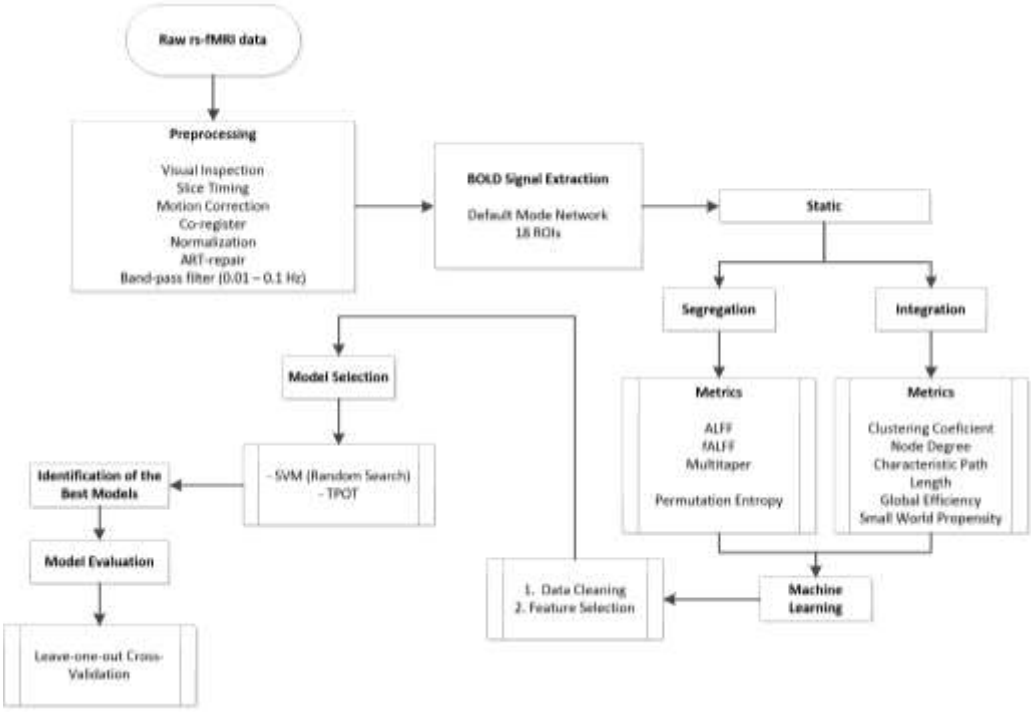

Figure 37. *flowchart representing a brief introduction to the methodology implemented in objective 4.*

7.1.1.1. Subjects

The validation was made with data from the Alzheimer's disease Neuroimaging Initiative ADNI-3. 13 AD and 149 MCI sessions were downloaded; 5 of the 13 AD sessions accomplished the technical inclusion criteria regarding equal acquisition parameters for all subjects; 59 of the 149 MCI session had rs-fMRI with the same acquisition parameters, only 14 of them had good quality after preprocessing. Once the MCI data was selected, CN subjects were downloaded matching for sex, they were selected by age such that it would not represent a statistically significant difference

between the groups. ADNI-3 initiative was chosen based on previous experiences of the research group with ADNI-2, concerning not good quality of the data (Súarez-Revelo, Ochoa-Gomez, Tobón-Quintero, & Duque-Grajales, 2014). Therefore, the analysis was performed with MCI subjects. Table 25 shows the demographics characteristics of the data. See supplementary material appendix 7 for more information about the downloaded data and appendix 8 for the selected subjects.

Table 25. *Demographic and clinical characteristics for the ADNI dataset.*

Parameter	**MCI** **Mean ± Standard Deviation**	**CN** **Mean ± Standard Deviation**	**P value**
n	14	14	-
Sex (female:male)	8:6	8:6	-
Hand dominance (right:left)	14:0	14:0	-
Age	74.43 ± 11.44	76.5 ± 8.35	> 0.10
Years of education	15.93 ± 3.40	17.57 ± 1.78	0.06
MMSE	27.21 ± 3.55	29.5 ± 0.76	< 0.01
CDR-SB	1.39 ± 1.00	-	-

MMSE: Mini-Mental State Examination
CDR-SB: Clinical Dementia Scale Sum of Boxes

7.1.1.2. Data acquisition

For rs-fMRI acquisition, echo-planar images were collected at rest using a 3T SIEMENS Scanner (MAGNETOM Prisma Fit, Siemens, Erlangen, Germany). The acquisition for each subject had 197 samples with parameters: echo time (TE) = 30 ms, repetition time (TR)= 3000 ms, flip angle (FA)= 90º and voxel size= 3.4 mm x 3.4 mm x 3.4 mm.

7.1.1.3. Image preprocessing

Preprocessing steps were performed on CONN (www.nitrc.org/projects/conn). Data were visually inspected to discard low-quality volumes. Volume realignment was performed taking the first

volume as reference. Functional data was slice timing corrected and therefore they were registered with the corresponding individual T1 image. Motion correction report was inspected to exclude subjects with excessive motion (translation > 3 mm and rotation > 3º in any direction). Selected data was normalized to the Montreal National Institute standard space, with the 2x2 x2 mm voxel size. Trends removal, removal of movement, white matter and cerebrospinal fluid related signals, as well as temporal bandpass filtering, within the 0.01 to 0.1 Hz frequency band, were applied.

7.1.1.4. DMN regions

BOLD signals were extracted using the ROIs approach for the 18 DMN regions described by table 5 and figure 5.

7.1.1.5. Estimation of Brain Function

For each region of the DMN, the ALFF, fALFF and Multitaper metrics on the slow-4, slow-5 and the [0.01-0.1] Hz frequency range; the SWP, CC, DG, PL and GE on the [0.01-0.1] Hz frequency range were computed and used as input features, 219 features were generated. Graph metrics were converted from fully connected functional brain networks to sparse brain networks using a proportional threshold function from [0.01 – 1] with an increment step of 0.01.

7.1.1.6. Machine Learning Techniques

7.1.1.6.1. Data Cleaning and Feature Selection

Data was inspected to detect atypical values, then a dimensionality reduction step was performed keeping the components with the 99% of the variance. The union between selected features by ES and MI was used to select the more meaningful features.

7.1.1.6.2. Model Selection and Model Evaluation

A randomized search was performed to find the best parameters for the classification. The search of *c* was carried out with the parameter described on section 6.1.1.1.

7.1.2. Results

The best model for SVM is described on table 22, the same model was found for 13 thresholds, 2 features were selected as the more meaningful for the classification. Leave one out cross-validation (LOOCV) was performed instead of k-fold cross-validation given the small number of subjects. TPOT was also used for finding the best classifier, however no good performance was found. See supplementary material appendix 9 for more details of the performance of the best TPOT model.

Table 26. *Best SVM models after feature selection with components that explained the 99% of the variability. Th: proportional threshold applied to the graph metrics for the ROI approach. Ac: accuracy LOOCV, FS: features selected.*

Th	Model Parameters	Performance precision-recall-f1-score-support	FS	Performance LOOCV precision-recall-f1-score-support	Ac
0.03	SVC(C=86.47761323199036, break_ties=False, cache_size=200, class_weight=None, coef0=0.0, decision_function_shape='ovr', degree=3, gamma=0.10471885619097257, kernel='linear', max_iter=-1, probability=False, random_state=None, shrinking=True, tol=0.001, verbose=False)	0 0.60 – 1.00 – 0.75 – 15 1 1.00 – 0.50 – 0.67 – 10	2	0 0.60 – 0.86 – 0.71 – 14 1 0.75 – 0.43 – 0.55 – 14	0.64
0.14				0 0.58 – 0.79 – 0.67 – 14 1 0.67 – 0.43 – 0.52 – 14	0.61
0.28				0 0.58 – 0.79 – 0.67 – 14 1 0.67 – 0.43 – 0.52 – 14	0.61
0.31				0 0.60 – 0.86 – 0.71 – 14 1 0.75 – 0.43 – 0.55 – 14	0.64
0.32				0 0.60 – 0.86 – 0.71 – 14 1 0.75 – 0.43 – 0.55 – 14	0.64
0.39				0 0.58 – 0.79 – 0.67 – 14 1 0.67 – 0.43 – 0.52 – 14	0.61
0.40				0 0.58 – 0.79 – 0.67 – 14 1 0.67 – 0.43 – 0.52 – 14	0.61
0.43				0 0.60 – 0.86 – 0.71 – 14 1 0.75 – 0.43 – 0.55 – 14	0.64
0.58				0 0.60 – 0.86 – 0.71 – 14 1 0.75 – 0.43 – 0.55 – 14	0.64
0.66				0 0.57 – 0.86 – 0.69 – 14 1 0.71 – 0.36 – 0.48 – 14	0.61
0.85				0 0.60 – 0.86 – 0.71 – 14 1 0.75 – 0.43 – 0.55 – 14	0.64
0.93				0 0.60 – 0.86 – 0.71 – 14 1 0.75 – 0.43 – 0.55 – 14	0.64
0.98				0 0.56 – 0.71 – 0.63 – 14	0.57

				1 0.60 – 0.43 – 0.50 – 14	

7.1.3. Discussion and conclusions

It was not possible to find a model with good performance for the MCI ADNI-3 dataset. TPOT did not represented a useful tool for this dataset, it was not possible to find a model better than the one obtained by implementing SVM with random search. Limitations of this analysis include the small number of subjects. Therefore, it is necessary to test the pipeline on other datasets from other neurodegenerative disorder with at least the same number of subjects used in section 6.

Although individuals with MCI has higher risk to convert to AD, and the MCI is considered a state between cognitively normal and AD, not all subjects develop AD (Sun, Van De Giessen, Lelieveldt, & Staring, 2017). Researchers have reported other causes that contribute to the MCI stage, some of them are cerebrovascular disease and Lewy Body disease (Knopman & Petersen, 2014).

Authors of a recent systematic review concerning resting state abnormalities of the DMN in MCI (Eyler et al., 2019) found variations in the pattern of its resting state function reported on the studies. They reported that there was not an index that could be considered a biomarker of MCI or risk of AD. The most robust finding that was present among studies was the reduction of functional connectivity in the posterior cingulate cortex in MCI, this finding was reported in 52% of the studies. To date, there is not a robust metric to be used with BOLD signals with the capacity to detect the differences and similarities between MCI and AD. Metrics used for the classification of AD might not be capturing differences between MCI and CN.

8. Overall discussion

It was possible to develop a methodology for the classification of subjects with AD. The implemented metrics for the estimation of brain function captured brain dynamics and differentiated AD from cognitively normal individuals with an accuracy of 0.74 ± 0.05, ROC-AUC of 0.75 ± 0.06 and specificity of 0.60 ± 0.01. PE and ALFF were found to have high relevance in feature selection, as well as GE and PL. The automated pipeline that integrates segregation and integration metrics can be found in the following link https://gitlab.com/neuro-tools/fmri/mlclassificationnd.git. Findings also revealed higher entropy in subjects with AD compared to CN.

In line with the results of this project, previous studies have reported an increase in entropy as a manifestation on reduced energy production in AD (Boccardi et al., 2017; B. Wang et al., 2017; Zheng et al., 2020). PE and ALFF were also found to have high relevance in feature selection, as well as GE and PL, also reported in a previous research (Kundu et al., 2019; Yang et al., 2018). Studies that have addressed the classification of AD subjects using rs-fMRI data have reached 100% accuracy using SVM and proportional threshold of 0.19 for the graph analysis in a small dataset, 20 subjects with AD and 20 subjects with AD from the ADNI-2 database. The analysis was performed over 90 regions of the Automated Anatomical Labelling Atlas (A. Khazaee et al., 2015). Another study reported 95% accuracy using SVM with linear kernel computing ALFF and fALFF features over regions from the Automated Anatomical Labelling Atlas analysis in a small dataset, 20 subjects with AD and 20 subjects with AD from the ADNI-2 database (Mao et al., 2017). Important limitations in those studies are the small number of subjects and none of them validate the proposed methodology in a different dataset. Results of this project also support

findings of the literature that suggest the use of SVM for machine learning for the classification of neurodegenerative diseases.

To date, all metrics are computed in python except for the SWP and the extraction of BOLD signals using DPARSFA, both require MATLAB. Future improvements will be made to include in the pipeline not only the extraction of BOLD signals but also preprocessing steps for rs-fMRI data.

The biggest limitation of the study is related to the use sparse connectivity matrix to compute graph properties of the network. It was necessary to use this approach given the outperformance of the model with fully connected matrices. It was not possible to validate the pipeline with the desired dataset. There exist limitations concerning the dataset from ADNI-3, there is lack of information regarding the cognitive status of the subjects. It was not possible to identify which subjects with MCI will convert to AD, therefore it is necessary to follow new acquisitions of ADNI-3 to enrich the dataset.

Future work is needed, the implementation of the dynamic analysis would be useful for tracking the progression of brain dynamics, not only for neurodegenerative diseases but also for neurodevelopmental disorders. However, more advances in the methodology are required. For example, to include different types of windows to perform the sliding window technique, use another connectivity metric for the construction of the vectorized dynamic correlation matrix. On the other hand, the pipeline was only tested for the DMN, therefore, other networks that have been reported to be affected in AD during the progression of the disease should be tested using this approach. It is also necessary to extent the application to other neurodegenerative diseases such as the analysis over the sensorimotor cortex for the classification of subjects with Parkinson's Disease. rs-fMRI preprocessing can be improved by including stronger denoising approaches such as ICA and machine learning techniques to discriminate noisy components. In addition,

improvements in the pipeline will be made by including other connectivity metrics not dependent on a threshold for replacing graph analysis with a proportional threshold.

9. Overall conclusion

It was developed a pipeline that integrates metrics based on biomedical signal processing for quantifying the static and dynamic brain function using segregation and integration approaches. An increase in entropy was found on the left Retrosplenial Cortex, Posterior Cingulate Cortex in subjects with AD. The pipeline was able to classify AD subjects from CN with an accuracy of 0.74 ± 0.05, specificity of 0.60 ± 0.01. The pipeline was able to classify MCI subjects from CN with accuracy of 0.64. Further investigations are required to improve the performance of the models and to generalize the methodology to other ND, primarily to local populations and including more subjects to improve specificity.

10. Research publication

Title: Alteration of Entropy in the Precuneus and Posterior Cingulate Cortex in Alzheimer's Disease: A Resting-State Functional Magnetic Resonance Study.

How to cite:

A. C. Puche, J. F. Ochoa-Gómez, Y. A. Agudelo-Londoño, J. K. Rodas-Marín, and C. A. Tobón-Quintero, "Alteration of Entropy in the Precuneus and Posterior Cingulate Cortex in Alzheimer's Disease: A Resting-State Functional Magnetic Resonance Study", TecnoL., vol. 24, no. 52, p. e2118, Dec. 2021.

Abstract

The human brain has been described as a complex system. Its study using neurophysiological signals has revealed the presence of linear and non-linear interactions. In this context, entropy metrics have been used to discover brain behavior in the presence and absence of neurological alterations. Entropy mapping is of great interest for the study of progressive neurodegenerative diseases such as Alzheimer's Disease (AD). The objective of this study was to characterize the dynamics of brain oscillations in AD using entropy and the Amplitude of Low-Frequency Fluctuations (ALFF) of BOLD signals from the default network and the executive control network in patients with AD and healthy individuals. For this purpose, the data was extracted from the Open Access Series of Imaging Studies (OASIS). The results revealed greater discriminatory power in Permutation Entropy (PE) than in ALFF and fractional ALFF metrics. An increase in PE was obtained in regions of the default network and the executive control network in patients. The posterior cingulate cortex and the precuneus exhibited a differential characteristic when PE was evaluated in both groups. There were no findings when the metrics were correlated with clinical scales. The results showed that PE can be used to characterize the brain function in patients with

AD and reveals information about non-linear interactions complementary to the characteristics obtained by calculating the ALFF.

11. Bibliography

Agosta, F., Pievani, M., Geroldi, C., Copetti, M., Frisoni, G. B., & Filippi, M. (2012). Resting state fMRI in Alzheimer's disease: beyond the default mode network. *Neurobiology of Aging*, *33*(8), 1564–1578. https://doi.org/10.1016/j.neurobiolaging.2011.06.007

Al-Zubaidi, A., Mertins, A., Heldmann, M., Jauch-Chara, K., & Münte, T. F. (2019). Machine Learning Based Classification of Resting-State fMRI Features Exemplified by Metabolic State (Hunger/Satiety). *Frontiers in Human Neuroscience*, *13*, 164. https://doi.org/10.3389/fnhum.2019.00164

An, L., Cao, Q.-J., Sui, M.-Q., Sun, L., Zou, Q.-H., Zang, Y.-F., & Wang, Y.-F. (2013). Local synchronization and amplitude of the fluctuation of spontaneous brain activity in attention-deficit/hyperactivity disorder: a resting-state fMRI study. *Neuroscience Bulletin*, *29*(5), 603–613. https://doi.org/10.1007/s12264-013-1353-8

Ansart, M., Epelbaum, S., Bassignana, G., Bône, A., Bottani, S., Cattai, T., … Durrleman, S. (2020). Predicting the Progression of Mild Cognitive Impairment Using Machine Learning: A Systematic, Quantitative and Critical Review. *Medical Image Analysis*, *67*, 101848. https://doi.org/10.1016/j.media.2020.101848

Azeez, A. K., & Biswal, B. B. (2017). A Review of Resting-State Analysis Methods. *Neuroimaging Clinics of North America*, *27*(4), 581–592. https://doi.org/10.1016/J.NIC.2017.06.001

Babadi, B., & Brown, E. N. (2014). A Review of Multitaper Spectral Analysis. *IEEE Transactions on Biomedical Engineering*, *61*(5), 1555–1564. https://doi.org/10.1109/TBME.2014.2311996

Bachmann, C., Jacobs, H. I. L., Porta Mana, P., Dillen, K., Richter, N., von Reutern, B., …

Morrison, A. (2018). On the Extraction and Analysis of Graphs From Resting-State fMRI to Support a Correct and Robust Diagnostic Tool for Alzheimer's Disease. *Frontiers in Neuroscience*, *12*, 528. https://doi.org/10.3389/fnins.2018.00528

Badhwar, A. P., Tam, A., Dansereau, C., Orban, P., Hoffstaedter, F., & Bellec, P. (2017). Resting-state network dysfunction in Alzheimer's disease: A systematic review and meta-analysis. *Alzheimer's and Dementia: Diagnosis, Assessment and Disease Monitoring*. https://doi.org/10.1016/j.dadm.2017.03.007

Bahrami, M., Lyday, R. G., Casanova, R., Burdette, J. H., Simpson, S. L., & Laurienti, P. J. (2019). Using Low-Dimensional Manifolds to Map Relationships Between Dynamic Brain Networks. *Frontiers in Human Neuroscience*, *13*. https://doi.org/10.3389/fnhum.2019.00430

Balthazar, M., Campos, B., Franco, A., Damasceno, B., & Cendes, F. (2013). Whole cortical and DMN mean functional connectivity as potential biomarkers for mild Alzheimer's disease. *Alzheimer's & Dementia*, *9*(4), P92. https://doi.org/10.1016/j.jalz.2013.05.150

Bandt, C., & Pompe, B. (2002). Permutation Entropy: A Natural Complexity Measure for Time Series. *Physical Review Letters*, *88*(17), 4. https://doi.org/10.1103/PhysRevLett.88.174102

Baron, J. C., Chételat, G., Desgranges, B., Perchey, G., Landeau, B., de la Sayette, V., & Eustache, F. (2001). In Vivo Mapping of Gray Matter Loss with Voxel-Based Morphometry in Mild Alzheimer's Disease. *NeuroImage*, *14*(2), 298–309. https://doi.org/10.1006/nimg.2001.0848

Bassett, D. S., & Gazzaniga, M. S. (2011, May). Understanding complexity in the human brain. *Trends in Cognitive Sciences*. NIH Public Access. https://doi.org/10.1016/j.tics.2011.03.006

Bayram, E., Caldwell, J. Z. K., & Banks, S. J. (2018). Current understanding of magnetic resonance imaging biomarkers and memory in Alzheimer's disease. *Alzheimer's & Dementia: Translational Research & Clinical Interventions*, *4*, 395–413.

https://doi.org/10.1016/J.TRCI.2018.04.007

Ben-Hur, A., & Weston, J. (2010). A user's guide to support vector machines. *Methods in Molecular Biology (Clifton, N.J.), 609*, 223–239. https://doi.org/10.1007/978-1-60327-241-4_13

Benjamini, Y., & Hochberg, Y. (1995). *Controlling the False Discovery Rate: A Practical and Powerful Approach to Multiple Testing*. *Source: Journal of the Royal Statistical Society. Series B (Methodological)* (Vol. 57). Retrieved from http://engr.case.edu/ray_soumya/mlrg/controlling_fdr_benjamini95.pdf

Bi, X. A., Shu, Q., Sun, Q., & Xu, Q. (2018). Random support vector machine cluster analysis of resting-state fMRI in Alzheimer's disease. *PLoS ONE*, *13*(3). https://doi.org/10.1371/journal.pone.0194479

Biswal, B. B. (2012, August 15). Resting state fMRI: A personal history. *NeuroImage*. Neuroimage. https://doi.org/10.1016/j.neuroimage.2012.01.090

Biswal, B., Bandettini, P., Jesmanowicz, A., SMRM, J. H.-P. of, 12th, U., & 1993, U. (1993). Time-frequency analysis of functional EPI time-course series. In *SMRM Twelfth Annual Scientific Meeting*. New York.

Biswal, B., Yetkin, F. Z., Haughton, V. M., & Hyde, J. S. (1995). Functional connectivity in the motor cortex of resting human brain using echo-planar MRI. *Magnetic Resonance in Medicine*, *34*(4), 537–541. Retrieved from http://www.ncbi.nlm.nih.gov/pubmed/8524021

Boccardi, V., Comanducci, C., Baroni, M., & Mecocci, P. (2017, December 9). Of energy and entropy: The ineluctable impact of aging in old age dementia. *International Journal of Molecular Sciences*. MDPI AG. https://doi.org/10.3390/ijms18122672

Buckner, R. L., Snyder, A. Z., Shannon, B. J., LaRossa, G., Sachs, R., Fotenos, A. F., … Mintun,

M. A. (2005). Molecular, Structural, and Functional Characterization of Alzheimer's Disease: Evidence for a Relationship between Default Activity, Amyloid, and Memory. *Journal of Neuroscience*, *25*(34), 7709–7717. https://doi.org/10.1523/JNEUROSCI.2177-05.2005

Buckner, Randy L., Andrews-Hanna, J. R., & Schacter, D. L. (2008). The brain's default network: anatomy, function, and relevance to disease. *Annals of the New York Academy of Sciences*, *1124*(1), 1–38. https://doi.org/10.1196/annals.1440.011

Busche, M. A., & Hyman, B. T. (2020, October 1). Synergy between amyloid-β and tau in Alzheimer's disease. *Nature Neuroscience*. Nature Research. https://doi.org/10.1038/s41593-020-0687-6

Cerutti, S., & Marchesi, C. (2011). *Advanced methods of biomedical signal processing*. Wiley.

Cha, J., Jo, H. J., Kim, H. J., Seo, S. W., Kim, H.-S., Yoon, U., … Lee, J.-M. (2013). Functional alteration patterns of default mode networks: comparisons of normal aging, amnestic mild cognitive impairment and Alzheimer's disease. *European Journal of Neuroscience*, *37*(12), 1916–1924. https://doi.org/10.1111/ejn.12177

Cheng, R., Qi, H., Liu, Y., Zhao, S., Li, C., Liu, C., & Zheng, J. (2017). Abnormal amplitude of low-frequency fluctuations and functional connectivity of resting-state functional magnetic resonance imaging in patients with leukoaraiosis. *Brain and Behavior*, *7*(6), e00714. https://doi.org/10.1002/brb3.714

Dai, Z., Lin, Q., Li, T., Wang, X., Yuan, H., Yu, X., … Wang, H. (2019). Disrupted structural and functional brain networks in Alzheimer's disease. *Neurobiology of Aging*, *75*, 71–82. https://doi.org/10.1016/J.NEUROBIOLAGING.2018.11.005

Dalianis, H., & Dalianis, H. (2018). Evaluation Metrics and Evaluation. In *Clinical Text Mining* (pp. 45–53). Springer International Publishing. https://doi.org/10.1007/978-3-319-78503-5_6

Damoiseaux, J. S., Rombouts, S. A. R. B., Barkhof, F., Scheltens, P., Stam, C. J., Smith, S. M., & Beckmann, C. F. (2006). Consistent resting-state networks across healthy subjects. *Proceedings of the National Academy of Sciences of the United States of America*, *103*(37), 13848–13853. https://doi.org/10.1073/pnas.0601417103

Dekhil, O., Hajjdiab, H., Shalaby, A., Ali, M. T., Ayinde, B., Switala, A., … El-Baz, A. (2018). Using resting state functional MRI to build a personalized autism diagnosis system. *PloS One*, *13*(10), e0206351. https://doi.org/10.1371/journal.pone.0206351

deSouza, N. M., Achten, E., Alberich-Bayarri, A., Bamberg, F., Boellaard, R., Clément, O., … Zech, C. J. (2019). Validated imaging biomarkers as decision-making tools in clinical trials and routine practice: current status and recommendations from the EIBALL* subcommittee of the European Society of Radiology (ESR). *Insights into Imaging*, *10*(1), 87. https://doi.org/10.1186/s13244-019-0764-0

Dickerson, B. C., Agosta, F., & Filippi, M. (2016). fMRI in Neurodegenerative Diseases: From Scientific Insights to Clinical Applications (pp. 699–739). Humana Press, New York, NY. https://doi.org/10.1007/978-1-4939-5611-1_23

Dillen, K. N. H., Jacobs, H. I. L., Kukolja, J., Richter, N., von Reutern, B., Onur, Ö. A., … Fink, G. R. (2017). Functional Disintegration of the Default Mode Network in Prodromal Alzheimer's Disease. *Journal of Alzheimer's Disease*, *59*(1), 169–187. https://doi.org/10.3233/JAD-161120

Dillen, K. N. H., Jacobs, H. I. L., Kukolja, J., von Reutern, B., Richter, N., Onur, Ö. A., … Fink, G. R. (2016). Aberrant functional connectivity differentiates retrosplenial cortex from posterior cingulate cortex in prodromal Alzheimer's disease. *Neurobiology of Aging*, *44*, 114–126. https://doi.org/10.1016/j.neurobiolaging.2016.04.010

Duff, E. P., Johnston, L. A., Xiong, J., Fox, P. T., Mareels, I., & Egan, G. F. (2008). The power of spectral density analysis for mapping endogenous BOLD signal fluctuations. *Human Brain Mapping*, *29*(7), 778–790. https://doi.org/10.1002/hbm.20601

Dyrba, M., Grothe, M., Kirste, T., & Teipel, S. J. (2015). Multimodal analysis of functional and structural disconnection in Alzheimer's disease using multiple kernel SVM. *Human Brain Mapping*, *36*(6), 2118–2131. https://doi.org/10.1002/hbm.22759

Erkkinen, M. G., Kim, M.-O., & Geschwind, M. D. (2017). Clinical Neurology and Epidemiology of the Major Neurodegenerative Diseases. *Cold Spring Harbor Perspectives in Biology*, *10*(4), a033118. https://doi.org/10.1101/CSHPERSPECT.A033118

Eyler, L. T., Elman, J. A., Hatton, S. N., Gough, S., Mischel, A. K., Hagler, D. J., … Kremen, W. S. (2019). Resting State Abnormalities of the Default Mode Network in Mild Cognitive Impairment: A Systematic Review and Meta-Analysis. *Journal of Alzheimer's Disease*. IOS Press. https://doi.org/10.3233/JAD-180847

Farahani, F. V., Karwowski, W., & Lighthall, N. R. (2019). Application of Graph Theory for Identifying Connectivity Patterns in Human Brain Networks: A Systematic Review. *Frontiers in Neuroscience*, *13*, 585. https://doi.org/10.3389/fnins.2019.00585

Frisoni, G. B., Testa, C., Zorzan, A., Sabattoli, F., Beltramello, A., Soininen, H., & Laakso, M. P. (2002). Detection of grey matter loss in mild Alzheimer's disease with voxel based morphometry. *Journal of Neurology, Neurosurgery, and Psychiatry*, *73*(6), 657–664. https://doi.org/10.1136/jnnp.73.6.657

Giménez, M., Guinea-Izquierdo, A., Villalta-Gil, V., Martínez-Zalacaín, I., Segalàs, C., Subirà, M., … Soriano-Mas, C. (2016). Brain alterations in low-frequency fluctuations across multiple bands in obsessive compulsive disorder. *Brain Imaging and Behavior*, 1–17.

https://doi.org/10.1007/s11682-016-9601-y

Glerean, E., Pan, R. K., Salmi, J., Kujala, R., Lahnakoski, J. M., Roine, U., … Jääskeläinen, I. P. (2016). Reorganization of functionally connected brain subnetworks in high-functioning autism. *Human Brain Mapping*, *37*(3), 1066–1079. https://doi.org/10.1002/hbm.23084

Gray, K. R., Aljabar, P., Heckemann, R. A., Hammers, A., Rueckert, D., & Alzheimer's Disease Neuroimaging Initiative. (2013). Random forest-based similarity measures for multi-modal classification of Alzheimer's disease. *NeuroImage*, *65*, 167–175. https://doi.org/10.1016/j.neuroimage.2012.09.065

Greicius, M. D., Srivastava, G., Reiss, A. L., & Menon, V. (2004). Default-mode network activity distinguishes Alzheimer's disease from healthy aging: Evidence from functional MRI. *Proceedings of the National Academy of Sciences*, *101*(13), 4637–4642. https://doi.org/10.1073/pnas.0308627101

Grieder, M., Wang, D. J. J., Dierks, T., Wahlund, L.-O., & Jann, K. (2018). Default Mode Network Complexity and Cognitive Decline in Mild Alzheimer's Disease. *Frontiers in Neuroscience*, *12*, 770. https://doi.org/10.3389/fnins.2018.00770

Habib, M., Mak, E., Gabel, S., Su, L., Williams, G., Waldman, A., … O'Brien, J. T. (2017). Functional neuroimaging findings in healthy middle-aged adults at risk of Alzheimer's disease. *Ageing Research Reviews*. https://doi.org/10.1016/j.arr.2017.03.004

Habib, R., Noureen, N., & Nadeem, N. (2018). Decoding Common Features of Neurodegenerative Disorders: From Differentially Expressed Genes to Pathways. *Current Genomics*, *19*(4), 300–312. https://doi.org/10.2174/1389202918666171005100549

Hentschke, H., & Stüttgen, M. C. (2011). Computation of measures of effect size for neuroscience data sets. *The European Journal of Neuroscience*, *34*(12), 1887–1894.

https://doi.org/10.1111/j.1460-9568.2011.07902.x

Hojjati, S. H., Ebrahimzadeh, A., Khazaee, A., & Babajani-Feremi, A. (2017). Predicting conversion from MCI to AD using resting-state fMRI, graph theoretical approach and SVM. *Journal of Neuroscience Methods*, *282*, 69–80. https://doi.org/10.1016/j.jneumeth.2017.03.006

Hojjati, S. H., Ebrahimzadeh, A., Khazaee, A., & Babajani-Feremi, A. (2018). Predicting conversion from MCI to AD by integrating rs-fMRI and structural MRI. *Computers in Biology and Medicine*, *102*, 30–39. https://doi.org/10.1016/j.compbiomed.2018.09.004

Hu, X., Chen, S., Huang, C.-B., Qian, Y., & Yu, Y. (2017). Frequency-dependent changes in the amplitude of low-frequency fluctuations in patients with Wilson's disease: a resting-state fMRI study. *Metabolic Brain Disease*, *32*(3), 685–692. https://doi.org/10.1007/s11011-016-9946-3

Hussain, R., Zubair, H., Pursell, S., & Shahab, M. (2018). Neurodegenerative Diseases: Regenerative Mechanisms and Novel Therapeutic Approaches. *Brain Sciences*, *8*(9). https://doi.org/10.3390/brainsci8090177

Hutchison, R. M., Womelsdorf, T., Gati, J. S., Everling, S., & Menon, R. S. (2013). Resting-state networks show dynamic functional connectivity in awake humans and anesthetized macaques. *Human Brain Mapping*, *34*(9), 2154–2177. https://doi.org/10.1002/hbm.22058

Ishii, K., Kawachi, T., Sasaki, H., Kono, A. K., Fukuda, T., Kojima, Y., & Mori, E. (2005). Voxel-based morphometric comparison between early- and late-onset mild Alzheimer's disease and assessment of diagnostic performance of z score images. *AJNR. American Journal of Neuroradiology*, *26*(2), 333–340. Retrieved from http://www.ncbi.nlm.nih.gov/pubmed/15709131

Jalili, M. (2017). Graph theoretical analysis of Alzheimer's disease: Discrimination of AD patients from healthy subjects. *Information Sciences*, *384*, 145–156. https://doi.org/10.1016/J.INS.2016.08.047

Jha, D., Kim, J.-I., & Kwon, G.-R. (2017). Diagnosis of Alzheimer's Disease Using Dual-Tree Complex Wavelet Transform, PCA, and Feed-Forward Neural Network. *Journal of Healthcare Engineering*, *2017*, 1–13. https://doi.org/10.1155/2017/9060124

Kabbara, A., EL Falou, W., Khalil, M., Wendling, F., & Hassan, M. (2017). The dynamic functional core network of the human brain at rest. *Scientific Reports*, *7*(1), 1–16. https://doi.org/10.1038/s41598-017-03420-6

Khalili-Mahani, N., Rombouts, S. A. R. B., van Osch, M. J. P., Duff, E. P., Carbonell, F., Nickerson, L. D., … van Gerven, J. M. (2017). Biomarkers, designs, and interpretations of resting-state fMRI in translational pharmacological research: A review of state-of-the-Art, challenges, and opportunities for studying brain chemistry. *Human Brain Mapping*, *38*(4), 2276–2325. https://doi.org/10.1002/hbm.23516

Khazaee, A., Ebrahimzadeh, A., & Babajani-Feremi, A. (2015). Identifying patients with Alzheimer's disease using resting-state fMRI and graph theory, *126*, 2132–2141. Retrieved from http://www.scopus.com/record/display.url?eid=2-s2.0-84927942784&origin=resultslist&sort=plf-f&src=s&sid=4B0F8DDFB2B6967432AB0CAE53654FC1.CnvicAmOODVwpVrjSeqQ:50&sot=a&sdt=a&sessionSearchId=4B0F8DDFB2B6967432AB0CAE53654FC1.CnvicAmOODVwpVrjSeqQ:50&relpos=37

Khazaee, Ali, Ebrahimzadeh, A., & Babajani-Feremi, A. (2015). Identifying patients with Alzheimer's disease using resting-state fMRI and graph theory. *Clinical Neurophysiology*,

126(11), 2132–2141. https://doi.org/10.1016/j.clinph.2015.02.060

Khazaee, Ali, Ebrahimzadeh, A., & Babajani-Feremi, A. (2017). Classification of patients with MCI and AD from healthy controls using directed graph measures of resting-state fMRI. *Behavioural Brain Research*, *322*(Pt B), 339–350. Retrieved from https://www.sciencedirect.com/science/article/pii/S0166432816304077?via%3Dihub

Khosla, M., Jamison, K., Ngo, G. H., Kuceyeski, A., & Sabuncu, M. R. (2019). Machine learning in resting-state fMRI analysis. *Magnetic Resonance Imaging*. https://doi.org/10.1016/j.mri.2019.05.031

Knopman, D. S., & Petersen, R. C. (2014, October 1). Mild cognitive impairment and mild dementia: A clinical perspective. *Mayo Clinic Proceedings*. Elsevier Ltd. https://doi.org/10.1016/j.mayocp.2014.06.019

Knyazev, G. G. (2007, January 1). Motivation, emotion, and their inhibitory control mirrored in brain oscillations. *Neuroscience and Biobehavioral Reviews*. Pergamon. https://doi.org/10.1016/j.neubiorev.2006.10.004

Koch, W., Teipel, S., Mueller, S., Benninghoff, J., Wagner, M., Bokde, A. L. W., … Meindl, T. (2012). Diagnostic power of default mode network resting state fMRI in the detection of Alzheimer's disease. *Neurobiology of Aging*, *33*(3), 466–478. https://doi.org/10.1016/j.neurobiolaging.2010.04.013

Kohavi, R., & John, G. H. (1997). Wrappers for feature subset selection. *Artificial Intelligence*, *97*(1–2), 273–324. https://doi.org/10.1016/s0004-3702(97)00043-x

Kraskov, A., Stoegbauer, H., & Grassberger, P. (2003). Estimating Mutual Information. *Physical Review E - Statistical Physics, Plasmas, Fluids, and Related Interdisciplinary Topics*, *69*(6), 16. https://doi.org/10.1103/PhysRevE.69.066138

Kundu, S., Lukemire, J., Wang, Y., Guo, Y., Weiner, M. W., Schuff, N., … Furst, A. J. (2019). A Novel Joint Brain Network Analysis Using Longitudinal Alzheimer's Disease Data. *Scientific Reports*, *9*(1). https://doi.org/10.1038/s41598-019-55818-z

LaMontagne, P. J., Benzinger, T. L. S., Morris, J. C., Keefe, S., Hornbeck, R., Xiong, C., … Marcus, D. (2019). OASIS-3: Longitudinal Neuroimaging, Clinical, and Cognitive Dataset for Normal Aging and Alzheimer Disease. *MedRxiv*, 2019.12.13.19014902. https://doi.org/10.1101/2019.12.13.19014902

Lassonde, M., Candel, S., Hacker, J., Quadrio-Curzio, A., Onishi, T., Ramakrishnan, V., & McNutt, M. (2017). The challenge of neurodegenerative diseases in aging population. Retrieved October 23, 2019, from https://royalsociety.org/-/media/about-us/international/g-science-statements/2017-may-aging-population.pdf?la=en-GB&hash=C665B04DAB77DE2C053D8F51E61E4379

Lees, A. J., Hardy, J., & Revesz, T. (2009). Parkinson's disease. *Lancet (London, England)*, *373*(9680), 2055–2066. https://doi.org/10.1016/S0140-6736(09)60492-X

Liu, C., Li1, C., Yin, X., Yang, J., Zhou, D., Gui, L., & Wang, J. (2014). Abnormal Intrinsic Brain Activity Patterns in Patients with Subcortical Ischemic Vascular DementiaLiu, C., Li1, C., Yin, X., Yang, J., Zhou, D., Gui, L., & Wang, J. (2014). Abnormal Intrinsic Brain Activity Patterns in Patients with Subcortical Ischemic V. *PLoS ONE*, *9*(2), e87880. https://doi.org/10.1371/journal.pone.0087880

Lizier, J. T., Heinzle, J., Horstmann, A., Haynes, J.-D., & Prokopenko, M. (2011). Multivariate information-theoretic measures reveal directed information structure and task relevant changes in fMRI connectivity. *Journal of Computational Neuroscience*, *30*(1), 85–107. https://doi.org/10.1007/s10827-010-0271-2

Lizier, J. T., Prokopenko, M., & Zomaya, A. Y. (2012). Local measures of information storage in complex distributed computation. *Information Sciences*, *208*, 39–54. https://doi.org/10.1016/j.ins.2012.04.016

Lustig, C., Snyder, A. Z., Bhakta, M., O'Brien, K. C., McAvoy, M., Raichle, M. E., … Buckner, R. L. (2003). Functional deactivations: Change with age and dementia of the Alzheimer type. *Proceedings of the National Academy of Sciences*, *100*(24), 14504–14509. https://doi.org/10.1073/pnas.2235925100

Lv, H., Wang, Z., Tong, E., Williams, L. M., Zaharchuk, G., Zeineh, M., … Wintermark, M. (2018). Resting-State Functional MRI: Everything That Nonexperts Have Always Wanted to Know. *American Journal of Neuroradiology*, *39*(8), 1390–1399. https://doi.org/10.3174/ajnr.A5527

Mao, S., Zhang, C., Gao, N., Wang, Y., Yang, Y., Guo, X., & Ma, T. (2017). A study of feature extraction for Alzheimer's disease based on resting-state fMRI. In *2017 39th Annual International Conference of the IEEE Engineering in Medicine and Biology Society (EMBC)* (pp. 517–520). IEEE. https://doi.org/10.1109/EMBC.2017.8036875

McKhann, G. M., Knopman, D. S., Chertkow, H., Hyman, B. T., Jack, C. R., Kawas, C. H., … Phelps, C. H. (2011). The diagnosis of dementia due to Alzheimer's disease: recommendations from the National Institute on Aging-Alzheimer's Association workgroups on diagnostic guidelines for Alzheimer's disease. *Alzheimer's & Dementia : The Journal of the Alzheimer's Association*, *7*(3), 263–269. https://doi.org/10.1016/j.jalz.2011.03.005

Mevel, K., Chételat, G., Eustache, F., & Desgranges, B. (2011). The default mode network in healthy aging and Alzheimer's disease. *International Journal of Alzheimer's Disease*, *2011*, 535816. https://doi.org/10.4061/2011/535816

Miri Ashtiani, S. N., Daliri, M. R., Behnam, H., Hossein-Zadeh, G.-A., Mehrpour, M., Motamed, M. R., & Fadaie, F. (2018). Altered topological properties of brain networks in the early MS patients revealed by cognitive task-related fMRI and graph theory. *Biomedical Signal Processing and Control*, *40*, 385–395. https://doi.org/10.1016/J.BSPC.2017.10.006

Mokhtari, F., Akhlaghi, M. I., Simpson, S. L., Wu, G., & Laurienti, P. J. (2019). Sliding window correlation analysis: Modulating window shape for dynamic brain connectivity in resting state. *NeuroImage*, *189*, 655–666. https://doi.org/10.1016/J.NEUROIMAGE.2019.02.001

Muldoon, S. F., Bridgeford, E. W., & Bassett, D. S. (2016). Small-world propensity and weighted brain networks. *Scientific Reports*, *6*(1), 1–13. https://doi.org/10.1038/srep22057

Nl, L. V. U., & Hinton, G. (2008). *Visualizing Data using t-SNE Laurens van der Maaten*. *Journal of Machine Learning Research* (Vol. 1).

Olson, R. S., Edu, O., & Moore, J. H. (2016). *AutoML Workshop* (Vol. 64). Retrieved from https://github.com/rhiever/tpot.

Pan, P., Zhang, Y., Liu, Y., Zhang, H., Guan, D., & Xu, Y. (2017). Abnormalities of regional brain function in Parkinson's disease: a meta-analysis of resting state functional magnetic resonance imaging studies. *Scientific Reports*, *7*, 40469. https://doi.org/10.1038/srep40469

Pedregosa, F., Michel, V., Grisel OLIVIERGRISEL, O., Blondel, M., Prettenhofer, P., Weiss, R., … Duchesnay EDOUARDDUCHESNAY, Fré. (2011). *Scikit-learn: Machine Learning in Python Gaël Varoquaux Bertrand Thirion Vincent Dubourg Alexandre Passos PEDREGOSA, VAROQUAUX, GRAMFORT ET AL. Matthieu Perrot*. *Journal of Machine Learning Research* (Vol. 12). Retrieved from http://scikit-learn.sourceforge.net.

Pellegrini, E., Ballerini, L., Hernandez, M. del C. V., Chappell, F. M., González-Castro, V., Anblagan, D., … Wardlaw, J. M. (2018). Machine learning of neuroimaging for assisted

diagnosis of cognitive impairment and dementia: A systematic review. *Alzheimer's & Dementia: Diagnosis, Assessment & Disease Monitoring*, *10*, 519–535. Retrieved from https://www.sciencedirect.com/science/article/pii/S2352872918300447

Penttonen, M., & Buzsáki, G. (2003). Natural logarithmic relationship between brain oscillators. *Thalamus & Related Systems*, *2*(2), 145–152. https://doi.org/10.1016/S1472-9288(03)00007-4

Prada, S. I., Takeuchi, Y., & Ariza, Y. (2014). *Costo monetario del tratamiento de la enfermedad deAlzheimer en Colombia / Monetary cost of treatment for Alzheimer's disease in Colombia*. *Acta neurol. colomb* (Vol. 30). Asociación Colombiana de Neurología. Retrieved from http://pesquisa.bvsalud.org/portal/resource/pt/lil-731701

Puche Sarmiento, A. C., Bocanegra García, Y., & Ochoa Gómez, J. F. (2019). Active information storage in Parkinson's disease: a resting state fMRI study over the sensorimotor cortex. *Brain Imaging and Behavior*. https://doi.org/10.1007/s11682-019-00037-3

Qiao, J., Lv, Y., Cao, C., Wang, Z., & Li, A. (2018). Multivariate Deep Learning Classification of Alzheimer's Disease Based on Hierarchical Partner Matching Independent Component Analysis. *Frontiers in Aging Neuroscience*, *10*, 417. https://doi.org/10.3389/fnagi.2018.00417

Rathore, S., Habes, M., Iftikhar, M. A., Shacklett, A., & Davatzikos, C. (2017). A review on neuroimaging-based classification studies and associated feature extraction methods for Alzheimer's disease and its prodromal stages. *NeuroImage*, *155*(April), 530–548. https://doi.org/10.1016/j.neuroimage.2017.03.057

Riedl, M., Müller, A., & Wessel, N. (2013, June 25). Practical considerations of permutation entropy: A tutorial review. *European Physical Journal: Special Topics*. Springer.

https://doi.org/10.1140/epjst/e2013-01862-7

Roh, Y., Heo, G., & Euijong Whang, S. (n.d.). *A Survey on Data Collection for Machine Learning A Big Data-AI Integration Perspective*.

Sánchez-Maroño, N., Alonso-Betanzos, A., & Tombilla-Sanromán, M. (n.d.). *Filter methods for feature selection. A comparative study*.

Savva, A. D., Mitsis, G. D., & Matsopoulos, G. K. (2019). Assessment of dynamic functional connectivity in resting-state fMRI using the sliding window technique. *Brain and Behavior*, *9*(4), e01255. https://doi.org/10.1002/brb3.1255

Schnaubelt, M., Dovern, J., Fischer, T., Krauss, C., & Glas, A. (2019). *A comparison of machine learning model validation schemes for non-stationary time series data A comparison of machine learning model validation schemes for non-stationary time series data The author has benefited from helpful discussions with Ingo* (No. 11/2019). *FAU Discussion Papers in Economics*. Erlangen-Núremberg. Retrieved from http://hdl.handle.net/10419/209136

Schumacher, J., Peraza, L. R., Firbank, M., Thomas, A. J., Kaiser, M., Gallagher, P., … Taylor, J.-P. (2018). Dynamic functional connectivity changes in dementia with Lewy bodies and Alzheimer's disease. *BioRxiv*, 374538. https://doi.org/10.1101/374538

Sepulcre, J., Sabuncu, M. R., & Johnson, K. A. (2012). Network assemblies in the functional brain. *Current Opinion in Neurology*, *25*(4), 1. https://doi.org/10.1097/WCO.0b013e328355a8e8

Shi, J., & Liu, B. (2020). Stage detection of mild cognitive impairment via fMRI using Hilbert Huang Transform based classification framework. *Medical Physics*, mp.14183. https://doi.org/10.1002/mp.14183

Shirer, W. R., Ryali, S., Rykhlevskaia, E., Menon, V., & Greicius, M. D. (2012). Decoding Subject-Driven Cognitive States with Whole-Brain Connectivity Patterns. *Cerebral Cortex*,

22(1), 158–165. https://doi.org/10.1093/cercor/bhr099

Siyah Mansoory, M., Oghabian, M. A., Jafari, A. H., & Shahbabaie, A. (2017). Analysis of Resting-State fMRI Topological Graph Theory Properties in Methamphetamine Drug Users Applying Box-Counting Fractal Dimension. *Basic and Clinical Neuroscience*, *8*(5), 371–385. https://doi.org/10.18869/nirp.bcn.8.5.371

Smelser, N. J., & Baltes, P. B. (2001). *International encyclopedia of the social & behavioral sciences*. Elsevier. Retrieved from https://www.sciencedirect.com/referencework/9780080430768/international-encyclopedia-of-the-social-and-behavioral-sciences

Sporns, O. (2013). Structure and function of complex brain networks. *Dialogues in Clinical Neuroscience*, *15*(3), 247–262. Retrieved from www.dialogues-cns.org

Strimbu, K., & Tavel, J. A. (2010). What are biomarkers? *Current Opinion in HIV and AIDS*, *5*(6), 463–466. https://doi.org/10.1097/COH.0b013e32833ed177

Súarez-Revelo, X., Ochoa-Gomez, J. F., Tobón-Quintero, C. A., & Duque-Grajales, J. E. (2014). Conectividad funcional en adultos mayores a partir de resonanciamagnética funcional como un posible indicador para la enfermedad deAlzheimer. *Acta Neurol. Colomb*, 273–281. Retrieved from http://acnweb.org/es/acta-neurologica/volumen-30-2014/157-volumen-30-no-4-octubre-diciembre-de-2014/1068-conectividad-funcional-en-adultos-mayores-a-partir-de-resonancia-magnetica-funcional-como-un-posible-indicador-para-la-enfermedad-de-alzheimer.html

Sun, Z., Van De Giessen, M., Lelieveldt, B. P. F., & Staring, M. (2017). Detection of conversion from mild cognitive impairment to Alzheimer's disease using longitudinal brain MRI. *Frontiers in Neuroinformatics*, *11*, 16. https://doi.org/10.3389/fninf.2017.00016

Tang, J., Alelyani, S., & Liu, H. (n.d.). *Feature Selection for Classification: A Review*.

Teipel, S. J., Grothe, M. J., Metzger, C. D., Grimmer, T., Sorg, C., Ewers, M., … Dyrba, M. (2017). Robust Detection of Impaired Resting State Functional Connectivity Networks in Alzheimer's Disease Using Elastic Net Regularized Regression. *Frontiers in Aging Neuroscience*, *8*, 318. https://doi.org/10.3389/fnagi.2016.00318

Telesford, Q. K., Simpson, S. L., Burdette, J. H., Hayasaka, S., & Laurienti, P. J. (2011, October 1). The Brain as a Complex System: Using Network Science as a Tool for Understanding the Brain. *Brain Connectivity*. Brain Connect. https://doi.org/10.1089/brain.2011.0055

Timme, N. M., & Lapish, C. (2018). A Tutorial for Information Theory in Neuroscience. *ENeuro*, *5*(3). https://doi.org/10.1523/ENEURO.0052-18.2018

Tom, S. E., Hubbard, R. A., Crane, P. K., Haneuse, S. J., Bowen, J., McCormick, W. C., … Larson, E. B. (2015). Characterization of dementia and Alzheimer's disease in an older population: updated incidence and life expectancy with and without dementia. *American Journal of Public Health*, *105*(2), 408–413. https://doi.org/10.2105/AJPH.2014.301935

Uhlhaas, P. J., & Singer, W. (2006). Neural Synchrony in Brain Disorders: Relevance for Cognitive Dysfunctions and Pathophysiology. *Neuron*, *52*(1), 155–168. https://doi.org/10.1016/j.neuron.2006.09.020

Vermunt, L., Sikkes, S. A. M., van den Hout, A., Handels, R., Bos, I., van der Flier, W. M., … Coley, N. (2019). Duration of preclinical, prodromal, and dementia stages of Alzheimer's disease in relation to age, sex, and APOE genotype. *Alzheimer's & Dementia*, *15*(7), 888–898. https://doi.org/10.1016/J.JALZ.2019.04.001

Vu, M. A. T., Adalı, T., Ba, D., Buzsáki, G., Carlson, D., Heller, K., … Dzirasa, K. (2018). A shared vision for machine learning in neuroscience. *Journal of Neuroscience*, *38*(7), 1601–

1607. https://doi.org/10.1523/JNEUROSCI.0508-17.2018

Wang, B., Niu, Y., Miao, L., Cao, R., Yan, P., Guo, H., … Zhang, H. (2017). Decreased Complexity in Alzheimer's Disease: Resting-State fMRI Evidence of Brain Entropy Mapping. *Frontiers in Aging Neuroscience*, *9*(NOV), 378. https://doi.org/10.3389/fnagi.2017.00378

Wang, J., Zhang, J.-R., Zang, Y.-F., & Wu, T. (2018). Consistent decreased activity in the putamen in Parkinson's disease: a meta-analysis and an independent validation of resting-state fMRI. *GigaScience*, *7*(6). https://doi.org/10.1093/gigascience/giy071

Wang, P., Yang, J., Yin, Z., Duan, J., Zhang, R., Sun, J., … Tang, Y. (2019). Amplitude of low-frequency fluctuation (ALFF) may be associated with cognitive impairment in schizophrenia: a correlation study. *BMC Psychiatry*, *19*(1), 30. https://doi.org/10.1186/s12888-018-1992-4

Williams, A. (2002). Defining neurodegenerative diseases. *BMJ (Clinical Research Ed.)*, *324*(7352), 1465–1466. https://doi.org/10.1136/bmj.324.7352.1465

Xie, H., Zheng, C. Y., Handwerker, D. A., Bandettini, P. A., Calhoun, V. D., Mitra, S., & Gonzalez-Castillo, J. (2019). Efficacy of different dynamic functional connectivity methods to capture cognitively relevant information. *NeuroImage*, *188*, 502–514. https://doi.org/10.1016/J.NEUROIMAGE.2018.12.037

Yang, L., Yan, Y., Wang, Y., Hu, X., Lu, J., Chan, P., … Han, Y. (2018). Gradual Disturbances of the Amplitude of Low-Frequency Fluctuations (ALFF) and Fractional ALFF in Alzheimer Spectrum. *Frontiers in Neuroscience*, *12*, 975. https://doi.org/10.3389/fnins.2018.00975

Zang, Y.-F., Zuo, X.-N., Milham, M., & Hallett, M. (2015). Toward a Meta-Analytic Synthesis of the Resting-State fMRI Literature for Clinical Populations. *BioMed Research International*, *2015*, 435265. https://doi.org/10.1155/2015/435265

Zhang, H.-Y., Wang, S.-J., Liu, B., Ma, Z.-L., Yang, M., Zhang, Z.-J., & Teng, G.-J. (2010). Resting Brain Connectivity: Changes during the Progress of Alzheimer Disease. *Radiology*, *256*(2), 598–606. https://doi.org/10.1148/radiol.10091701

Zhang, T., Zhao, Z., Zhang, C., Zhang, J., Jin, Z., & Li, L. (2019). Classification of early and late mild cognitive impairment using functional brain network of resting-state fMRI. *Frontiers in Psychiatry*, *10*(AUG), 572. https://doi.org/10.3389/fpsyt.2019.00572

Zheng, H., Onoda, K., Nagai, A., & Yamaguchi, S. (2020). Reduced Dynamic Complexity of BOLD Signals Differentiates Mild Cognitive Impairment From Normal Aging. *Frontiers in Aging Neuroscience*, *12*. https://doi.org/10.3389/fnagi.2020.00090

Zhou, F., Zhuang, Y., Gong, H., Zhan, J., Grossman, M., & Wang, Z. (2016). Resting state brain entropy alterations in relapsing remitting multiple sclerosis. *PLoS ONE*, *11*(1), 146080. https://doi.org/10.1371/journal.pone.0146080

Zhou, J., Greicius, M. D., Gennatas, E. D., Growdon, M. E., Jang, J. Y., Rabinovici, G. D., … Seeley, W. W. (2010). Divergent network connectivity changes in behavioural variant frontotemporal dementia and Alzheimer's disease. *Brain*, *133*(5), 1352–1367. https://doi.org/10.1093/brain/awq075

Zou, Q.-H., Zhu, C.-Z., Yang, Y., Zuo, X.-N., Long, X.-Y., Cao, Q.-J., … Zang, Y.-F. (2008). An improved approach to detection of amplitude of low-frequency fluctuation (ALFF) for resting-state fMRI: Fractional ALFF. *Journal of Neuroscience Methods*, *172*(1), 137–141. https://doi.org/10.1016/J.JNEUMETH.2008.04.012

Zuo, X.-N., Di Martino, A., Kelly, C., Shehzad, Z. E., Gee, D. G., Klein, D. F., … Milham, M. P. (2010). The oscillating brain: complex and reliable. *NeuroImage*, *49*(2), 1432–1445. https://doi.org/10.1016/j.neuroimage.2009.09.037